

12-2019

ASSESSMENT OF NEW INNOVATIONS IN PET/CT FOR RESPIRATORY MOTION CORRECTION

Joseph Meier

Follow this and additional works at: https://digitalcommons.library.tmc.edu/utgsbs_dissertations



Part of the [Medicine and Health Sciences Commons](#)

Recommended Citation

Meier, Joseph, "ASSESSMENT OF NEW INNOVATIONS IN PET/CT FOR RESPIRATORY MOTION CORRECTION" (2019). *The University of Texas MD Anderson Cancer Center UTHealth Graduate School of Biomedical Sciences Dissertations and Theses (Open Access)*. 983.
https://digitalcommons.library.tmc.edu/utgsbs_dissertations/983

This Dissertation (PhD) is brought to you for free and open access by the The University of Texas MD Anderson Cancer Center UTHealth Graduate School of Biomedical Sciences at DigitalCommons@TMC. It has been accepted for inclusion in The University of Texas MD Anderson Cancer Center UTHealth Graduate School of Biomedical Sciences Dissertations and Theses (Open Access) by an authorized administrator of DigitalCommons@TMC. For more information, please contact digitalcommons@library.tmc.edu.

ASSESSMENT OF NEW INNOVATIONS IN PET/CT FOR RESPIRATORY
MOTION CORRECTION

by

Joseph Gabriel Meier, B.S.

APPROVED:

Osama R. Mawlawi, Ph.D.
Advisory Professor

Jeremy J. Erasmus, M.D.

Tinsu Pan, Ph.D.

Christine B. Peterson, Ph.D.

Richard Wendt, III, Ph.D.

APPROVED:

Dean, The University of Texas
MD Anderson Cancer Center UTHealth Graduate School of Biomedical Sciences

ASSESSMENT OF NEW INNOVATIONS IN PET/CT FOR RESPIRATORY
MOTION CORRECTION

A

DISSERTATION

Presented to the Faculty of

The University of Texas

MD Anderson Cancer Center UTHealth

Graduate School of Biomedical Sciences

in Partial Fulfillment

of the Requirements

for the Degree of

DOCTOR OF PHILOSOPHY

by

Joseph Gabriel Meier, B.S.

Houston, Texas

December 2019

Dedication

To Kristine, the love of my life, who has been there with me for every step on my Medical Physics journey. I could not have gotten here without your everlasting support. No matter what life has in store for us, I can't wait to be there with you always and catchup on all of the scrabble and father of the bride that we have missed during my time as a student!

To all of the cancer patients who are in need of the technologies that we as a field are pushing towards clinical realization.

Acknowledgements

I will forever be grateful to Dr. Mawlawi for giving me the opportunity to be his student. On top of the many responsibilities his work and life entails, he has provided me unwavering support and encouragement throughout my time as a student. He has spent countless hours in helping me develop my research, editing our publications, and giving feedback on my practice presentations for which I am eternally grateful. In addition, he has given me unparalleled exposure to our field from both a clinical and research perspective. To say that you have gone above and beyond doesn't even begin to cover it. Thank you!

Next I would like to thank my committee members for their guidance throughout my time as a graduate student. To Dr. Wendt, thank you for your constant encouragement and guidance. Thank you as well for involving me in the PET/MR shielding investigation. To Dr. Pan, thank you for all of our discussions on and your contagious enthusiasm about 4DPET, 4DCT, average CT, as well as for providing my first introduction to these issues. To Dr. Peterson for all the time you spent suggesting and explaining the statistical analyses in my work as well as considering alternative methods. It moved me past many roadblocks and was a great learning experience. To Dr. Erasmus, thank you for providing your expertise when assessing the PET images in our investigation. It is an invaluable experience to be able to have the opinion of you and your team who are experts in reading thoracic PET/CT. To the past members of my committee, Dr. Kundra, Dr. Ma, and Dr. Rao, your time and expertise was greatly appreciated.

To Dr. Kappadath who I worked with on the electronic personal dosimeter investigation before I was a student. This was a very formative experience as I was able to substantially contribute to the experimental design, data acquisition, and publications.

To the PET technologists, for providing me the invaluable experience of learning how the clinic works, and how my research would fit into the routine operations.

To all of the industrial scientists that I have worked with and have learned so much from: Jim Hamill, Judd Jones, Inki Hong, Paul Schleyer, and Tim Deller.

To all of the patients who consented to be in these studies and endure the annoyances of prolonged examination durations.

For all of the knowledge and good times coming from my time as a physics technologist working with Colby Anger, Tony Blatnica, Mike Silosky, Brandan Darensbourg, Paul Stauduhar, and Navya Kurre. For all of the mentorship and knowledge given to me while a physics technologist from the physicists: Jeff Shepard, Donna Reeve, Bill Erwin, Dr. Rong, Dr. Jones, Dr. Willis, Dr. Nishino, Dr. Stafford.

For being along on the adventure with my classmates especially those in Nuclear Medicine: Ben Lopez, Wendy Siman, and Justin Mikell.

To Nikki Franklin, for all of her help getting me organized for all of the important meetings, trips, and exams. To Frances for helping all the students out faster than anything that is fast. To Anne and Betsy for all that you do/have done to keep our paths as clear as possible.

To my family who have given unwavering support in my life through all of my ups and downs, but most of all for always being excited like puppies to see each other.

Finally, I want to thank the UTGSBS and especially Dr. Mattox and Brenda Gaughn. They have helped me out on many occasions and are truly dedicated to the success and well being of all of the student body.

ASSESSMENT OF NEW INNOVATIONS IN PET/CT FOR RESPIRATORY MOTION CORRECTION

Joseph Gabriel Meier, B.S.

Advisory Professor: Osama R. Mawlawi, Ph.D.

In oncological imaging, Positron Emission Tomography/Computed Tomography (PET/CT) is a vital tool used for staging and treatment response assessment of patients due to its ability to visualize and accurately quantify the bio-distribution of radiolabeled pharmaceuticals. However, due to the long acquisition times, respiratory motion blur is unavoidable in PET images especially in the lower lung and upper abdomen. This leads to reductions in measured radiotracer concentration and lesion detectability all of which can potentially result in incorrect management of patients. Multiple methods exist to correct for respiratory motion but are rarely used in the routine clinical setting because of: 1) increased image noise due to the rejection of motion blurred data; 2) burdensome workflows which require setup and troubleshooting of external hardware needed to track patient breathing; 3) and ineffective respiratory motion correction due to irregular patient breathing potentially caused by the abrupt bed transitions during step and shoot (SS) whole body PET acquisition.

Our goal of this Ph.D. dissertation is to address these three issues by evaluating 1) a pre-commercial version of a vendor designed elastic motion correction (EMC) algorithm which uses all of the acquired PET data resulting in reduced image noise; 2) a pre-commercial version of a vendor designed data driven gating (DDG) algorithm, which determines the respiratory waveform from the PET data alone, thereby removing the need for and challenges of external hardware; 3) the effect of using continuous bed motion (CBM) as compared to SS as a means to minimize the irregularity of patient breathing.

The results of these evaluations showed that the EMC algorithm performed similarly to conventional respiratory motion correction techniques with respect to radiotracer quantification, however, due to using all of the acquired PET data, the EMC algorithm showed improved performance resulting in the lowest amount of image noise, improved contrast to noise ratio, and had the highest overall image quality scores as assessed by independent observers. Evaluation of the CBM DDG algorithm showed that in comparison to an external device, the measured respiratory waveforms, radiotracer quantification, and assessment of the presence of respiratory motion blur were similar, demonstrating that the CBM DDG algorithm holds promise as a replacement to external hardware devices currently needed to measure respiratory waveforms and hence could potentially simplify the data acquisition workflow. Finally, we found no statistically significant differences between the CBM and SS PET acquisition modes with respect to the regularity of respiratory waveforms, radiotracer quantification, contrast to noise ratio and perceptions of respiratory motion blur.

In conclusion, although no reductions of irregular breathing were found between CBM and SS, improvements in image quality through the use of EMC and reductions of workflow complexity through the use of DDG will hopefully facilitate the routine adoption of respiratory motion correction in PET/CT.

Table of Contents

DEDICATION.....	III
ACKNOWLEDGEMENTS	IV
ABSTRACT.....	VI
TABLE OF CONTENTS	VIII
LIST OF ILLUSTRATIONS.....	XI
LIST OF TABLES	XIV
LIST OF ABBREVIATIONS	XV
CHAPTER 1: INTRODUCTION.....	1
1.1 BACKGROUND	1
1.1.1 INTRODUCTION TO PET	1
1.2 SIGNIFICANCE AND INNOVATION	6
1.2.1 SIGNIFICANCE	6
1.2.2 INNOVATION	12
1.3 CENTRAL HYPOTHESIS AND SPECIFIC AIMS.....	14
1.3.1 CENTRAL HYPOTHESIS	14
1.3.2 SPECIFIC Aim 1	14
1.3.3 SPECIFIC Aim 2	14
1.3.4 SPECIFIC Aim 3	15
1.4 DISSERTATION ORGANIZATION.....	15
CHAPTER 2: COMPARISON OF THE PERFORMANCE OF A PRE-COMMERCIAL VERSION OF A VENDOR DESIGNED ELASTIC MOTION CORRECTION ALGORITHM IN COMPARISON TO CONVENTIONAL MOTION CORRECTION TECHNIQUES.....	16
2.1 ABSTRACT	16
2.2 INTRODUCTION	17
2.3 MATERIALS AND METHODS	20
2.3.1 RECONSTRUCTION ALGORITHMS	20
2.3.2 PHANTOM EVALUATION	22
2.3.3 PATIENT EVALUATION	25

2.3.4	PET/CT ACQUISITION AND IMAGE RECONSTRUCTION	25
2.3.5	IMAGE ANALYSIS.....	26
2.3.6	IMAGE QUALITY ASSESSMENT	26
2.3.7	STATISTICAL ANALYSIS	26
2.4	RESULTS	27
2.4.1	PHANTOM EVALUATION.....	27
2.4.2	PATIENT TUMOR QUANTIFICATION.....	29
2.4.3	SUBJECTIVE IMAGE QUALITY	32
2.5	DISCUSSION	34
2.6	CONCLUSION	37
2.7	DISCLOSURE	37
2.8	ACKNOWLEDGEMENTS	37
	CHAPTER 3: EVALUATION OF THE PERFORMANCE OF A PRE-COMMERCIAL VERSION OF A VENDOR DESIGNED CBM_DDГ TECHNIQUE IN COMPARISON TO A CONVENTIONAL EXTERNAL DEVICE	38
3.1	ABSTRACT	38
3.2	INTRODUCTION	40
3.3	MATERIALS AND METHODS	42
3.3.1	CONTINUOUS BED MOTION DATA DRIVEN GATING ALGORITHM	42
3.3.2	PHANTOM EVALUATION.....	46
3.3.3	PATIENTS	47
3.3.4	PET SCAN AND IMAGE RECONSTRUCTION.....	48
3.3.5	PATIENT WAVEFORM COMPARISON AND IMAGE QUANTIFICATION	48
3.3.6	PHYSICIAN ASSESSMENT OF IMAGE QUALITY	49
3.3.7	STATISTICAL ANALYSIS	50
3.4	RESULTS	50
3.4.1	PHANTOM EVALUATION.....	50
3.4.2	PATIENT WAVEFORM COMPARISON AND IMAGE QUANTIFICATION	54
3.4.3	PHYSICIAN VISUAL ASSESSMENT.....	57
3.5	DISCUSSION	57
3.6	CONCLUSION	64

CHAPTER 4: EVALUATION OF THE IMPACT OF STEP AND SHOOT AND CONTINUOUS BED MOTION PET ACQUISITION MODES ON RESPIRATORY MOTION CORRECTION.....	65
4.1 ABSTRACT	65
4.2 INTRODUCTION.....	66
4.3 METHODS	68
4.3.1 PATIENTS	68
4.3.2 PET/CT ACQUISITION AND IMAGE RECONSTRUCTION	69
4.3.3 RESPIRATORY WAVEFORM ANALYSIS	70
4.3.4 RESPIRATORY MOTION QUANTIFICATION AND IMAGE QUALITY ASSESSMENT	73
4.3.5 PHYSICIAN ASSESSMENT OF IMAGE QUALITY	73
4.3.6 STATISTICAL ANALYSIS	76
4.4 RESULTS	76
4.4.1 RESPIRATORY WAVEFORM ANALYSIS	76
4.4.2 RESPIRATORY MOTION QUANTIFICATION AND IMAGE QUALITY	80
4.4.4 PHYSICIAN ASSESSMENT OF IMAGE QUALITY	81
4.5 DISCUSSION	82
4.6 CONCLUSION	88
4.7 ACKNOWLEDGEMENTS	88
CHAPTER 5: DISCUSSION	89
5.1 SPECIFIC AIM 1	89
5.2 SPECIFIC AIM 2	91
5.3 SPECIFIC AIM 3	92
5.4 FUTURE APPLICATIONS	94
5.5 CONCLUSION	98
APPENDIX.....	99
6.1 EMOCO SUPPLEMENTAL MATERIALS	99
BIBLIOGRAPHY	102
VITA.....	114

List of Illustrations

Figure 1-1. Diagram of positron annihilation with an electron and detection of the 2 x 511 keV photons between detector pairs(left). Discovery MI 5-ring(25 cm axial) PET detector (right). ...	3
Figure 1-2. Examples of PET image reconstruction to demonstrate the differences in image quality(noise) and sphere detectability. Spheres range from 10 mm to 28 mm in diameter. Filtered backprojection(top row). Iterative reconstruction(bottom row). Non-Time of Flight (left column). With Time of Flight (right column).	5
Figure 1-3 A 63 year old male with a history of heavy smoking underwent PET/CT with and without motion correction for characterizing a 12 mm diameter right lung nodule on CT (B: black arrow). A) Maximum intensity projection image. C) Fused PET/CT. With no motion correction(D) very faint uptake was visible (black arrow; SUVmax 1.5) resulting in a negative score for disease. With motion correction(E) the radiotracer concentration was increased significantly (black arrow; SUVmax 2.8) resulting in a positive score for disease. Based on the motion corrected images, the patient underwent surgery and histology classified the tumor as an adenocarcinoma. Republished with permission (License ID =4687661090461 from www.copyright.com) from: Guerra L, De Ponti E, Elisei F, Bettinardi V, Landoni C, Picchio M, Gilardi MC, Versari A, Fioroni F, Dziuk M, Koza M, Ahond-Vionnet R, Collin B, Messa C, Carla Gilardi M, Versari A, Fioroni F, Dziuk M, Koza M, Ahond-Vionnet R, Collin B, Messa C, Guerra L, Elisei F, Messa C, De Ponti E, Bettinardi V, Landoni C, Picchio M, Gilardi MC, Versari A, Fioroni F, Dziuk M, Koza M, Ahond-Vionnet R, Collin B. Respiratory gated PET/CT in a European multicentre retrospective study: added diagnostic value in detection and characterization of lung lesions. Eur J Nucl Med Mol Imaging. 2012;39(9):1381-1390. doi:10.1007/s00259-012-2148-2.....	7

Figure 1-4 Respiratory motion correction methodologies which utilize fractions of the data.	
Phase Based Gating(top) and Amplitude Based End of Expiration(bottom).	9
Figure 1-5 Phantom images reconstructed with decreasing fractions of data	9
Figure 1-6 Examples of external hardware used to obtain a respiratory waveform and the steps of the setup process which sometimes have to be repeated. Varian patient setup courtesy of Dr. Tinsu Pan at MD Anderson Cancer Center, Houston, TX.....	10
Figure 2-1 Workflow of the EMDB Algorithm.....	21
Figure 2-2 Phantom experimental setup and resultant images	24
Figure 2-3 Phantom experimental measurements. (A and B) SUVmax normalized to SWB (RSmax) (A) and SUVpeak normalized to SWB (RSpeak) (B) variation caused by to sphere displacement. (C) SUV SD in background across all reconstructions. (D) CNR ratio normalized to SWB (RCNR) variation due to sphere displacement. Data are for the average of all spheres.	28
Figure 2-4 Patient Quantification Results. SUVmax and SUVpeak for 65 lesions (A), SUV SD for lung and liver tissue (B), and CNR for lung and liver lesions (C). *P < 0.01.	30
Figure 2-5 Example patient images. (Top) Maximum intensity projection images of all reconstructions. (Middle) Coronal plane view of right lung tumors. (Bottom) Zoomed view of middle row.	31
Figure 2-6 Mean image quality score for different reconstructions. Error bars represent 1 SD. *P < 0.01.	33
Figure 3-1 Overview of the CBM_DDG workflow.....	45
Figure 3-2 Segment of the respiratory waveform when the scanner was centered over the phantom spheres.....	51
Figure 3-3 Maximum intensity projection images of the phantom for the acquisitions with varying motion amplitudes and reconstructions used in this study: ANZ_EMDB(top row) and	

DDG_EMDB(middle row). Subtraction images (ANZ_EMDB – DDG_EMDB) of a coronal slice along with a corresponding SUV scale (bottom row).	52
Figure 3-4 Phantom Acquisition Measurements: A)DDG_EMDB SUVmax normalized to ANZ_EMDB SUVmax for each acquisition (RSmax), B)DDG_EMDB SUVpeak normalized to ANZ_EMDB SUVpeak for each acquisition(RSpeak). Error bars represent +/- 1 SD.	53
Figure 3-5 Example patient respiratory waveforms from a) CBM_DDG and Anzai along with a plot of a 30 s sliding window correlation coefficient and anatomical landmark identifiers. b) ANZ_EMDB and DDG_EMDB reconstructions along with SUVmax measurements of a lower liver lesion show little difference in motion blur in the images and show similar SUVmax quantification.	55
Figure 3-6 Box-plots of patient F18-FDG foci (lung/liver/spleen tumor, gastric, and kidney medulla) for a) SUVmax and b) SUVpeak for both the ANZ_EMDB and DDG_EMDB reconstructions.	56
Figure 4-1 An example patient respiratory waveform at bed position four along with the four different analysis techniques.....	72
Figure 4-2 Patient images of the (a) non-motion corrected SWB and (b) the motion corrected EMDB reconstructions for physician interpretation. The images are from a CBM acquisition.	75
Figure 4-3 Bar Plot of the frequencies of the motion blur score differences for the CBM and SS motion blur visual analysis.	81
Figure 4-4 Examples of repetitive (top) and non-repetitive(bottom) respiratory waveforms and respective analyses.....	84
Figure 6-1 Top view of the phantom tank.	99
Figure 6-2 Setup of motion phantom. Surrogate motion platform and set up of Anzai belt on the platform (red arrow).....	101

List of Tables

Table 4-1 Comparison of the four different analysis methods between CBM and SS for the entire waveform duration for bed position four.....	77
Table 4-2 Waveform analysis of the first and last 30 s of bed position four.....	79
Table 4-3 Results for the motion quantification measurements. The scores are summarized as the median [interquartile].....	80

List of Abbreviations

ANZ – Anzai External Respiratory Waveform Measurement Device

ANZ_EMDB - EMDB reconstruction using the Anzai respiratory waveform

BMI – Body Mass Index

CIRS - Computerized Imaging Reference Systems

CBM – Continuous Bed Motion PET Acquisition Mode

CBM_DDГ – Continuous Bed Motion Data Driven Gating

CNR – Contrast to Noise Ratio

COV – Coefficient of Variation

cps – Counts Per Second

CT - Computed Tomography

DDG – Data Driven Gating

DDG_EMDB - EMDB reconstruction using the DDG respiratory waveform

EMC – Elastic Motion Correction

EMBD – Elastic Motion Deblurring Respiratory Motion Correction Algorithm

FWHM – Full Width at Half Maximum

¹⁸F-FDG - 2-deoxy-2-(¹⁸F)fluoro-D-glucose

HDC – HDChest Respiratory Motion Correction Algorithm

ICC – Intraclass Correlation Coefficient

MBq – megabecquerel

MDACC IRB – MD Anderson Cancer Center Institutional Review Board

MPOF – Mass Preservation Optical Flow

MRI – Magnetic Resonance Imaging

NIH – National Institutes of Health

OG – HDChest Optimal Gate

PBG – Phase Based Gating Respiratory Motion Correction Algorithm

PBG_{ave} – average of all PBG bins

PBG_{max} – maximum of all PBG bins

PET - Positron Emission Tomography

PET/CT – Hybrid Positron Emission Tomography Computed Tomography

RCA – Respiratory Cycle Amplitude

RCD – Respiratory Cycle Duration

RCNR – CNR (of motion correction method) normalized to SWB CNR

RPM – Real-time Position Management

RS_{max} – SUV_{max} (of motion correction method) normalized to SWB SUV_{max}

RS_{peak} – SUV_{peak} (of motion correction method) normalized to SWB SUV_{peak}

RSP – Respiratory Frequency Signal Prominence

SD – Standard Deviation

SPECT- Single Photon Emission Computed Tomography

SS – Step and Shoot PET Acquisition Mode

SUV – Standardized Uptake Value

SUV_{mean} - mean Standardized Uptake Value of a region of interest

SUV_{max} – maximum Standardized Uptake Value of a region of interest

SUV_{max,sp} - SUV_{max} of sphere

SUV_{max,bg} - SUV_{max} of background

SUV_{peak} – peak Standardized Uptake Value of a region of interest

SWB – Static Whole Body – reconstruction with no motion correction

WF- respiratory waveforms

Chapter 1: Introduction

This work aims to enable routine correction for the uncertainties in quantification and visualization of radiotracer activity concentration caused by respiratory motion blur of tumors in positron emission tomography (PET) images. These uncertainties can lead to decreased confidence in diagnosis or treatment response assessment in cancer imaging, as well as failure to find tumors of low detectability, all of which could result in incorrect management of patients.

1.1 Background

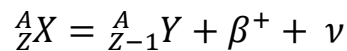
1.1.1 Introduction to PET

Non-invasive medical imaging originated from the discovery of X-rays by Wilhelm Conrad Röntgen in 1895 and the subsequent observation that these X-rays penetrated materials such as tissue, bone, or metal to varying degrees[1]. This laid the foundation for anatomical imaging with ionizing radiation for radiography, fluoroscopy, mammography, angiography, and x-ray computed tomography(CT). Further advances in anatomical imaging led to harnessing non-ionizing radiation for Ultrasound and Magnetic Resonance Imaging(MRI). Nuclear medicine imaging on the other hand is primarily a functional imaging modality and is capable of imaging a vast array of biological processes with an ever-expanding arsenal of radiotracers. The advantage that nuclear medicine imaging has over every imaging modality is its unparalleled lower limits of detection in vivo. MRI typically has a lower limit of detection in the millimolar concentration range ($\sim 6 \times 10^{17}$ molecules per mL tissue range), while nuclear medicine studies routinely detect in the nanomolar to picomolar range ($\sim 6 \times 10^{11}$ to 6×10^8 molecules per mL tissue range)[2]. Consequentially, nuclear medicine can image biological processes, such as glucose metabolism, myocardial perfusion, and indicators of Alzheimer's disease such as tau

protein deposition, with trace amounts of radionuclides, preventing perturbation of the underlying biological processes being imaged.

Accurate quantification and visualization of the biodistribution of these radionuclides in nuclear medicine requires Single Photon Emission Computed Tomography (SPECT) or PET systems. SPECT detects single photons and so must use physical collimation to determine the direction from which the photon was emitted. In contrast, for PET imaging two photons are produced for each positron that is emitted from the radionuclide, and so physical collimation is not required, resulting in improved performance over SPECT[3]. In a comparison of the Siemens mCT Flow PET to the Siemens Symbia Intevo SPECT, the measured sensitivity for PET was 9632 cps MBq⁻¹ when using Flourine-18 (F-18) and for SPECT was 119 cps MBq⁻¹ when using Technetium-99m, showing that PET sensitivity is ~2 orders of magnitude higher[4]. This increased sensitivity greatly improves image quality which can be traded for decreased injected activities or shorter acquisition times. This study also showed that PET has better resolution at the center of the field of view as measured by the full width at half maximum (FWHM) of 4.3 mm when using F-18, compared to 13.1 mm for SPECT when using Tc-99m.

Central to the improved performance of PET is harnessing positron emission which occurs in nuclei with a low neutron to proton ratio by conversion of a proton to a neutron via positron(β^+) emission:



The excess transition energy from the nucleus is shared in the form of kinetic energy between the β^+ and the neutrino(ν). The β^+ deposits its kinetic energy through coulombic interactions as it travels from the nucleus. The mean energy and range of different positron emitters impacts the resultant image resolution[5]. When the β^+ has slowed down sufficiently, it combines with an electron and since the β^+ is the antimatter counterpart of the electron, the particles annihilate

and the mass of the electron and β^+ is converted into energy in the form of two 511 keV photons. If annihilation occurs when the particles are at rest, the photons will be emitted 180 degrees with respect to each other to conserve momentum. However, the annihilation usually occurs before the particles have come to rest and so the photons are not emitted at 180 degrees apart. These two 511 keV photons that are emitted from each annihilation enable PET cameras to forgo utilization of physical collimation resulting in the substantial improvements in sensitivity and resolution in comparison to SPECT.

For PET scanners, electronic collimation is used to locate the annihilation events. Clinical PET scanners such as the 5 ring Discovery MI[6] seen in figure 1.1 are composed of a cylindrical array of PET detectors.

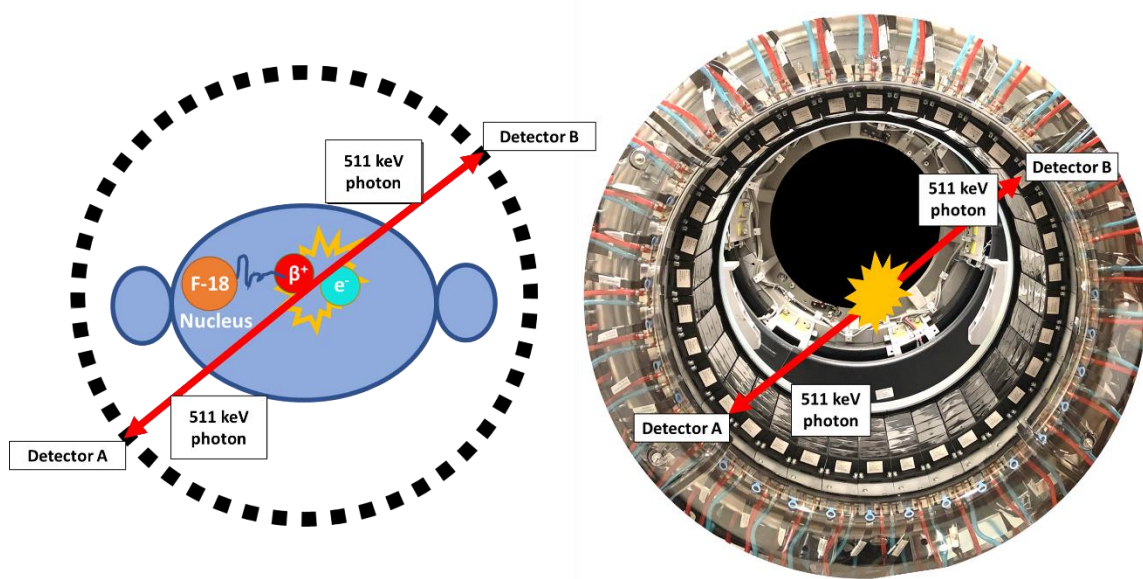


Figure 1-1. Diagram of positron annihilation with an electron and detection of the 2 x 511 keV photons between detector pairs(left). Discovery MI 5-ring(25 cm axial) PET detector (right).

Each PET detector operates in coincidence mode with the other PET detectors. In figure 1-1, the two annihilation photons interact with detector A and detector B respectively, and in order for these two interactions to be registered as a coincidence event, they must fall within a coincidence

timing window (for example: Siemens mCT Flow: 4.07 ns [7]), and an energy window (for example: Siemens mCT Flow: 435 – 650 keV). The line connecting each detector pair is known as a line of response. For each detected coincidence event, the time the events were detected, and which detector pair detected the coincidence event are recorded. Advancements in the detector scintillators, photomultipliers, and electronic circuitry has substantially improved the timing resolution of scanners enabling time of flight imaging. The best clinically available timing resolution is 210 ps (Siemens Biograph Vision PET [8]) leading to an uncertainty in coincidence event localization of 3.15 cm, as opposed to assigning the coincidence event location to the entire line of response upwards of 80 cm in length.

To create images of the biodistribution of the PET radiotracers, the recorded lines of response are reconstructed into image space. Figure 1-2 shows an example reconstruction of a phantom with varying sphere sizes using filtered backprojection and Iterative Reconstruction when incorporating or not incorporating time of flight information. Iterative Reconstruction, which is the currently used clinical method, dramatically reduces image noise in comparison to filtered back projection. Utilization of time of flight information improves the visibility of the spheres for both reconstructions, most notably in the smallest spheres.

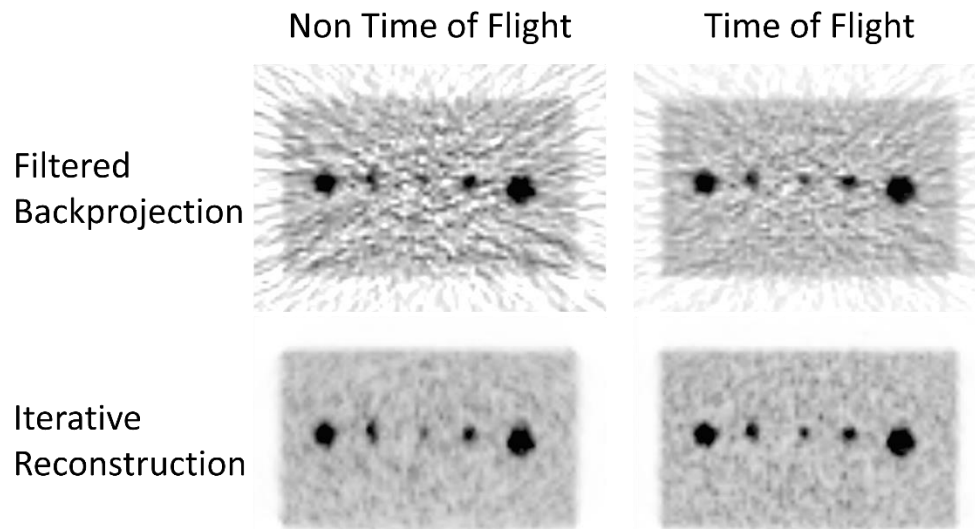


Figure 1-2. Examples of PET image reconstruction to demonstrate the differences in image quality(noise) and sphere detectability. Spheres range from 10 mm to 28 mm in diameter. Filtered backprojection(top row). Iterative reconstruction(bottom row). Non-Time of Flight (left column). With Time of Flight (right column).

In order to achieve accurate image quantification of the radiopharmaceutical concentration in patients, as well as reproducible measurements from scan to scan, there are many potential inaccuracies that must be accounted for[9]. These come from PET scanner related issues to correct the acquired PET data such as scatter, dead time, randoms, partial volume effects due to scanner resolution, well counter calibration, and detector normalization. For examinations performed with ^{18}F -FDG many factors must be monitored in patients such as blood sugar level, quality of injection, correct assay and recording of pre and post injection activities and correct entering of patient weight and assayed activities. Finally, there is patient motion that comes in three forms: bulk, cardiac, and respiratory motion. All of these motions can lead to degraded image resolution, underestimated activity concentration, and misalignment with anatomical images such as CT or MRI[10]. Unless respiratory motion is corrected for, improvements in PET scanner resolution will never be realized in the thorax and abdomen where respiratory motion is most severe[11].

1.2 Significance and Innovation

1.2.1 Significance

PET produces images which represent the biodistribution of administered radiopharmaceuticals. This capability has had a tremendous impact on the management of cancer by imaging glucose metabolism, cellular proliferation, hypoxia, and receptor density (Farwell 2014). The quantitative nature of PET images allows the radiologist to determine the extent of radiopharmaceutical accumulation in areas of interest. In this regard, PET plays a critical role in the staging and assessment of treatment response[12]. However, PET acquisitions typically last 2-3 minutes per bed position, which can result in degraded image quality and quantification due to respiratory motion blur particularly for tumors located in the lower thorax and upper abdomen which are affected the most by this motion. Based on a review article, the mean (range) superior-inferior excursion in mm due to respiratory motion for the lung was 10.3 (1 - 31.9), for the diaphragm was 14.9 (2.6 – 38.2) and for the liver was 12.3 (4.9 – 30.4)[13]. Respiratory motion results in underestimated measurements of activity concentration, overestimation of lesion volume, decreases in lesion detectability and mis-alignments with anatomical imaging, all of which could negatively impact patient management[14–16]. Many methodologies have been developed to overcome the challenges of respiratory motion correction, and their positive impact has been demonstrated[17]. One such study performed an investigation as to whether respiratory motion correction of PET/CT studies helps to overcome these challenges and improve detection and characterization of lung lesions[15]. This study showed improvements in quantification as measured by the maximum Standardized Uptake Value (SUVmax) which increased on average by 30.8 %. The most impactful finding was the visual analysis which showed that the number of equivocal lesions when reading the PET images with no motion correction was reduced from 50/206(24.3%) to 9/206(4.4%) when

motion correction was applied. Reducing equivocal findings improves the confidence that physicians have in characterizing lesions. In addition, this study showed cases, for example as seen in Figure 1-3, where the diagnosis of a lesion changed from negative to positive with application of respiratory motion correction. This resulted in a change of patient management to have surgery to remove what was found to be an adenocarcinoma.

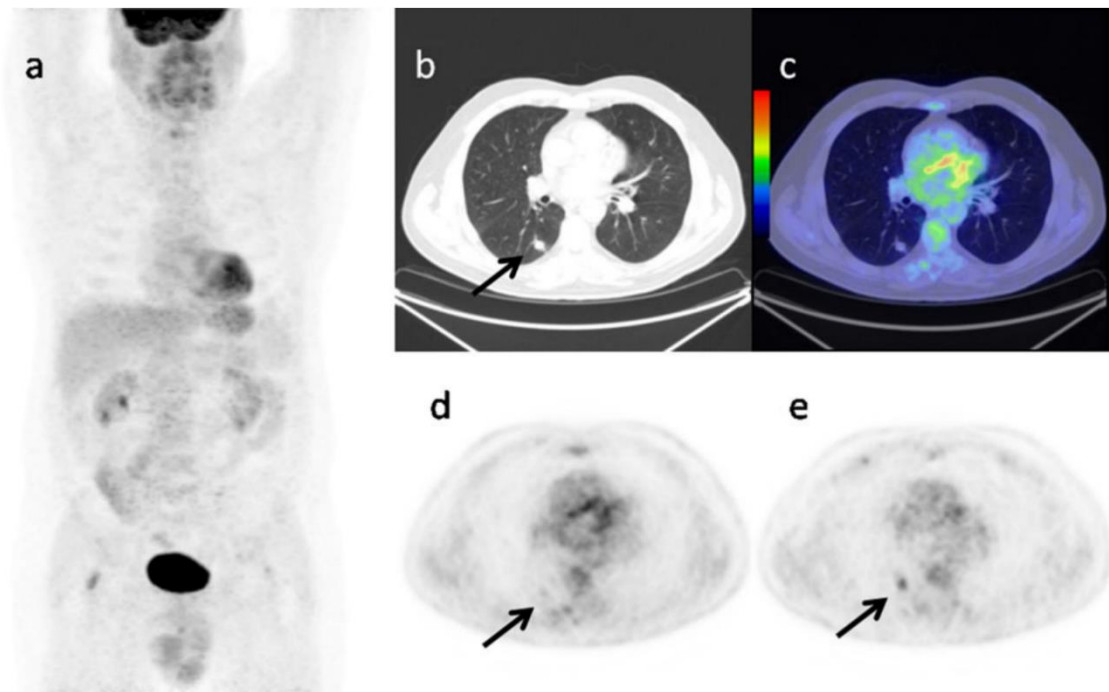


Figure 1-3 A 63 year old male with a history of heavy smoking underwent PET/CT with and without motion correction for characterizing a 12 mm diameter right lung nodule on CT (B: black arrow). A) Maximum intensity projection image. C) Fused PET/CT. With no motion correction (D) very faint uptake was visible (black arrow; SUVmax 1.5) resulting in a negative score for disease. With motion correction (E) the radiotracer concentration was increased significantly (black arrow; SUVmax 2.8) resulting in a positive score for disease. Based on the motion corrected images, the patient underwent surgery and histology classified the tumor as an adenocarcinoma. Republished with permission (License ID =4687661090461 from www.copyright.com) from: Guerra L, De Ponti E, Elisei F, Bettinardi V, Landoni C, Picchio M, Gilardi MC, Versari A, Fioroni F, Dziuk M, Koza M, Ahond-Vionnet R, Collin B, Messa C, Carla Gilardi M, Versari A, Fioroni F, Dziuk M, Koza M, Ahond-Vionnet R, Collin B, Messa C, Guerra L, Elisei F, Messa C, De Ponti E, Bettinardi V, Landoni C, Picchio M, Gilardi MC, Versari A, Fioroni F, Dziuk M, Koza M, Ahond-Vionnet R, Collin B. Respiratory gated PET/CT in a European multicentre retrospective study: added diagnostic value in detection and characterization of lung lesions. *Eur J Nucl Med Mol Imaging*. 2012;39(9):1381-1390. doi:10.1007/s00259-012-2148-2

In 2018, an estimated 2 million oncologic PET/CT examinations were performed in the United States with an expected annual growth rate of 7% [18]. In a study which acquired 847 PET scans, 25% of the patients had lung or liver tumor(s)[19], leading to an estimation that 0.5 million patients who had PET scans in 2018 had lung or liver tumors. In cancer imaging, lung and liver tumors are the most likely to be impacted by respiratory motion. Even though the benefits of respiratory motion correction have been demonstrated and while every PET/CT scan could have been performed with respiratory motion correction, virtually none to a very small number were performed with this correction[17]. This dissertation addresses three major obstacles that currently exist which prevent the adoption of routine use of respiratory motion correction methods. These obstacles are: 1) poor resultant image quality of motion corrected images due to increased image noise, 2) increased workflow complexity due to the need to use external breathing tracking devices, and 3) irregular patient breathing which limits the success of motion correction techniques.

Typical clinical PET images use all the data that is acquired without application of motion correction, resulting in images with varying severity of respiratory motion blur. Conventional respiratory motion corrected images have poor image quality, because smaller percentages of the data which contain less amounts of respiratory motion are used for image reconstruction resulting in increased image noise. The first strategy known as phase-based gating (PBG), divides each respiratory cycle into $1/n$ fractions of data or bins, as seen in figure 1-4. As the number of bins increase, the motion reduction improves, but the image noise increases and this tradeoff must be considered[20]. Based on the observation that patients spend more time at the end of expiration, strategies have been developed to select this more abundant and relatively motion free data based on either a phase[21] or amplitude[22] analysis of the respiratory waveform.

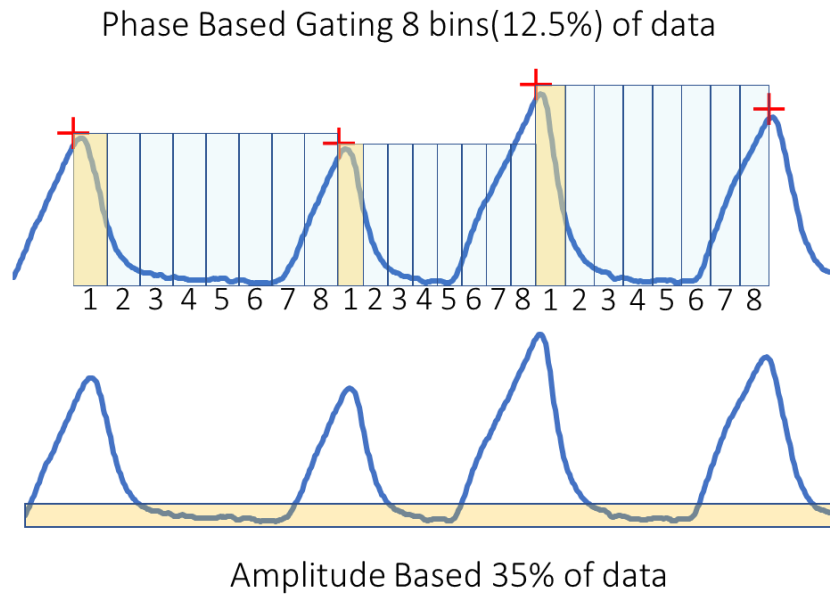


Figure 1-4 Respiratory motion correction methodologies which utilize fractions of the data. Phase Based Gating(top) and Amplitude Based End of Expiration(bottom).

As seen in figure 1-5, the image noise increases severely when using decreasing fractions of data from 100% down to 12.5%, as could be used with conventional motion correction.

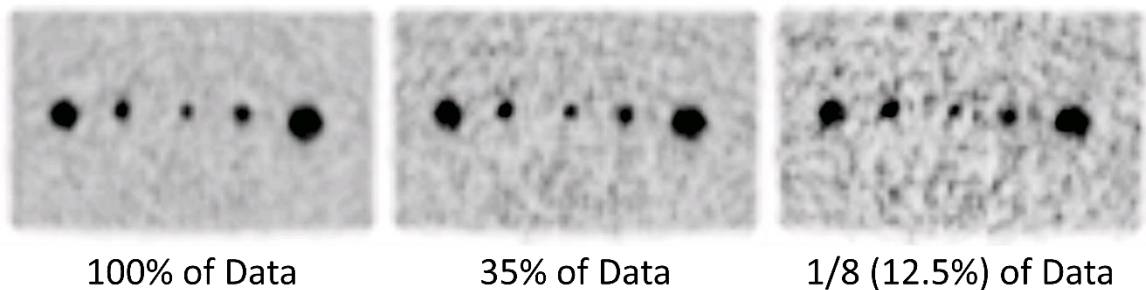


Figure 1-5 Phantom images reconstructed with decreasing fractions of data

To counteract this resultant poor image quality, the acquisition times must be increased accordingly. This is undesirable in routine clinical practice and results in decreased patient

throughput, increased patient discomfort, and increased probability of bulk patient motion of the body which results in gross misalignment between PET and CT data.

The second obstacle to routine utilization of respiratory motion correction is that it is necessary to use external devices to measure respiratory waveforms. The two systems most commonly utilized clinically are the Varian realtime positioning monitor(Varian Medical Systems, Palo Alto, CA, USA) and the pressure sensitive Anzai Belt(Anzai Medical, Tokyo, Japan). These systems require setup of either a reflective box or a pressure sensitive belt to acquire a respiratory waveform as seen in figure 1-6.

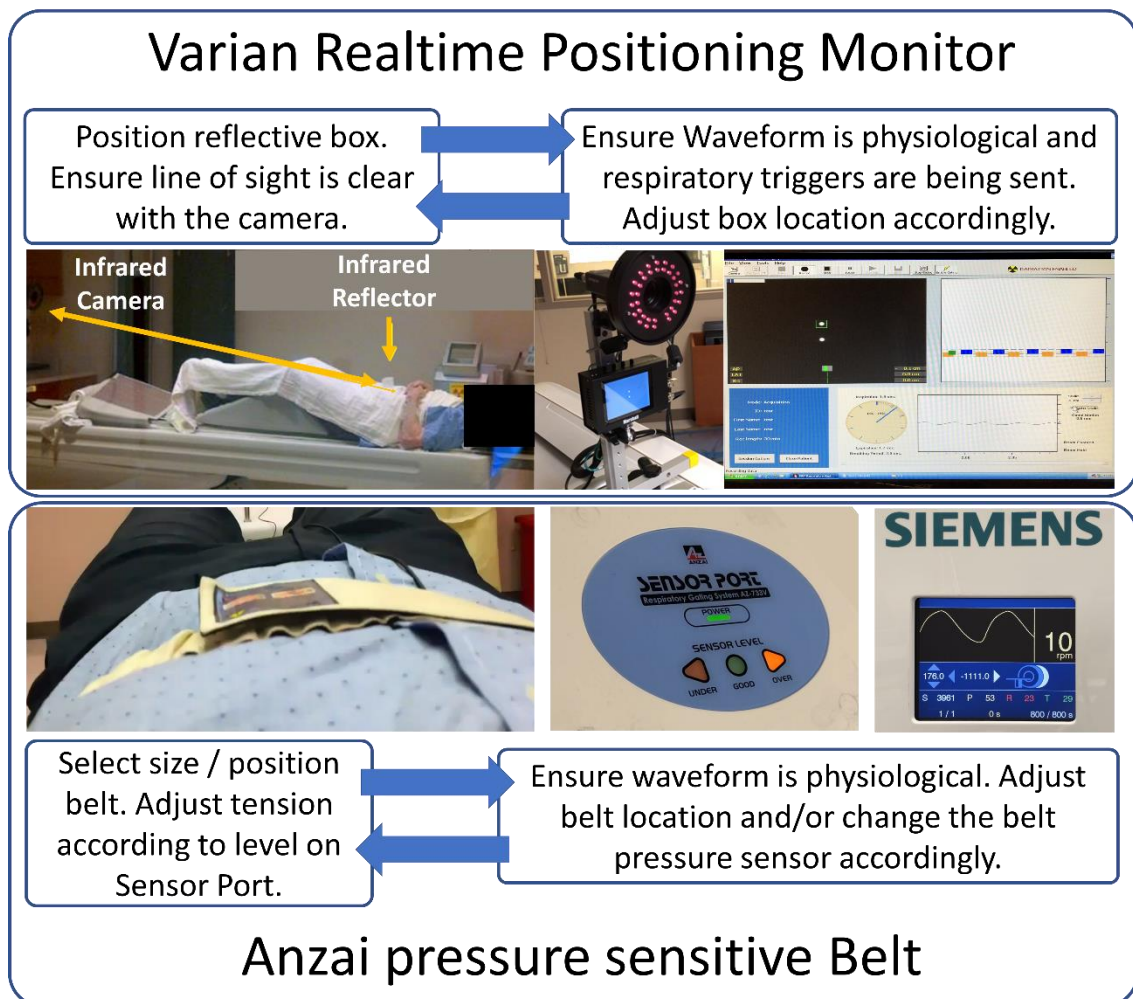


Figure 1-6 Examples of external hardware used to obtain a respiratory waveform and the steps of the setup process which sometimes have to be repeated. Varian patient setup courtesy of Dr. Tinsu Pan at MD Anderson Cancer Center, Houston, TX.

As seen in figure 1-6, the setup, adjustment, and troubleshooting of these devices and requisite software adds additional time to the examination and increases the overall examination complexity. The quality of these respiratory waveforms is highly dependent on the setup of the devices, and so reproducibility of the respiratory waveform measurement is of concern with respect to the between user variation of device positioning and the varying habitus of each patient. In addition, in the diagnostic setting, setup is much more challenging as patients prefer to wear blankets during their scan which can degrade the mechanical coupling between the reflective box or the belt with the patient surface, resulting in degraded respiratory waveforms. Even with proper setup at the beginning of the patient, these devices are prone to fail or produce unusable respiratory waveforms, rendering motion correction of the PET images not possible.

Irregular patient breathing is the third and final obstacle to respiratory motion correction that is considered in this dissertation. Irregular breathing has been shown to reduce the efficacy of PET/CT respiratory motion correction techniques by degrading image quantification and lesion detectability [23,24], even to the point that the motion corrected images become uninterpretable. Irregular breathing has a high incidence as shown in a study which performed an analysis of 1295 respiratory waveforms and showed that 20% of patients have highly irregular breathing, 20% breathe with some irregularities, and that 60% had regular breathing[25]. Heightened anxiety can have a profound impact on breathing [26], potentially leading to irregular breathing. Studies have shown that during a PET/CT imaging session, that patients experience anxiety for a multitude of reasons[27], and it is possible that reducing the anxiety that a patient experiences during the examination could reduce the incidence of irregular patient breathing thereby improving respiratory motion correction.

Given the increasing reliance of radiologists on PET image quality and quantification for managing oncologic patients, coupled with the limitations of current respiratory motion correction techniques, there is an urgent and unmet need to validate alternate methods that have

been recently developed to overcome these challenges. Surmounting these obstacles will facilitate advancement towards the routine use of respiratory motion correction in PET imaging thereby improving image interpretation which ultimately will help patient management.

1.2.2 Innovation

In this work, novel solutions created by Siemens Healthineers are validated to determine if they can address each of these three challenges facing the routine use of respiratory motion correction in PET imaging. To overcome increased noise in motion corrected images, elastic motion correction (EMC) techniques have been developed to use all the acquired PET data [28], rather than only a fraction of the data as in current approaches for respiratory motion correction. The resultant EMC images show remarkably less amounts of image noise while correcting for respiratory motion blur. Elastic motion correction with image deblurring (EMDB)[29] is a novel EMC technique that was developed to decrease the reconstruction time required for typical EMC methodologies, especially for joint correction of cardiac and respiratory motion. This work is the first to evaluate the impact on image quality and quantification of the EMDB algorithm in comparison to conventional respiratory motion techniques in a large and comprehensive clinical evaluation which is necessary to determine the efficacy of routine utilization of the EMDB algorithm.

To overcome the burdens of utilizing external hardware to measure the patient respiratory waveform, Data Driven Gating (DDG) techniques have been developed to determine the patient's respiratory waveform directly from the acquired PET data. For organs and tumors that have radiotracer uptake and that are under the influence of respiratory motion, a respiratory waveform can be determined from the motion information contained in the acquired PET data through a multitude of methodologies. This eliminates the need for external devices to obtain the respiratory waveform and results in reduced PET workflow complexity and examination

duration [30]. Although success of the DDG algorithms has been demonstrated with PET data acquired in step and shoot(SS) mode, no DDG technique has been developed for PET data acquired in continuous bed motion (CBM)[31]. This work will validate the first CBM_DDG technique, which was recently created by Siemens Healthineers[32], and will show its ability to replace external devices to record patient respiratory waveforms thereby reducing workflow complexity.

The development of CBM as opposed to SS to continuously translate the patient into the scanner during a PET imaging session has been shown to be preferred by patients due to the smooth movement of CBM (Schatka 2016). Due to this, CBM could potentially reduce breathing irregularities caused by heightened patient anxiety by providing a more comfortable examination experience. However, the effect that CBM has on patient breathing regularity and consequentially on motion corrected PET image quality and quantification has not been investigated. This work will be the first to evaluate whether CBM can improve breathing regularity and consequentially improve motion corrected PET image quality and quantification. This will provide necessary insight into which imaging mode (SS versus CBM) should be used for the routine application of respiratory motion correction.

This dissertation will validate whether these three proposed solutions can overcome three respective challenges that currently impede the routine use of respiratory motion correction in PET imaging.

1.3 Central Hypothesis and Specific Aims

1.3.1 Central Hypothesis

The central hypothesis is that the application of EMC, DDG, and CBM for respiratory motion correction in PET imaging will result in improved image quantification and quality, decreased workflow complexity, and reduced patient breathing irregularity during PET/CT imaging.

This central hypothesis will be tested through the following three specific aims, each specific aim containing multiple studies:

1.3.2 Specific Aim 1

SA 1. Compare the performance of a pre-commercial version of a vendor designed EMC algorithm in comparison to conventional motion correction techniques.

Working Hypothesis: due to utilization of all the acquired PET data during image reconstruction, the EMDB algorithm will have superior performance characteristics when compared to conventional motion correction methodologies.

- **Study 1.1:** Evaluation of EMDB using a phantom scan
- **Study 1.2:** Objective Evaluation with Patient Data
- **Study 1.3:** Subjective Image Quality Assessment

1.3.3 Specific Aim 2

SA 2. Evaluate the performance of a pre-commercial version of a vendor designed CBM_DDГ technique in comparison to a conventional external device.

Working Hypothesis: CBM_DDГ motion corrected images will be non-inferior to hardware-based motion corrected images.

- **Study 2.1:** Waveform Evaluation

- **Study 2.2:** Quantitative Assessment of Patient Studies
- **Study 2.3:** Qualitative Image Assessment of Patient Studies

1.3.4 Specific Aim 3

SA 3. Evaluate the impact of step and shoot (SS) and CBM PET acquisition modes on respiratory motion correction.

Working Hypothesis: CBM acquisition will reduce breathing irregularities in comparison to SS acquisition and therefore, the motion corrected CBM images will have superior motion reduction in comparison to the SS images.

- **Study 3.1:** Determine the impact of SS and CBM on patient respiratory waveforms
- **Study 3.2:** Determine the quantitative impact of SS and CBM on respiratory motion corrected images
- **Study 3.3:** Physician assessment of motion reduction

1.4 Dissertation Organization

The primary body of this dissertation is composed of three chapters. Each chapter is written in format for submission to peer-review journals. Chapter 2 addresses specific aim 1. Chapter 3 addresses specific aim 2. Chapter 4 addresses specific aim 3. In the last chapter, this work is summarized and future research directions for this work are proposed.

Chapter 2: Comparison of the performance of a pre-commercial version of a vendor designed elastic motion correction algorithm in comparison to conventional motion correction techniques

This chapter is based upon:

Meier J G, Wu C C, Betancourt Cuellar S L, Truong M T, Erasmus J R, Einstein S and Mawlawi O 2018 Evaluation of a novel elastic respiratory motion correction algorithm on quantification and image quality in abdomino-thoracic PET/CT. JNM 60 279–84

The permissions for reuse of this material were obtained from the Journal of Nuclear Medicine

2.1 Abstract

Our aim was to evaluate in phantom and patient studies a recently developed elastic motion deblurring (EMDB) technique that makes use of all the acquired PET data and compare its performance with other conventional techniques such as phase-based gating (PBG) and HDChest (HDC), both of which use fractions of the acquired data. Comparisons were made with respect to static whole-body (SWB) images with no motion correction.

Methods: A phantom simulating respiratory motion of the thorax with lung lesions (5 spheres with internal diameters of 10–28 mm) was scanned with 0, 1, 2, and 3 cm of motion. Four reconstructions were performed: SWB, PBG, HDC, and EMD. For PBG, the average (PBGave) and maximum bin (PBGmax) were used. To compare the reconstructions, the ratios of SUVmax, SUVpeak, and contrast-to-noise ratio (CNR) were calculated with respect to SWB. Additionally, 46 patients with lung or liver tumors less than 3 cm in diameter were studied. Measurements of SUVmax, SUVpeak, and CNR were made for 46 lung and 19 liver lesions. To evaluate image noise, the SUV SD was measured in healthy lung and liver tissue and in the

phantom background. Finally, the subjective image quality of patient examinations was scored on a 5-point scale by 4 radiologists.

Results: In the phantom, EMDB increased SUVmax and SUVpeak over SWB but to a lesser extent than the other reconstruction methodologies. The ratio of CNR with respect to SWB for EMDB, however, was higher than all other reconstructions (0.68 with EMDB . 0.54 with HDC . 0.41 with PBGmax . 0.31 with PBGave). Similar results were seen in patient studies. SUVmax and SUVpeak were higher by, respectively, 19.3% and 11.1% with EMDB, 21.6% and 13.9% with HDC, 22.8% and 12.8% with PBGave, and 45.6% and 26.8% with PBGmax, compared with SWB. Lung and liver noise increased with EMDB by, respectively, 3% and 15%, with HDC by 35% and 56%, with PBGave by 100% and 170%, and with PBGmax by 146% and 219%. CNR increased in lung and liver tumors only with EMDB (18% and 13%, respectively) and decreased with HDC (−14% and −23%), PBGave (−39% and −63%), and PBGmax (−18% and −46%). The average radiologist scores of image quality were 4.0 ± 0.8 with SWB, 3.7 ± 1.0 with EMDB, 3.1 ± 1.0 with HDC, and 1.5 ± 0.7 with PBG.

Conclusion: The EMDB algorithm had the least increase in image noise, improved lesion CNR, and had the highest overall image quality score.

2.2 Introduction

Static whole-body (SWB) PET acquisitions typically last 2-3 min per bed position, which can result in degraded PET image quality due to respiratory motion, particularly for tumors in the lower thorax and upper abdomen [14,16,17]. This degradation potentially results in decreased measurements of activity concentration, overestimated measured metabolic volume, and decreased lesion detectability, all of which could negatively affect patient management. Many solutions exist to correct respiratory motion artifacts in PET/CT [22,33–38].

However, all such methods first require the acquisition of the patient's respiratory waveform using external devices or data-driven techniques. One of the first motion correction methods proposed was multibin respiratory gating, which divides the acquired PET data into multiple bins corresponding to different respiratory phases or amplitudes of the breathing cycle. Fractioning the data into multiple bins increases the amount of noise per bin, however, which biases quantitative measures such as SUVmax and decreases image quality. These drawbacks can be overcome by a longer acquisition time but come at the expense of decreased patient comfort and reduced scanner throughput. Furthermore, whereas this approach allows the full range of tumor motion to be determined, which is crucial for radiation therapy planning, it increases the complexity of the interpretation because it results in multiple image volumes corresponding to the different bins. Another approach to reduce motion while avoiding the complexity of multibin respiratory gating is end-expiration respiratory gating [22,39]. End-expiration respiratory gating is based on the observation that patients tend to spend more time in the end expiration quiescent period of the breathing cycle, which corresponds to the least amount of motion [25]. In comparison to an individual bin of multibin respiratory gating, end-expiration respiratory gating has the advantage of using a larger fraction of the acquired PET data, resulting in less image noise while reducing motion blur, and creates only one PET volume for interpretation. End-expiration respiratory gating can be implemented using the amplitude or phase of the respiratory waveforms. In the phase-based approach, PET data corresponding to a preset phase offset and window width from the onset of each breathing cycle are retained. This approach is implemented commercially on GE Healthcare PET/CT scanners as Q.Static[21] (13). 'In the amplitude-based approach of end-expiration respiratory gating, implemented commercially as HD-Chest (HDC) on Siemens PET/CT scanners, the user selects a percentage of the acquired PET data to preserve [22,40–42]. The HDC algorithm analyzes the respiratory waveform to find the minimum amplitude range that contains the user-selected percentage of

PET data, typically about 35%. End-expiration respiratory gating, whether phase or amplitude based, has emerged as the most common respiratory motion correction because of its simplicity and ease of use. Elastic motion correction is another approach for respiratory motion correction that retains all the acquired PET data to create the final image. Using the entirety of PET data improves image quality, thereby reducing the acquisition times that are typical in respiratory motion corrected examinations. Two primary approaches exist for elastic motion correction. In one strategy, multibin respiratory gating images are reconstructed, nonrigidly registered, and then averaged into a single volume [43]. This approach has been implemented commercially by GE Healthcare as Q.Freeze. A more recent approach (implemented commercially by Siemens and known as OncoFreeze) first derives a blurring kernel from subimages (SWB and HDC) that are later used during image reconstruction to generate the final motion-free image [29,44]. To our knowledge, there has been no independent evaluation of the elastic motion deblurring (EMDB) algorithm with the exception of one small-scale study (5 patients) presented as an abstract[45]. In this study, we evaluated these various respiratory motion correction methodologies (multibin respiratory gating, amplitude-based optimal gating, and EMD) in comparison to SWB with no motion correction. Initially, a phantom evaluation was performed to provide a comparison of these algorithms with respect to the ground truth. We then assessed the impact of these various approaches on clinical PET lesion quantification as well as objective and subjective image quality. Numerous publications have studied the impact of multibin respiratory gating and HDC, but to the best of our knowledge, this is the first investigation that systematically compared the EMD algorithm with other motion-correction techniques.

2.3 Materials and Methods

2.3.1 Reconstruction Algorithms

In this study, 4 PET reconstructions were investigated. The first was SWB, which used all the data, with no respiratory motion correction. The second was multibin respiratory gating, which reconstructed 8 gates (each containing 12.5% of the PET data). The third was HDC, which used the manufacturer recommended 35% duty cycle for reconstruction. The fourth was the EMDB algorithm[29,44], which used 100% of the acquired PET data to reconstruct a motion-corrected image.

The EMDB algorithm initially performs an SWB reconstruction with 100% of the data and an HDC reconstruction that applies a baseline shift-correction to the patient respiratory waveform. In this study, we used a 35% duty cycle for the HDC image. The EMDB algorithm uses mass preservation optical flow [46] to non-rigidly register the reference volume (HDC) to the target volume (SWB) as seen in Figure 2-1. The HDC volume and the SWB volume have the same integral activity, but because of motion blur, the objects in each respective volume have different brightness, necessitating the mass preservation optical flow algorithm to register the 2 volumes. Mass preservation optical flow does not require that the motion vectors correspond to physically realizable motion. EMDB uses mass preservation optical flow to determine a fully 3-dimensional blurring kernel to redistribute the activity between the HDC SWB volumes. In the EMDB reconstruction, the blurring kernel is applied to the current image estimate before forward projection. The transpose of the blurring kernel, the deblurring kernel, is applied after backprojection and results in a motion-corrected image estimate as seen in Figure 2-1.

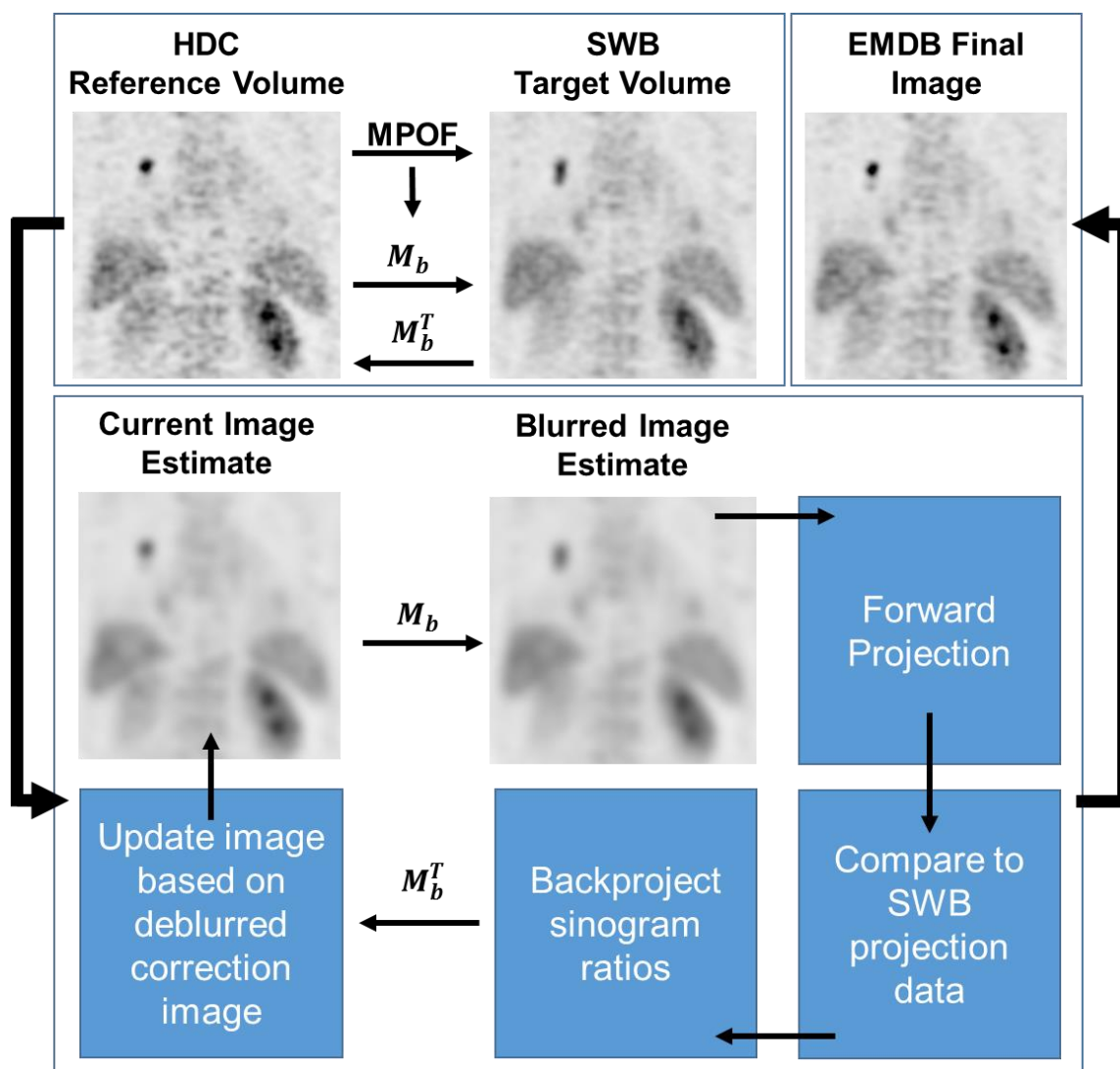


Figure 2-1 Workflow of the EMDB Algorithm

2.3.2 Phantom Evaluation

A phantom was constructed to move 5 spheres in 3 dimensions to simulate the elastic motions of the abdomen and thorax. A detailed phantom description is provided as supplemental material (supplemental materials are available at <http://jnm.snmjournals.org>). The spheres had inner diameters of 10, 13, 17, 22, and 28 mm. The spheres were placed in an acrylic tank containing 16 L of water, and the sphere-to-background ratio was set to 5:1. A motor drove the spheres using a repeated patient respiratory cycle that had a duration of 6 s. Four acquisitions were performed in which the spheres were driven with amplitudes of 0, 1, 2, and 3 cm. The phantom motion was programmed such that the spheres always returned to the same location for all acquisitions. The phantom was scanned on a 4-ring Siemens Biograph mCT Flow system, which has previously been characterized [7]. CT-based attenuation correction data were acquired while the spheres were motionless and at the initial position. The PET data were acquired during continuous bed motion for 60 cm. In each acquisition, 3 table-speed zones were prescribed: 1 mm/s for the 15 cm superior to the acrylic tank, 0.5 mm/s for the 30 cm covering the phantom tank, and 1 mm/s for the 15 cm inferior to the phantom tank. During PET acquisition, the respiratory waveform was acquired with the AZ-733V respiratory gating system (Anzai Medical Co.) [47] by wrapping the belt around the surrogate motor platform (Figure 2-2B). The phantom and setup are shown in Figures 2-2A and 2-2B and the supplemental material. Each phantom scan was 15 min. Care was taken to ensure that each acquisition had similar counting statistics, using list-mode rebinning of the acquired data. SWB, EMDB, HDC, and phase-based gating (PBG) reconstructions were performed for all phantom scans. All reconstructions were performed with the default clinical parameters: 2 iterations, 21 subsets, time-of-flight information, point-spread-function correction, a 200 x 200 matrix, 4.07 x 4.07 x 3 mm voxels, and isotropic gaussian postfiltration of 5 mm in full width at half maximum. For each motion amplitude and reconstruction algorithm, we measured SUVmax, SUVpeak, and

SUV SD. SUVmax and SUVpeak were determined from a region of interest encompassing each sphere. All measurements were made in MIM, version 6.6 (MIM Software, Inc.). SUV SD was measured in the uniform background of the phantom with a 3 cm diameter spherical region of interest. Contrast to noise ratio (CNR) for each sphere was also calculated according to Equation 2-1 using the sphere SUVmax (SUV_{max,sp}), background SUVmax (SUV_{max,bg}), and background SUV SD (σ).

$$CNR = \frac{SUV_{max,sp} - SUV_{max,bg}}{\sigma} \quad (2-1)$$

For each sphere, phantom scan, and reconstruction, the SUV ratio and the CNR ratio relative to the SUV and CNR of the ground truth SWB reconstruction with no motion was calculated for SUVmax, SUVpeak, and CNR. For the measurements made on the 8 gates of the PBG reconstruction, the average value of all 8 gates was used (PBGave), as well as the gate with the highest value (PBGmax) for each respective measurement of SUVmax, SUVpeak, SUV SD, and CNR. The average SUV SD was calculated for all background spheres, phantom scans, and reconstruction algorithms.

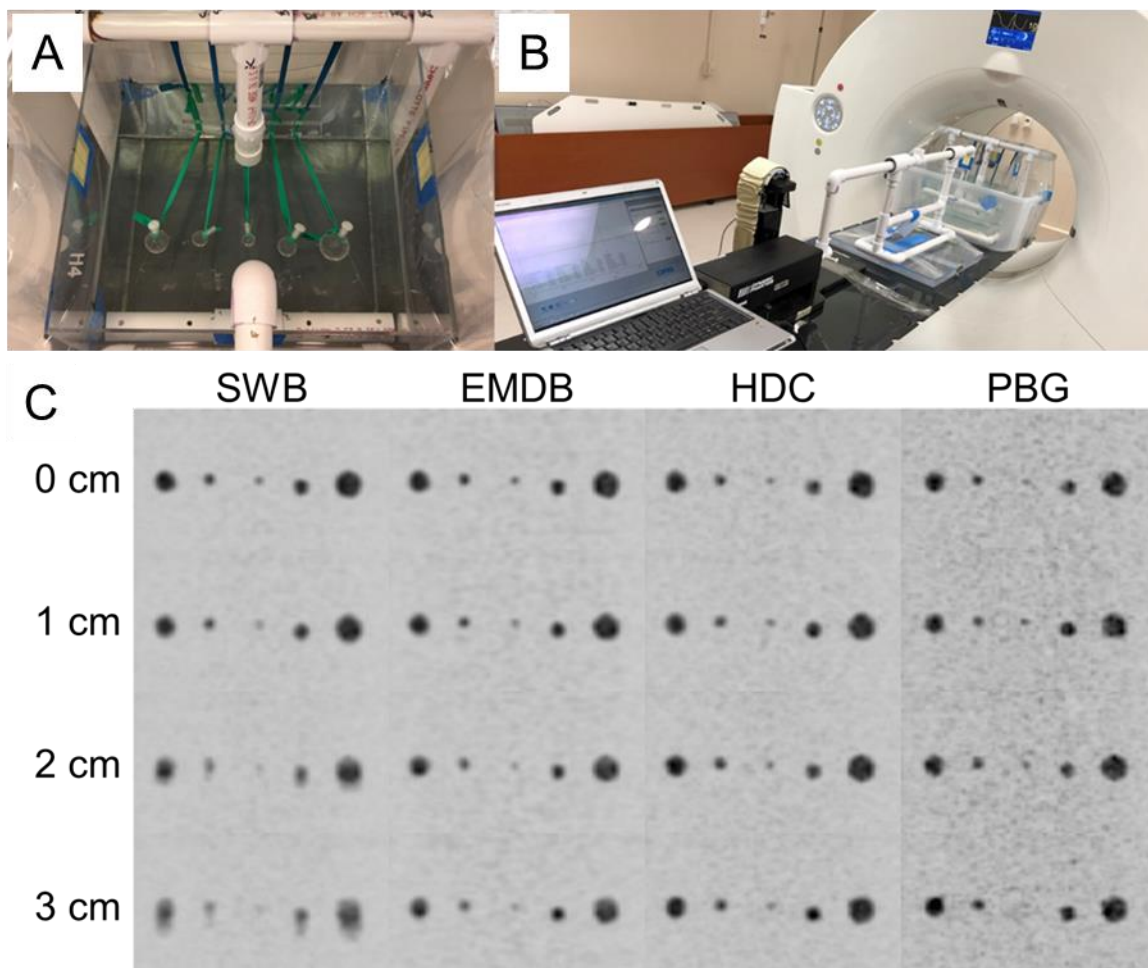


Figure 2-2 Phantom experimental setup and resultant images

2.3.3 Patient Evaluation

Forty-six patients (23 men and 23 women; mean age, 62.9 ± 14.8 y; mean body mass index, 28.2 ± 6.7) with 65 lung ($n = 46$) or liver ($n = 19$) lesions in regions affected by respiratory motion and less than 3 cm in diameter were prospectively recruited for this study. The institutional review board approved this study (approval 2015-0989), and all subjects gave written informed consent before undergoing imaging. Patients fasted for 6 h before injection of 323 ± 56 MBq of ^{18}F -FDG. The PET scan followed the ^{18}F -FDG injection by 69.2 ± 9.1 min.

2.2.4. PET/CT Acquisition and Image Reconstruction

All patients were scanned with the same PET/CT system and protocols as used for the phantom scans, except that the patient PET data were acquired in continuous bed motion with a table speed of 0.8–1 mm/s, depending on patient body mass index. Over the lung/ liver region where the tumor was affected by motion, a table speed of 0.5 mm/s was used for a 30-cm section of the scan. Patient respiratory waveforms were acquired with the Anzai system. All CT scans were acquired with free breathing. SWB, EMDB, HDC, and PGB reconstructions were performed for all patient scans, with the same reconstruction parameters as used for the phantom scans.

2.3.4 PET/CT Acquisition and Image Reconstruction

All patients were scanned with the same PET/CT system and protocols as used for the phantom scans, except that the patient PET data were acquired in continuous bed motion with a table speed of 0.8–1 mm/s, depending on patient body mass index. Over the lung/ liver region where tumor was affected by motion, a table speed of 0.5 mm/s was used for a 30-cm section of the scan. Patient respiratory waveforms were acquired with the Anzai system. All CT scans were acquired with free breathing. SWB, EMDB, HDC, and PGB reconstructions were performed for all patient scans, with the same reconstruction parameters as used for the phantom scans.

2.3.5 Image Analysis

SUV_{max} and SUV_{peak} normalized by body weight were measured for each tumor. SUV SD (a surrogate for image noise) was measured using a 3-cm diameter spherical region of interest in lung and liver tissue that we assessed to be free of disease. The CNR was calculated analogously to Equation 2-1. All measurements were made in MIM, version 6.6. For the PBG reconstruction, both PBG_{ave} and PBG_{max} were analyzed.

2.3.6 Image Quality Assessment

Four radiologists who were experienced in PET/CT imaging subjectively scored the image quality of the 4 reconstructions on a Likert-type scale of 1 (poor) to 5 (excellent). In total, 184 reconstructions (46 patients x 4 reconstructions) were assessed. For the PBG reconstructions, gate 5/8 was selected for presentation because it contained the least motion. Only one reconstruction at a time was displayed for assessment. The order of the presentation was randomized by reconstruction method and patient. Only the images acquired from the 30 cm region scanned with a 0.5 mm/s table speed were presented for image quality scoring. To assess intrareader reliability, 20 cases were repeated.

2.3.7 Statistical Analysis

All statistical analyses were performed with R (version 3.5.0 and package “irr,” version 0.84). Wilcoxon signed-rank tests, with Bonferroni adjustments, were performed to determine significance. The α -test of Krippendorff [48] was used to assess inter and intrareader reliability in image quality assessment.

2.4 Results

2.4.1 Phantom Evaluation

All motion correction methodologies successfully reduced image blur (Fig. 2-2C). The average values of SUV_{max} normalized to SWB over all spheres and motion amplitudes were 0.85 with SWB, 0.96 with EMDB, 1.01 with HDC, 1.06 with PBGave, and 1.23 with PBGmax (Fig. 2-3A). The average values of SUV_{peak} normalized to SWB were 0.87 with SWB, 0.94 with EMDB, 0.99 with HDC, 1.00 with PBGave, and 1.10 with PBGmax (Fig. 2-3B). Only the SWB and EMDB reconstructions had decreasing SUV_{max} normalized to SWB and SUV_{peak} normalized to SWB with increasing sphere motion amplitude. The sphere with the smallest inner diameter (10mm) had the largest decreases in SUV_{max} normalized to SWB and in SUV_{peak} normalized to SWB as the motion amplitude increased. The percentage increases in SUV SD compared with the SWB reconstruction were 24.6% with EMDB, 61.6% with HDC, 171.7% with PBGave, and 216.2% with PBGmax (Fig. 2-3C). The average values of CNR ratio normalized to SWB were 0.31 with PBGave, 0.41 with PBGmax, 0.54 with HDC, 0.68 with EMDB, and 0.74 with SWB (Fig. 2-3D). Motion correction did not increase CNR ratio normalized to SWB above the SWB value until the motion amplitude reached 3 cm, and this was only for the EMDB and HDC reconstructions (Fig. 2-3D). Decreases in CNR ratio normalized to SWB relative to motion amplitude were observed only for the SWB and EMDB reconstructions (Fig. 2-3D).

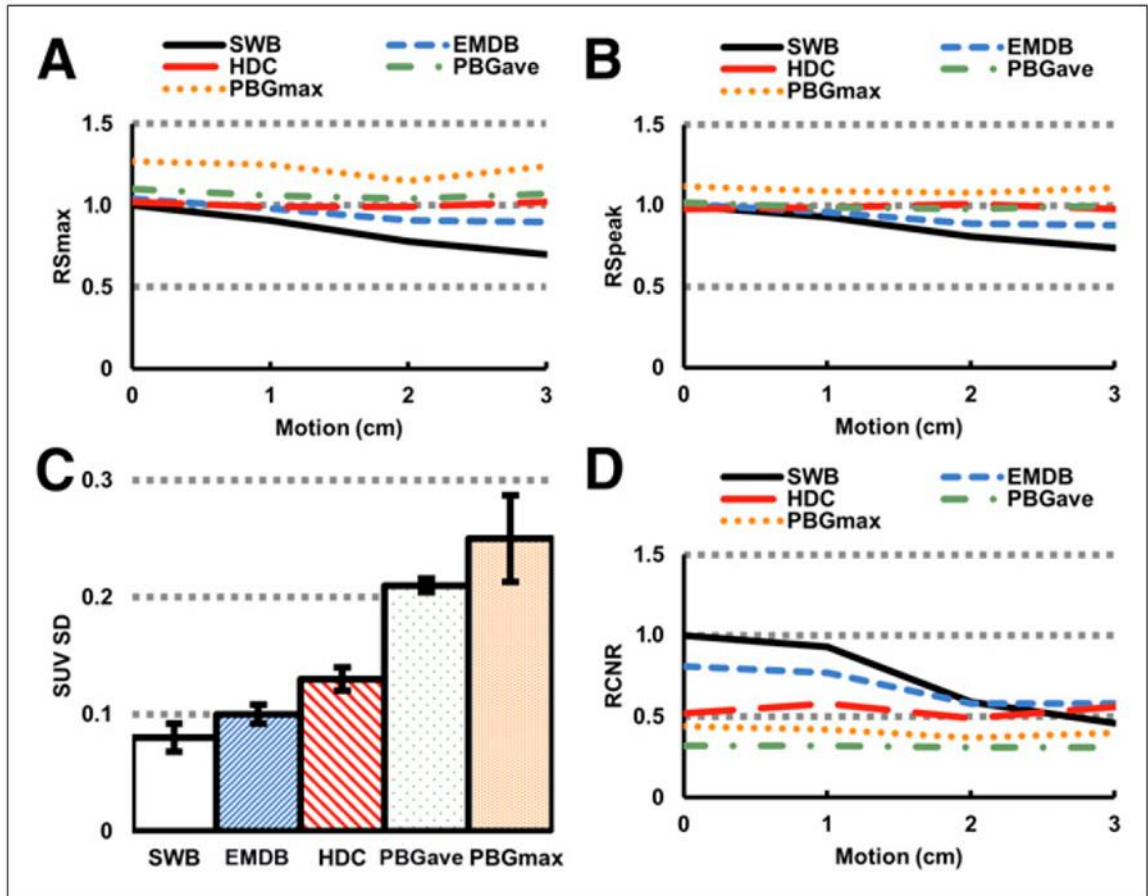


Figure 2-3 Phantom experimental measurements. (A and B) SUVmax normalized to SWB (RS_{max}) (A) and SUVpeak normalized to SWB (RS_{peak}) (B) variation caused by to sphere displacement. (C) SUV SD in background across all reconstructions. (D) CNR ratio normalized to SWB ($RCNR$) variation due to sphere displacement. Data are for the average of all spheres.

2.4.2 Patient Tumor Quantification

In comparison to the SWB reconstruction, all motion correction reconstruction algorithms displayed significant increases in SUVmax and SUVpeak (Fig. 2-4A). The percentage increases in SUVmax in comparison to SWB for EMDB, HDC, PBGave, and PBGmax were 19.3%, 21.6%, 22.8%, and 45.6%, respectively. The percentage increases in SUVpeak in comparison to SWB for EMDB, HDC, PBGave, and PBGmax were 11.1%, 13.9%, 12.8%, and 26.8%, respectively. For measurements of both SUVmax and SUVpeak, PBGmax had the largest increase in comparison to SWB, whereas PBGave, HDC, and EMDB had relatively similar increases, with EMDB consistently having the lowest values. The percentage increases in lung and liver SUV SD in comparison to SWB for EMDB, HDC, PBGave, and PBGmax were, respectively, 3.3% and 14.8%, 35.1% and 55.8%, 100.0% and 169.6%, and 145.8% and 219.0% (Fig. 2-4B), showing that EMDB consistently had the least increase in lung and liver SUV SD. Across all motion correction methodologies, the increases in SUV SD were higher in the liver than in the lung. The percentage increases for lung and liver lesion CNR in comparison to SWB for EMDB, HDC, PBGave, and PBGmax were, respectively, 17.8% and 13.3%, 213.9% and 223.2%, 238.6% and 262.7%, and 218.2% and 246.0%. EMDB was the only motion correction method that increased lesion CNR (the others had negative results), although the increase in liver lesion CNR was not significant ($P = 0.58$). Example patient images of all 4 reconstructions are shown in Figure 2-5.

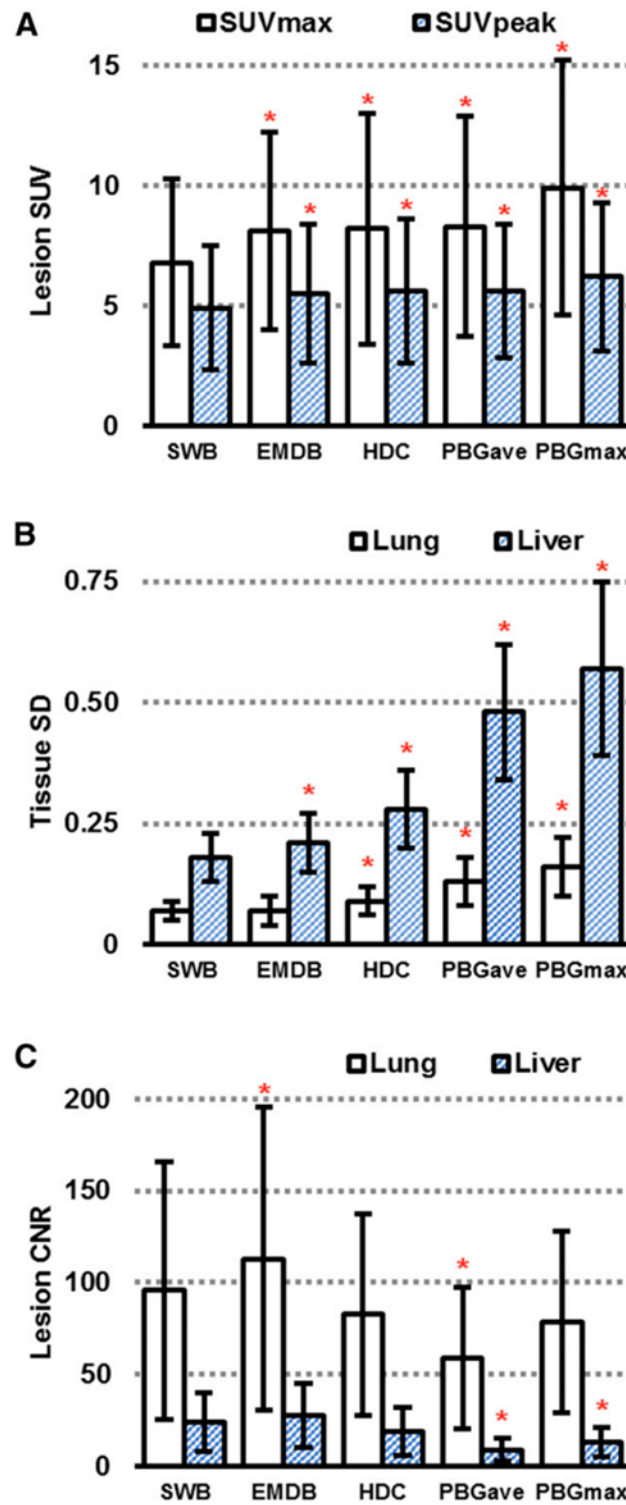


Figure 2-4 Patient Quantification Results. SUVmax and SUVpeak for 65 lesions (A), SUV SD for lung and liver tissue (B), and CNR for lung and liver lesions (C). *P < 0.01.

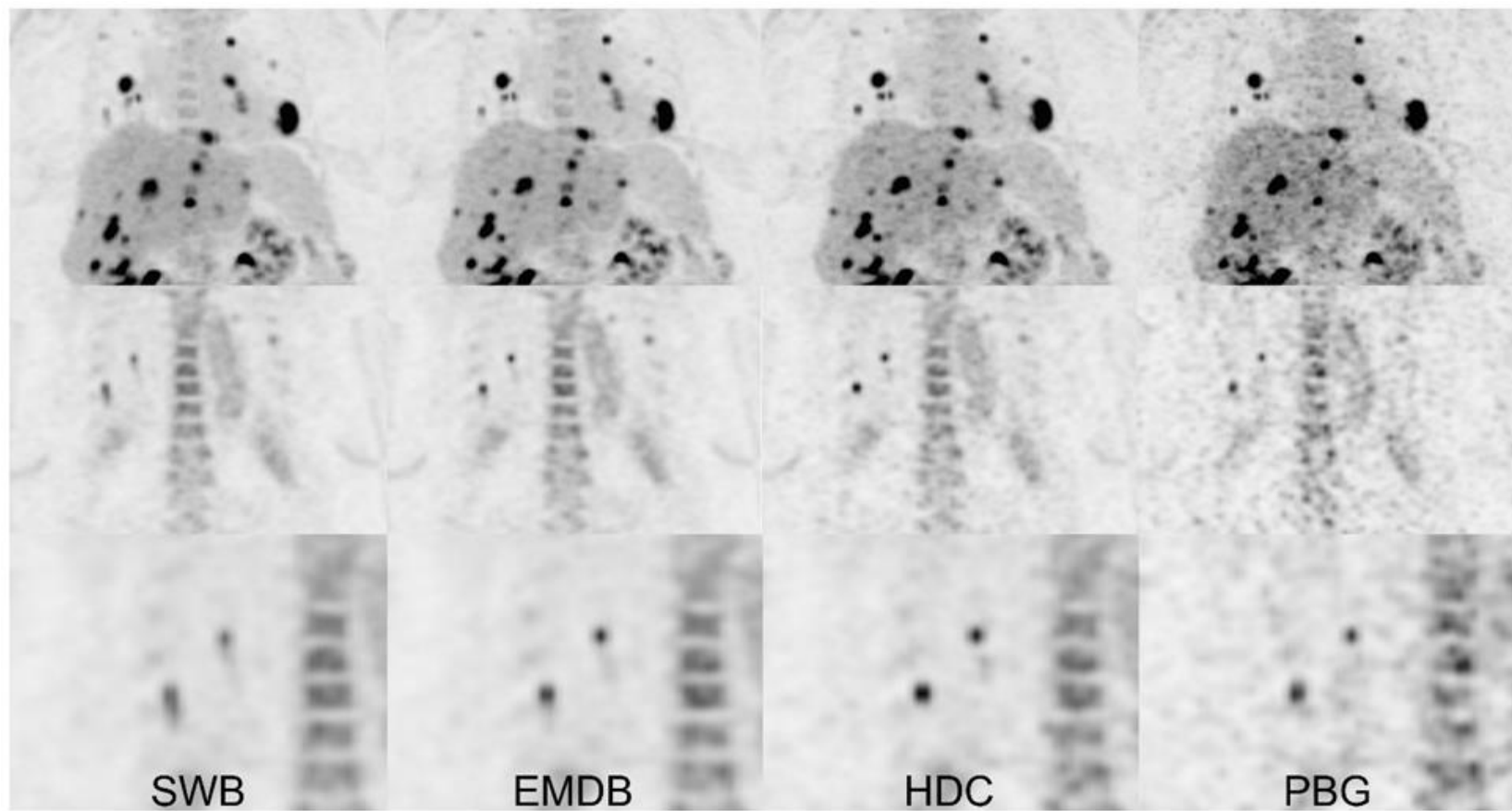


Figure 2-5 Example patient images. (Top) Maximum intensity projection images of all reconstructions. (Middle) Coronal plane view of right lung tumors. (Bottom) Zoomed view of middle row.

2.4.3 Subjective Image Quality

Of the motion correction methods, EMDB was scored as having the best overall image quality (Fig. 2-6). The percentage changes in image quality in comparison to SWB for EMDB, HDC, and PBG were 29.7%, 222.6%, and 263.7%, respectively. The intrareader repeatability α scores were 0.75, 0.77, 0.78, and 0.87, respectively. The interreader repeatability α score was 0.81.

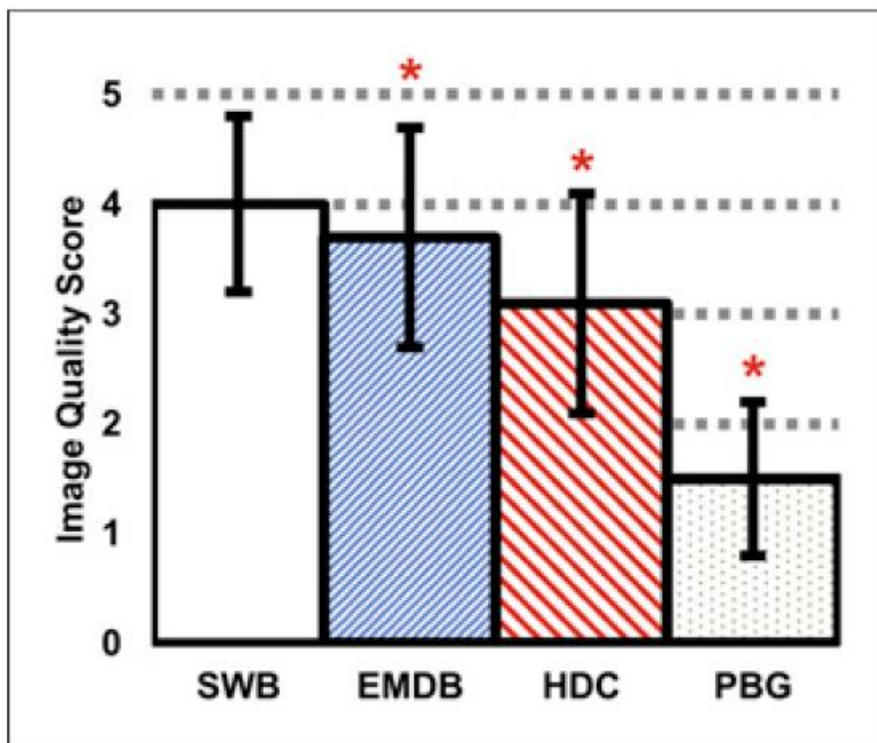


Figure 2-6 Mean image quality score for different reconstructions. Error bars represent 1 SD. *P < 0.01.

2.5 Discussion

We assessed the impact of various motion correction methodologies on PET/CT imaging, with a primary interest in evaluating the EMDB technique. To our knowledge, this is the first published study on the impact of the EMDB algorithm in comparison with other motion correction methodologies in a relatively large cohort of patients.

The most important finding was that the EMDB algorithm had the smallest increase in image noise while reducing motion blur and improving lesion contrast. The primary cause of the reduced image noise was that the algorithm used all the acquired PET data, as opposed to use of a smaller fraction of the data by the other motion correction methodologies. These findings were consistent for both phantom and patient studies and were corroborated by the objective physician evaluation.

Although the EMDB algorithm used all the acquired PET data in the reconstruction, the resultant images still had increased noise when compared with SWB. We postulate that this noise resulted from the determination of the blurring kernel between the noisy HDC image and the SWB image in the EMDB algorithm. Specifically, the blurring kernel is influenced by the noise in the HDC image. In this regard, the choice of the percentage duty cycle for the HDC image has an important consequence on EMDB image quality. Increasing the duty cycle would reduce noise but at the expense of increased image blur, whereas decreasing the duty cycle has the opposite effect.

Several investigators have previously shown that image blur is reduced when using PET data corresponding to only a small fraction of the breathing cycle [20,49]. However, one significant consideration when implementing such motion correction approaches is the artifactual increase in measured SUV_{max} and SUV_{peak} due to increased image noise. As seen in our phantom and patient results, SUV_{max} and SUV_{peak} increased for all motion correction

methodologies. However, these increases were amplified with decreasing amounts of PET data. Our phantom results indicate that image noise increased with methods that use decreasing amounts of PET data (increasing from 24.6% for EMDB to 216.2% for the PBGmax approach). In this regard, an increase in SUVmax or SUVpeak when using such correction techniques should be attributed not only to motion correction but also to an increase in image noise. In this work, we used CNR as a metric to capture both these image attributes (SUVmax and noise), and the results clearly show a decrease in CNR with correction methodologies that use decreasing amounts of PET data (Fig. 2-3D), reflecting the larger increase in image noise compared with a true increase in SUVmax.

One important finding about the EMDB algorithm is its degraded performance with increasing motion amplitude. Our results indicate that although all other motion correction methodologies resulted in an SUVmax and SUVpeak that were relatively independent of motion amplitude, the EMDB algorithm decreased these values with increasing motion but to a lower extent than SWB (Figs. 2-3A and 2-3B). It is not clear why this performance was observed, and further investigation is warranted.

In patient data, the percentage increases in SUVmax and SUVpeak were similar for EMDB, HDC, and PBGave. However, PBGmax had the highest percentage increases. The large differences seen between SUV for PBGmax and for the other motion correction methodologies is attributed to increases in image noise. EMDB had the least noise increase, yet the increases in SUVmax and SUVpeak were similar to HDC and PBGave, which use much less of the data. We can infer that the increases in SUV for the EMDB algorithm were influenced more by reductions in motion blur and less by increases due to noise bias.

EMDB was the only method that improved CNR, although not significantly for liver lesions, primarily because of the relatively high noise in the liver that neutralized any increase in liver SUV. Overall, however, EMDB increased SUVmax and SUVpeak yet had the least

increase in image noise and, as a result, was the only method to improve lesion CNR. Although SUVmax and SUVpeak increased for the other motion correction methodologies, all of them decreased the CNR of the lesions.

Our image quality scores confirmed our expectations of low scores with increased image noise. Of the motion correction methodologies, the EMDB algorithm had the highest overall score, presumably because it contained the least image noise. The SWB images incurred substantial respiratory motion blur in comparison to the motion correction methodologies; however, the image quality scores showed that the primary concern in overall image quality was the amount of image noise present. In addition, we found good agreement between readers. A meta-analysis of the physician scores showed that in 50% of the cases, the physicians scored the EMDB images as having quality similar to or better than the SWB images. This number was 25% for cases in which the physicians scored the EMDB as strictly better than the SWB images. These results suggest that physicians either preferred images with reduced blur or could not perceive changes in background noise between these 2 reconstruction algorithms.

One limitation of this study was that patient CT-based attenuation correction data were acquired under free-breathing conditions. The literature has shown that mismatches in free-breathing CT and PET data often occur in areas affected by respiratory motion and can affect SUV quantification [50,51]. It is possible that the quantification results of this study were affected by these attenuation correction mismatches. Recent work in collaboration with our group has investigated the effects of these mismatches and have developed approaches to mitigate them [52]. However, it would be interesting to assess the effect of such mismatches specifically on the performance of the EMDB algorithm as compared with other techniques.

Another limitation of this study was that all motion correction methods with the exception of the EMDB were performed without baseline shift correction of the respiratory waveform. (The EMDB algorithm had this feature embedded in the software.) In some patients,

however, there can be a baseline drift in the respiratory waveform throughout the course of the examination that could affect the results of the various correction methods. In this regard, this data processing difference might have biased the results in favor of the EMDB algorithm. Analysis of the results with baseline shift for all the other correction methods will be a focus of future investigations.

2.6 Conclusion

All methods of motion correction reduced image blur but increased image noise, resulting in increased SUVs. The EMDB algorithm had the least noise increase, which resulted in improved CNR and higher image quality scores.

2.7 Disclosure

Siemens Medical Solutions USA Inc. provided the EMDB software under a research agreement. No other potential conflict of interest relevant to this article was reported.

2.8 Acknowledgements

We thank Drs. James Hamill, Judson Jones, and Inki Hong from Siemens for technical support. We also thank Drs. Lawrence Court and Arvind Rao at M.D. Anderson Cancer Center for providing the dynamic thorax phantom and advice on statistical analysis, respectively.

Chapter 3: Evaluation of the performance of a pre-commercial version of a vendor designed CBM_DDГ technique in comparison to a conventional external device

3.1 Abstract

Data Driven Respiratory Gating (DDG) has been developed in an effort to eliminate the need for external devices to measure respiratory waveforms(WF) in PET imaging. Recently a DDG method has been introduced that leverages continuous bed motion (CBM_DDГ) to overcome the longstanding challenge of maintaining a consistent respiratory waveform polarity in relation to the true anatomical respiratory motion. Our goal was to determine the performance of this CBM_DDГ algorithm in comparison to the Anzai (ANZ) external device in phantom and patient studies while comparing resultant WFs, SUV quantification, and physician evaluation of respiratory gated patient images.

Methods

A phantom simulating abdominothoracic motion drove 5 spheres(10-28 mm inner diameter) in 4 acquisitions with amplitudes of 0, 1, 2, and 3 cm. Two reconstructions were performed: Elastic Motion Deblurring (EMDB) for respiratory motion correction using the ANZ WF(ANZ_EMDB) and the CBM_DDГ WF(DDГ_EMDB) respectively. To compare the waveforms, the Pearson correlation coefficient was calculated. To assess the impact on phantom image quantification, the ratio of DDГ_EMDB to ANZ_EMDB was calculated for SUVmax and SUVpeak respectively. In 43 patients, the WF correlation coefficient was calculated between the aortic arch and the center of the right kidney. SUVmax and SUVpeak were measured on F18-FDG foci (lung/liver/spleen tumor, gastric, kidney medulla) influenced by respiratory motion. Physicians assessed the motion corrected images in a side by side

comparison of the ANZ_EMDB to the DDG_EMDB images by scoring the presence of relative motion blur(0(no blur) to 3(significantly more blur)) in a single F18-FDG focus for each patient.

Results

The phantom WF correlation coefficients were 0.00, -0.40, 0.82, and 0.93 for the 0, 1, 2, and 3 cm amplitude acquisitions respectively, showing that the CBM_DDG WF improves as the amount of sphere motion increases. Over all spheres, the average phantom SUVmax ratios were 1.01(0 cm), 0.93(1 cm), 0.93(2 cm), and 0.96(3 cm), while for SUVpeak were 1.00(0 cm), 0.97(1 cm), 0.95(2 cm), and 0.97(3 cm). For the patient studies, the average WF correlation coefficient was 0.71 +/- 0.24. For quantification of patient 18F-FDG foci, in comparison to ANZ_EMDB, DDG_EMDB was lower by 2.4 % and 2.8 % for the average SUVmax and average SUVpeak values respectively. Similarity in quantification of the DDG_EMDB to the ANZ_EMDB images was shown for both SUVmax and SUVpeak when using non-inferiority statistical tests with a non-inferiority margin of -5% with respect to the ANZ_EMDB images. The physician image evaluation of relative motion blur showed that the DDG_EMDB images were similar to the ANZ_EMDB images when using a non-inferiority statistical test with a margin of 0.5 blurring points with respect to the ANZ_EMDB images.

Conclusion

The CBM_DDG algorithm shows promise as a replacement for the Anzai external device to measure patient respiratory waveforms, as comparison to the Anzai WF, image quantification and physician image assessment showed similar performance.

3.2 Introduction

Clinical PET imaging of the abdominothoracic regions typically lasts between 2-3 minutes per bed position and can result in degraded image quality due to the respiratory motion blur incurred from multiple respiratory cycles. Respiratory motion blur can negatively impact patient management due to underestimated activity concentration measurements, decreased lesion detectability, and overestimated volume measurements[14,16,17].

Multiple methods exist to correct for respiratory motion blur, the majority of which require the acquisition of a respiratory waveform [14,21,53–56,22,28,29,33–36,38]. External devices have been primarily used to acquire the respiratory waveforms. One such system is the real-time position management optical system (Varian Medical Systems, Palo Alto, CA, USA) which tracks the position of a box placed on the chest or abdomen of the patient. Another is the AZ-733V respiratory gating system (Anzai Medical, Tokyo, Japan) in which an elastic belt with a load cell is placed around the chest or abdomen of the patient and measures the changes in belt tension as the patient breathes in and out. However, external devices have technical challenges in that they require additional time for both setup and troubleshooting and are prone to both user setup error and hardware failure. In one study which investigated the feasibility of routine respiratory motion correction, 82 out of 741 examinations had unusable respiratory waveforms due to hardware failures or irregular breathing[19]. A proposed method to reduce hardware failures was to further train the technologists and to provide more frequent calibration of the sensors, demonstrating that successful implementation of the external devices is highly user dependent. In addition, several other studies have shown that the chest or abdominal wall motion captured by external devices does not always represent the motion of the internal anatomy[57–59].

Data driven gating(DDG) which relies on determining the respiratory waveform entirely from the acquired PET data from the patient has been introduced as an alternative to external devices to record the respiratory waveform. DDG is based on the knowledge that organs and diseases which exhibit radiotracer uptake and are under the influence of respiratory motion, will show periodic changes in the acquired PET data which can be detected and used to determine a respiratory waveform. DDG eliminates the need for extra time to set up external devices, and the resulting respiratory waveform is reproducible since it is entirely independent of the variability in user setup exhibited with external devices for each unique patient. In addition, the DDG signal is determined from the motion of internal anatomy rather than external surfaces.

Many different types of DDG techniques exist and have been in development over the past decade[60–68]. One DDG methodology determines the center of mass of a regional radioactive uptake that is influenced by respiratory motion and has been implemented in various ways[60–62]. Another DDG methodology exploits the geometric sensitivity profile of clinical PET scanners[63,64]. Other image based methodologies have also shown success, but are computationally expensive and require image reconstructions for each timepoint, typically every 0.5s[65]. To overcome this challenge, other methods that work in sinogram space have been developed such as the Sinogram Region Fluctuation[65] Spectral Analysis Method[66], Principle Component Analysis[67], and Laplacian Eigenmaps[68].

All of these DDG methodologies have been made exclusively for PET data acquired in Step and Shoot mode. However, no DDG method has been created for PET data acquired in Continuous Bed Motion(CBM)[31] until very recently [32]. In CBM acquisitions, the patient is continuously translated through the scanner, while in comparison to Step and Shoot, the patient is imaged in multiple stationary and overlapping bed positions[69]. In this DDG approach, the Spectral Analysis Method[66], which was originally developed for Step and Shoot, was adapted by Schleyer et al. to work with CBM data[32] in order to account for the combination of

anatomical motion due to both respiratory motion and continuous table motion. One challenge that all Step and Shoot DDG methodologies must account for is inversions in the DDG signal polarity that can occur between adjacent bed positions due to the arbitrary relationship between DDG signal polarity and the direction of object motion influenced by respiratory motion. In comparison to Step and Shoot, acquisition of the data in CBM enables continuous unlisting of short axial extent volumes with a high percentage of axial overlap. The DDG analysis of these volumes allows identifying a consistent relationship between the signal polarity and the physical direction of object motion influenced by respiratory motion.

In this work we evaluate the performance of this novel CBM DDG (CBM_DDГ) algorithm in comparison to an external device (Anzai) approach in a phantom and clinical evaluation. The evaluation is based on a comparison of the CBM_DDГ and Anzai waveforms from phantom and patient acquisitions. Additionally, assessments of the impact on tumor quantification is also performed by comparing the results of images without motion correction to the images with motion correction when using the Anzai and CBM_DDГ waveforms respectively. Finally, to assess the impact on subjective image quality, the perception of respiratory motion blur was scored for images generated using Anzai and CBM_DDГ waveforms for motion correction respectively. To our knowledge, this investigation is the first to perform a comprehensive phantom and clinical evaluation while using the CBM_DDГ algorithm in comparison to an external device approach for respiratory motion correction.

3.3 Materials and Methods

3.3.1 Continuous Bed Motion Data Driven Gating Algorithm

The CBM-DDG algorithm has been previously introduced [32]. Here we briefly describe its general framework. The algorithm starts by dynamically framing the list mode data

set into 500 ms frames. As seen in Figure 3-1, for each frame, a histo-projection volume is created by placing each event onto the Cartesian coordinate that the event was most likely emitted from using time of flight information. Each one of these volumes is collapsed onto the y-axis, and the standard deviation for each 500 ms frame is calculated. At inspiration the standard deviation of the collapsed frames will be highest, and so as patients breathe, the standard deviation along the anterior posterior direction will vary periodically. The Fast Fourier Transform of the standard deviation signal is used to estimate the global respiratory frequency, which in turn is used to define the frequency peak and window used in the Spectral Analysis Method.

The 500 ms histo-projection volumes created from the entire axial extent of the CBM acquisition are then combined into 80 mm axial range volumes which are overlapped by 70 mm. Each 80 mm volume is composed of 500 ms frames. From each 80 mm volume, the Spectral Analysis Method creates a 3D mask which identifies the regions in the volume that are impacted by respiratory motion. Leading and trailing edges of moving objects can destructively interfere with each other, and so each mask location is multiplied by the cosine of the phase at each mask location to enable these locations to contribute constructively to the respiratory signal. To ensure that the signal polarity remains consistent across all 80 mm volumes, an optimal phase angle is determined to minimize the difference in phase between the masks of adjacent 80 mm volumes. The phase difference minimization is initialized at the 80 mm volume centered on the dome of the liver which typically has the strongest DDG signal as a result of typically being under the influence of respiratory motion and having physiologic uptake of F18-FDG above background levels.

These phase adjusted masks are then averaged into one final 3D weighted mask. The product of each 500 ms histo-volume and the 3D weighted mask is summed over all dimensions for each 500 ms histo-volume to produce each 500 ms time point of the one-dimensional

respiratory signal. To ensure that the global polarity of the 3D weighted mask signal is consistent with the physiological respiratory motion direction, the correlation between the y-standard deviation signal, and the 3D mask signal multiplied by 1 or -1 is calculated. The 3D mask signal when multiplied by 1 or -1 which has the highest correlation is assumed to have the correct signal polarity with respect to the underlying respiratory motion and is used as the CBM_DDG respiratory signal.

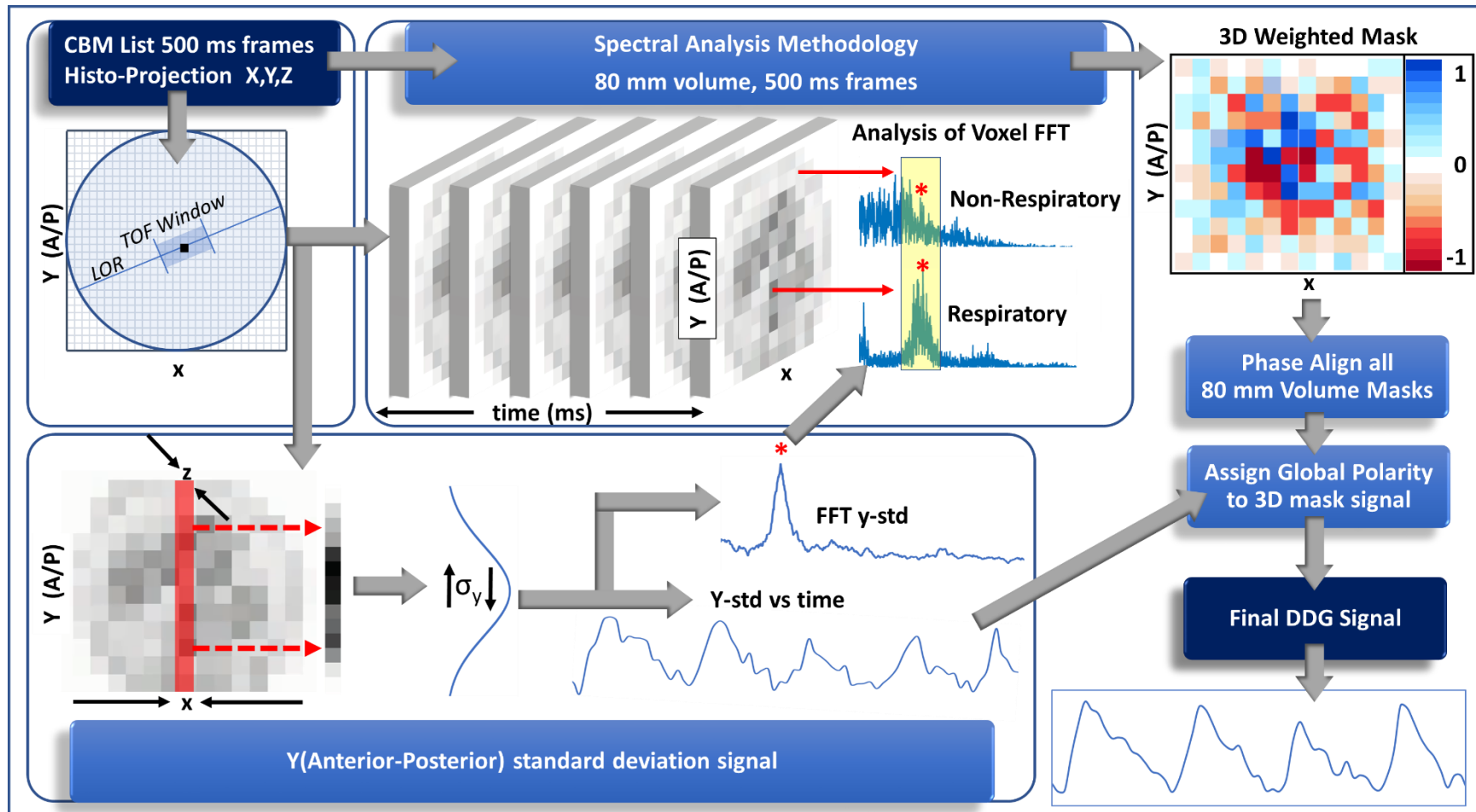


Figure 3-1 Overview of the CBM_DDG workflow

3.3.2 Phantom Evaluation

A phantom was utilized that moves 5 spheres in the superior-inferior, medio-lateral, and anterior-posterior directions, simulating the elastic motion found in the abdomen and thorax. A detailed description of this phantom and the setup was previously provided[54]. The inner diameters of the spheres were 10, 13, 17, 22, and 28 mm. The spheres were suspended in a cuboidal tank which was filled with 16 liters of water and prepared to achieve a 5:1 sphere-to-background ratio. Four acquisitions were performed in which the spheres were driven with amplitudes of 0, 1, 2, and 3 cm. The CIRS dynamic thorax phantom (Norfolk, Virginia) motor drove the spheres with a single, 6 s, repeated cycle of a representative patient's respiratory waveform. The phantom scan was acquired on a 4-ring Siemens Biograph mCT Flow system[7]. The CT used for attenuation correction was acquired while the spheres were motionless and at the end of expiration. All PET acquisitions were performed using CBM. Three table-speed zones were used for each acquisition: 1 mm/s for 15 cm superior to the phantom, 0.5 mm/s for the 30 cm covering the phantom, and 1 mm/s for 15 cm inferior to the phantom. All respiratory waveforms were acquired with the AZ-733V respiratory gating system (Anzai Medical Co.) by placing the belt around the surrogate motion platform. When necessary the PET list datasets were down sampled to achieve similar counting statistics.

Two respiratory motion correction reconstructions were performed using the Elastic Motion Deblurring (EMDB)[54] algorithm which uses 100% of the PET data during the image reconstruction and is known commercially as OncoFreeze. For the EMDB algorithm, a 35 % duty cycle was used to reconstruct the HDChest reference image. One of the EMDB reconstructions was performed using the Anzai waveform (ANZ_EMDB), and the other was performed using the CBM_DDГ waveform (DDГ_EMDB). For both reconstructions, the following parameters were used: 2 iterations, 21 subsets, time-of-flight information, point

spread function correction, 200 x 200 matrix, 4.07 mm x 4.07 mm x 2.03 mm voxel size, and 5 mm full-width at half-maximum isotropic Gaussian post-filtration.

To compare the DDG and the Anzai waveforms, the Pearson correlation coefficient was calculated for all the phantom acquisitions. The correlation coefficient was calculated for the time portion of the waveforms corresponding to an 80 mm axial extent centered around the axial motion extent of the phantom spheres. To assess the impact on quantification, for all acquisitions and reconstructions, we measured SUVmax and SUVpeak. Measurements of SUVmax and SUVpeak were made by drawing an encompassing region of interest around the spheres. All measurements were made in MIM 6.6 (MIM Software, Inc.; Cleveland, OH). To compare the relative performance in quantification between the two reconstructions, the ANZ_EMDB reconstruction was considered to be the ground-truth measurement. For each acquisition, the ratio of DDG_EMDB SUV to ANZ_EMDB SUV was calculated for each sphere and then averaged across all spheres. This was calculated for SUVmax (RSmax) and SUVpeak (RSpeak) respectively, and was the metric used for comparison of reconstruction quantification.

3.3.3 Patients

Forty-three patients (22 males and 21 females mean age: 62.4 ± 15.1 ; mean BMI: 28.3 ± 6.6) having at least one lung or liver tumor less than 3 cm in diameter and located in regions impacted by respiratory motion were recruited for this study (MDACC IRB 2015-0989). Informed consent was obtained prior to imaging. Patients were instructed to fast for 6 hours before injection of 322 ± 56 MBq ^{18}F -FDG. The injection to scan delay time was 68.9 ± 9.3 min.

3.3.4 PET Scan and Image Reconstruction

All patient scans were performed with the same PET/CT system and protocol as the phantom scan except that the CT used for attenuation correction was acquired under free breathing and the PET table speed was 0.8-1mm/s depending on the patient BMI. Over the lung/liver region with the tumor(s) of interest, a 30 cm section of the scan was prescribed with a table speed of 0.5 mm/s. The Anzai system was used to acquire all external device respiratory waveforms. While the new DDG software was used to derive the CBM_DDG waveform, the ANZ_EMDB and the DDG_EMDB reconstructions were performed using the same reconstruction parameters as those of the phantom scan.

3.3.5 Patient Waveform Comparison and Image Quantification

The Pearson correlation coefficient was used to compare the Anzai and the CBM_DDG respiratory signals for the patient respiratory waveforms between the aortic arch and the center of the right kidney. These anatomical locations were chosen because they are impacted the most by respiratory motion. Other areas such as the upper lungs and the lower abdomen are less affected by respiratory motion.

To assess the impact of the motion correction algorithms on tumor quantification, SUVmax and SUVpeak were measured. At the time of the examination, some patients' tumors had resolved or did not have a discernable uptake and so measurements of FDG foci (renal medullae, spleen, and gastrointestinal) which were under the influence of respiratory motion were made. Only one measurement per patient was made to avoid bias from patients with multiple tumors. The mean SUVpeak and SUVmax across all patients was calculated for each reconstruction, and the percent change of DDG_EMDB was calculated with respect to ANZ_EMDB. To assess the similarity in quantification of the ANZ_EMDB and the

DDG_EMDB images, a one-sided 95 % confidence interval non-inferiority test was used to determine if the DDG_EMDB images would remain within a -5% non-inferiority margin with respect to the ANZ_EMDB images for both SUVmax and SUVpeak. The one-sided 95 % confidence interval was calculated according to equation 3-1:

$$95\% \text{ C.I.} = \text{mean}(\text{DDG SUVmax}) - \text{mean}(\text{ANZ SUVmax}) - 1.645 \sqrt{\frac{s^2}{n}} \quad (3-1)$$

where s is the standard deviation of the difference between the two reconstructions across all patients and n is the number of patients. [70].

3.3.6 Physician Assessment of Image Quality

To assess whether the use of a CBM_DDГ waveform visually reduces respiratory motion blur in the images in a comparable manner to the Anzai waveform, a subjective assessment of respiratory motion blur was made by three radiologists experienced in PET/CT interpretation. One patient was assessed at a time and the coronal plane of both the ANZ_EMDB and DDG_EMDB reconstructions was displayed side by side in a randomized left to right order. The radiologists were asked to assess if there was any difference in motion blur for a specific lesion when comparing the two reconstructions. If there was no difference, both image series were assigned a score of zero. If one image series had more blur, then it was scored on a continuous scale (no motion blur (0), slightly more motion blur (1), moderately more motion blur (2), significantly more motion blur (3)). The image series with less blur was scored with a zero. The intrareader reliability of each reader was assessed by repeating 10 randomly selected patient studies. The mean motion blur score was calculated for each reconstruction. To assess the similarity in subjective image quality of the ANZ_EMDB and the DDG_EMDB images, a

non-inferiority test was utilized to determine if the DDG_EMDB images would remain within a non-inferiority margin of 0.5 motion blurring points. The 95% one-sided confidence interval was calculated according to equation 3-1, when using the motion blur scores and also changing the final term of equation 3-1 ($1.645 \cdot \sqrt{(s^2/n)}$) to be added rather than subtracted.

3.3.7 Statistical Analysis

All statistical analyses were performed using the R computing language (version 3.5.0). A two-way random effects, absolute agreement, multiple raters intraclass correlation coefficient was used to assess interreader reliability regarding the respiratory motion blur scores, whereas a two-way mixed effects, absolute agreement, multiple raters intraclass correlation coefficient was used to assess intrareader reliability regarding these scores[71].

3.4 Results

3.4.1 Phantom Evaluation

The correlation coefficients between the Anzai and CBM_DDG waveforms were 0.00, -0.40, 0.82, and 0.93 for the 0, 1, 2, and 3 cm amplitude acquisitions respectively suggesting that the quality of the CBM_DDG waveform improves as the amplitude of the phantom motion increases. Representative plots of the DDG and the Anzai respiratory waveforms are seen in Figure 3-2. Figure 3-3 shows images of the two reconstructions and a subtraction image ($ANZ_EMDB - DDG_EMDB$) for each acquisition. The subtraction image shows that the largest differences occur for the 1 cm and 2 cm acquisitions. Quantitative analysis of the phantom sphere data is shown in Figure 3-4 for RSmax and RSpeak. As the phantom motion amplitude increased, the RSmax and RSpeak values decreased beneath 1 to a lowest value of

0.93 and 0.95 for RSmax and RSpk respectively. However, the RSmax and RSpk values increased from the 2 to 3 cm acquisition.

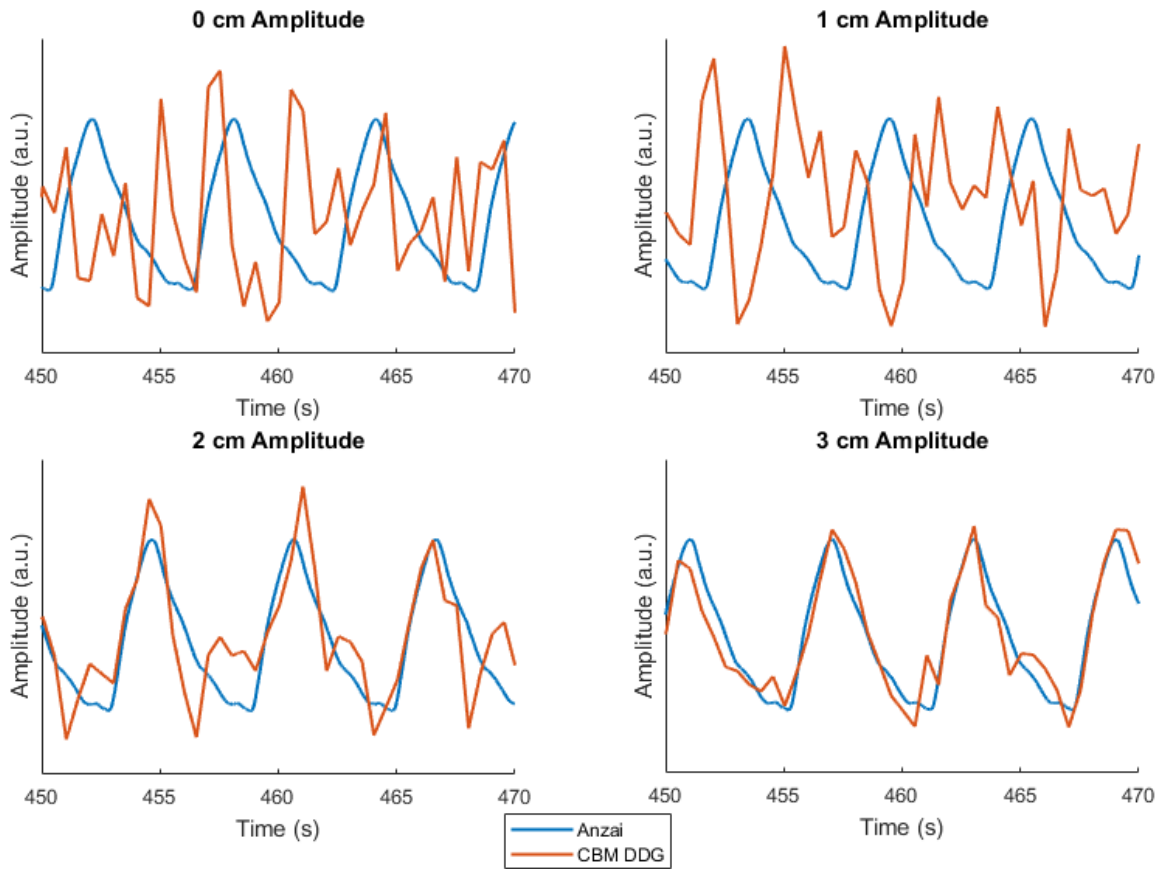


Figure 3-2 Segment of the respiratory waveform when the scanner was centered over the phantom spheres.

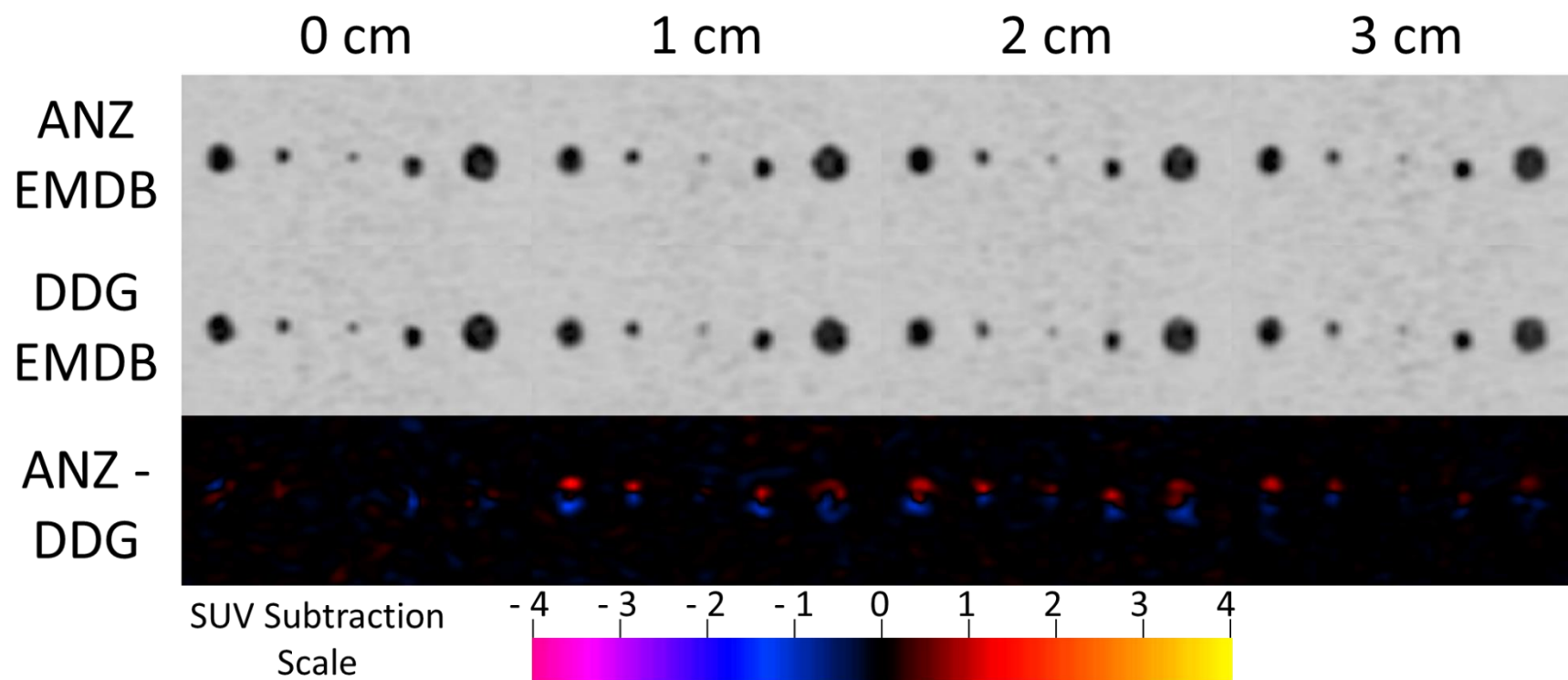


Figure 3-3 Maximum intensity projection images of the phantom for the acquisitions with varying motion amplitudes and reconstructions used in this study: ANZ_EMDB(top row) and DDG_EMDB(middle row). Subtraction images (ANZ_EMDB – DDG_EMDB) of a coronal slice along with a corresponding SUV scale (bottom row).

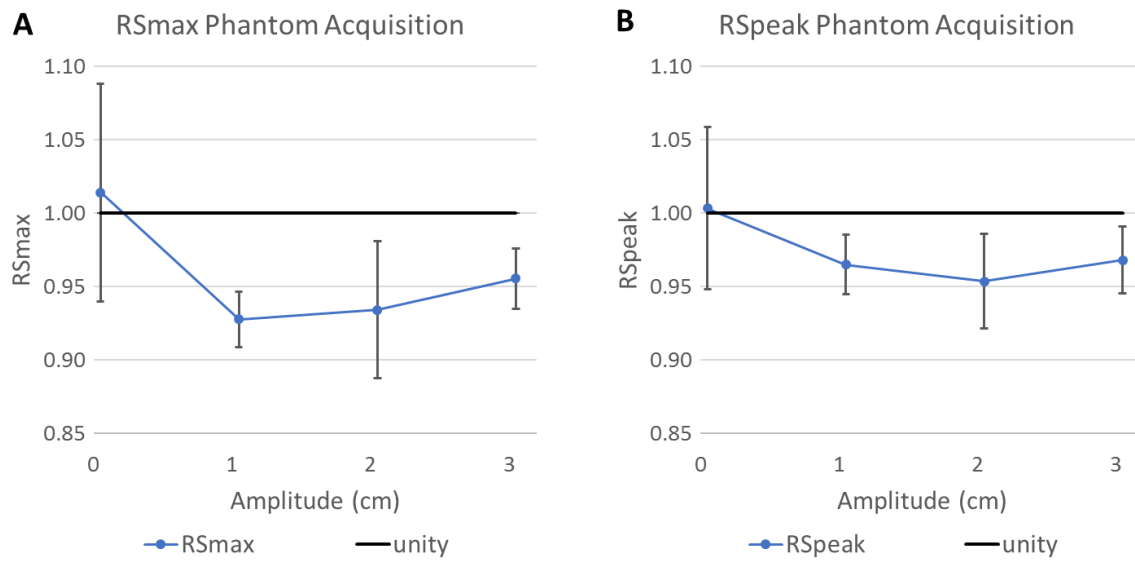


Figure 3-4 Phantom Acquisition Measurements: A)DDG_EMDB SUVmax normalized to ANZ_EMDB SUVmax for each acquisition (RSmax), B)DDG_EMDB SUVpeak normalized to ANZ_EMDB SUVpeak for each acquisition(RSpeak). Error bars represent +/- 1 SD.

3.4.2 Patient Waveform Comparison and Image Quantification

For the comparison of the patient CBM_DDГ to the Anzai respiratory waveforms, the mean \pm standard deviation of the Pearson Correlation coefficient of the zone between the aortic arch and the center of the right kidney was 0.71 \pm 0.24. A plot of the waveforms, correlations, images, and SUVs for the patient with the highest waveform correlation coefficient of 0.95, is seen in Figure 3-5.

For evaluation of the F18-FDG foci, in comparison to ANZ_EMDB, the mean DDГ_EMDB SUVmax and SUVpeak values were lower by 2.4% and 2.8% respectively. Figure 3-6 shows boxplots of SUVmax and SUVpeak of the F18-FDG foci for the two reconstructions. When compared to the non-inferiority margin of -5%, the one-sided 95% confidence interval of the percent difference between ANZ_EMDB and DDГ_EMDB was -3.9% and -4.8% for SUVmax and SUVpeak respectively. This shows that for both SUVmax and SUVpeak, DDГ_EMDB demonstrated non-inferiority in comparison to ANZ_EMDB by being within the non-inferiority margin of -5%.

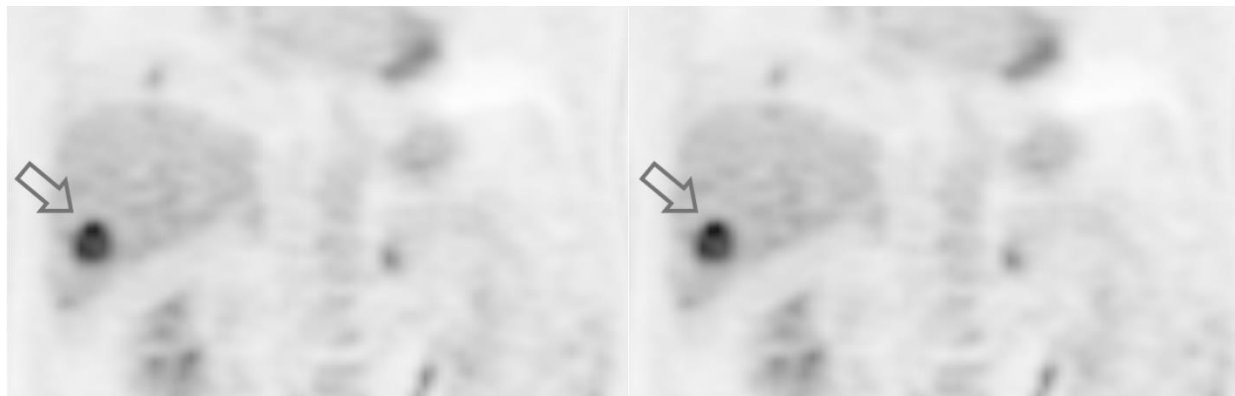
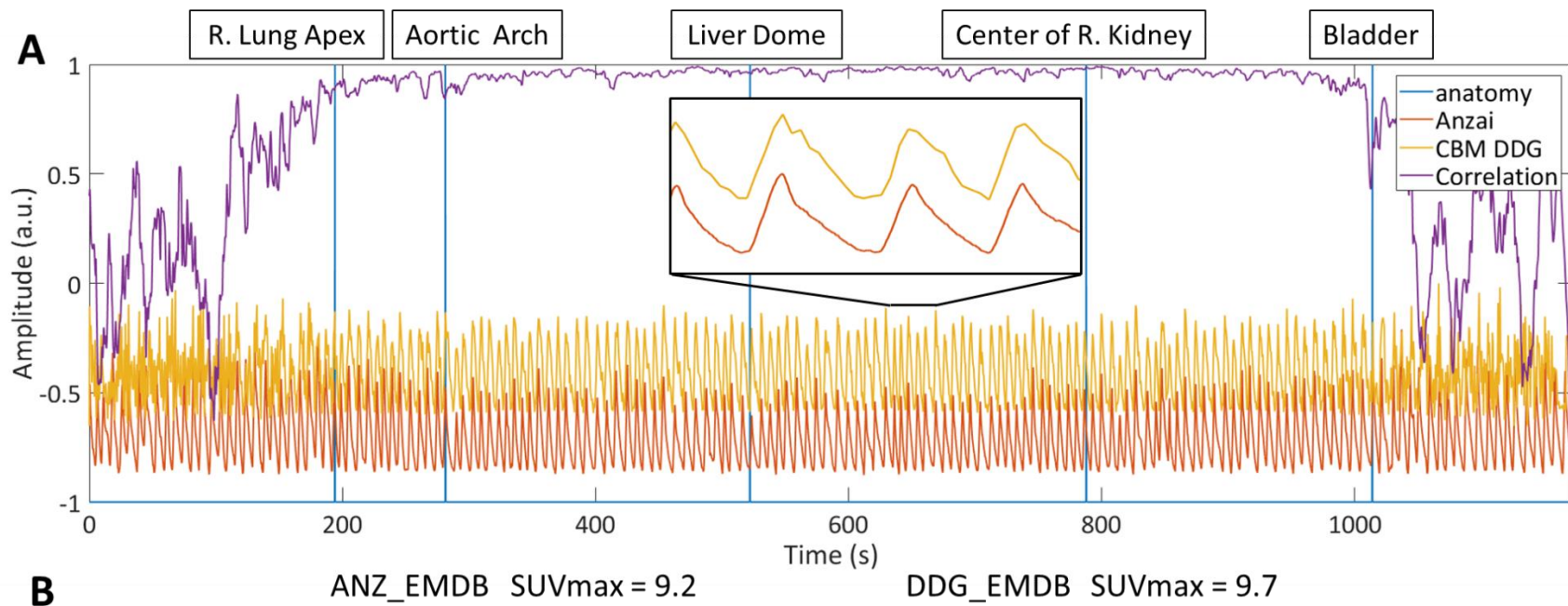


Figure 3-5 Example patient respiratory waveforms from a) CBM_DDG and Anzai along with a plot of a 30 s sliding window correlation coefficient and anatomical landmark identifiers. b) ANZ_EMDB and DDG_EMDB reconstructions along with SUVmax measurements of a lower liver lesion show little difference in motion blur in the images and show similar SUVmax quantification.

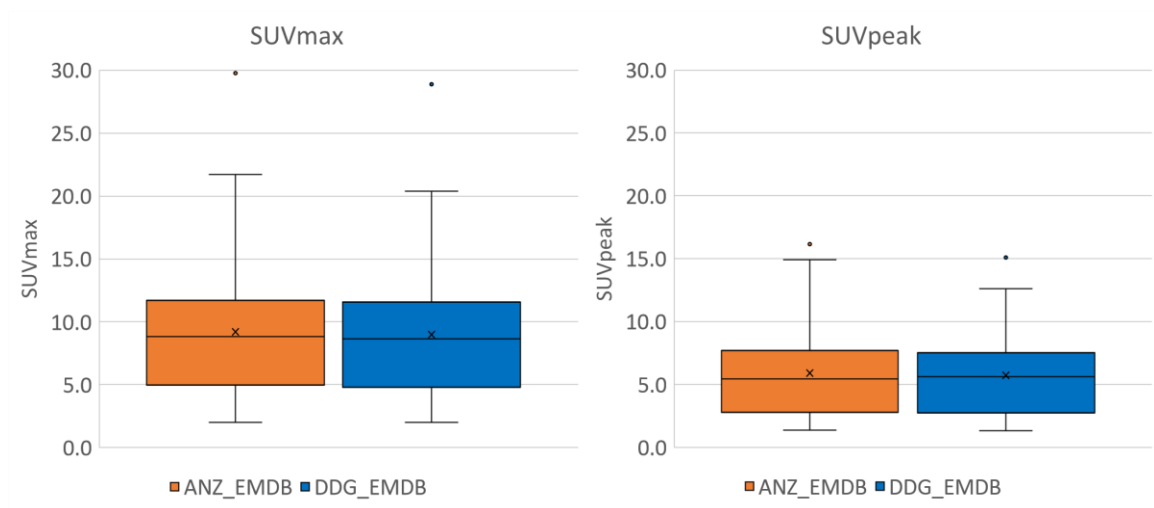


Figure 3-6 Box-plots of patient F18-FDG foci (lung/liver/spleen tumor, gastric, and kidney medulla) for a) SUVmax and b) SUVpeak for both the ANZ_EMDB and DDG_EMDB reconstructions.

3.4.3 Physician Visual Assessment

The physician average \pm standard deviation motion blur scores were 0.37 \pm 0.63 and 0.41 \pm 0.69 for ANZ_EMDB and DDG_EMDB respectively. The one-sided 95% confidence interval of the difference between the DDG_EMDB and ANZ_EMDB motion blur scores was 0.30. This demonstrated that the DDG_EMDB images as assessed by motion blur were non-inferior, falling in the non-inferiority margin of 0.5 motion blurring points. The inter-reader intraclass correlation coefficient was -0.06 indicating poor reliability between the readers (95% confidence interval, -0.43 : 0.24). The intra-rater intraclass correlation coefficients were -0.27, 0.09, and -0.30 indicating poor within-reader reliability.

3.5 Discussion

In this work we investigated the performance of the novel CBM_DDG algorithm in comparison to the Anzai external device with respect to respiratory waveforms, SUV quantification, and physician visual assessment of respiratory motion blur. To the best of our knowledge, this is the first published comprehensive evaluation of the CBM_DDG algorithm with both a phantom study and a relatively large patient population that also included quantitative (SUV analysis) and qualitative evaluation (physician reads of image quality). Our investigation showed that this CBM_DDG algorithm holds promise as an alternative to external devices. This is supported by experienced radiologists finding that the DDG_EMDB images are non-inferior to the ANZ_EMDB images, and that waveform correlations in the phantom and patient scans were relatively high. This is also supported by the measured similarity in quantification between the DDG_EMDB and ANZ_EMDB patient images which showed that the DDG_EMDB images are non-inferior to the ANZ_EMDB images as measured by SUV_{max} and SUV_{peak}.

As expected in the phantom, the correlation of the respiratory waveforms between the Anzai and DDG increased as the amplitude increased. However, with 1 cm of motion amplitude, the CBM_DDG algorithm had a negative correlation coefficient most probably due to a signal polarity flip, resulting in a value of -0.43. This polarity inversion is seen in Figure 3-2 as the troughs of the CBM_DDG waveform align with the peaks of the Anzai waveform. The CBM_DDG algorithm uses the y-standard deviation signal from the Anterior-Posterior changes in the chest and abdominal wall as the patient breathes to determine the polarity, and this phantom was not designed to mimic this surface movement, providing a potential explanation for the negative correlation coefficient. Even though the polarity was incorrectly assigned, the absolute value of the correlation was still poor at 0.43. However, as the amplitude increased, the correlation with the Anzai waveform increased up to 0.93 when using the largest motion amplitude of 3 cm. The phantom demonstrates a challenge that the CBM_DDG and all DDG algorithms face in that as there is less underlying respiratory motion of the anatomy, the quality of the DDG signal will degrade. However, as the amount of respiratory motion decreases, so too does the importance of performing respiratory motion correction, because the presence of motion blur and decreases in measured activity concentration eventually subsides.

When viewing the ANZ_EMDB and DDG_EMDB phantom images it is hard to see any differences, however, the subtraction images showed that the largest differences between the two reconstructions occurred for the 1 cm and 2 cm acquisitions. This can be explained by the fact that of the acquisitions with motion, the 1 and 2 cm acquisitions had the lowest waveform correlation coefficients. The differences in waveforms results in selection of different PET data for the reference image of the EMD algorithm. The subtraction images with motion show that with respect to the location around each sphere, the most positive(red) values, which indicate the ANZ_EMDB values were higher, occur in the superior locations corresponding to the end of expiration breathing position, while the most negative(blue) values, which indicate the

DDG_EMDB values were higher, occur in the inferior locations corresponding to a sphere position during inhalation. These subtraction images show that the Anzai waveform results in a better selection of the data from the end of expiration for the 1 cm and 2 cm acquisitions. However, for the 3 cm acquisition the subtraction image is much lower in intensity due to the DDG waveform improving as the sphere motion increases.

Based on the results of the waveform analysis and phantom subtraction images, it follows that as the amount of motion increased, that the RSmax and RSpeak values for DDG_EMDB were lowest for the 1 and 2 cm acquisitions with values of 0.93 and 0.95 for RSmax and RSpeak respectively. As expected, the values then improved for the 3 cm acquisition with values of 0.96 and 0.97 for RSmax and RSpeak respectively. Respiratory motion causes the most severe blurring and underestimation of activity concentration at the most extreme motion amplitudes, however, in this scenario, when motion correction is most needed the phantom evaluation showed that the CBM_DDG algorithm performs its best with respect to image quantification.

For the analysis of the patient respiratory waveforms, the average correlation coefficient was not as high as seen in previous DDG publications, typically above 0.8 [32,62,68]. However, in our results we did not remove cases with Anzai waveforms of poor quality, which when interpreting the correlation coefficient give the impression that the CBM_DDG waveforms were of poor quality. We performed a second analysis in which we removed waveforms from the average correlation coefficient calculation that were non-physiologic in appearance, and those that had high percentages of signal saturation at either the minimum or maximum values. When these cases (11/43) were removed, the average correlation coefficient increased from 0.71 +/- 0.24 to 0.80 +/- 0.16, which is more aligned with previous findings. Figure 3-5 shows the patient with the highest correlation coefficient between the aortic arch and the center of the right kidney. The figure shows that the correlation between the two waveforms increases dramatically when nearing the apex of the lungs, reaches its highest values between the liver

dome and the center of the right kidney, slowly falls off until the center of the bladder, then sharply falls off afterwards. Viewing a multi bin gated reconstruction of this patient reveals that there are substantial amounts of motion between the aortic arch through the top of the bladder in which respiratory motion is apparent. In addition to the normal physiologic radiotracer distribution, this patient had liver metastasis and high uptake levels in the bowel. In this patient scenario the CBM_DDG algorithm is expected to perform very well. Of the acceptable Anzai waveforms, the lowest correlation coefficient was 0.15 due to a poor DDG waveform. In contrast to the previous patient, this patient did not have as much respiratory motion and the only region with high contrast uptake was the kidneys. Approaching the kidneys, the correlation increased dramatically above 0.8, then steadily fell off after the kidneys most likely due to low amounts of radiotracer accumulation influenced by respiratory motion.

Consequently, in the CBM_DDG multi bin gated images, the kidney region shows that the respiratory motion is captured, while the heart and the dome of the liver are not in motion, contrary to the corresponding Anzai images which show heart and liver dome motion. This highlights that when there are lower amounts of motion and radioactivity present, the CBM_DDG algorithm will not perform as well as external devices.

The comparison of waveforms in patients does not tell the entire story. Since the CBM_DDG waveform is derived from the internal motion, rather than external devices which are surrogates of internal motion, outcome measures on the impact of quantification were necessary. To demonstrate that the CBM_DDG algorithm can replace the Anzai external device for measuring a patient's respiratory waveform with respect to SUV quantification, we performed non-inferiority tests for both SUV_{max} and SUV_{peak}. We chose a non-inferiority margin of -5% of the average ANZ_EMDB SUV. If the one-sided 95% confidence interval of $(SUV(DDG_EMDB) - SUV(ANZ_EMDB))$ was $> -5\%$ of the average ANZ_EMDB SUV, then the non-inferiority of DDG_EMDB to ANZ_EMDB was established. Previous evaluations of

the EMDB algorithm[54] showed an average increase in comparison to non-motion corrected images of 19.3% and 11.1% with respect to SUV_{max} and SUV_{peak}. We chose -5% for the non-inferiority margin as a difference that is acceptable in comparison to the current gold standard ANZ_EMDB measurement, because the -5% non-inferiority margin is narrow enough to avoid accepting the DDG_EMDB algorithm if its quantification results are too close to the non-motion corrected images. Non-inferiority was proven for the measurements of SUV_{max} and SUV_{peak} having one-sided 95% confidence intervals of -3.9 % and -4.8 %. When considering this and that the DDG_EMDB SUV_{max} and SUV_{peak} measurements were lower than ANZ_EMDB by only 2.4% and 2.8% respectively, this shows that the CBM_DDГ algorithm can replace the Anzai external device for measuring the patients' respiratory waveform with respect to SUV quantification in patients.

The physician visual evaluation of image quality showed that the DDG_EMDB images are non-inferior to the ANZ_EMDB images with respect to the presence of respiratory motion blur. We chose the non-inferiority margin as 0.5 blurring points, being between 0(no blur) and 1(slightly more blur), as a value that signified negligible increases in the visual perception of respiratory motion blur. For the visual evaluation, we only performed an assessment of the presence or respiratory motion blur as this was the most pertinent subjective assessment to make in a respiratory motion correction study and because the overall image quality of the EMDB algorithm has been previously evaluated when using the Anzai for the respiratory waveform[54]. Overall image quality scores are dependent on image noise, however, both the ANZ_EMDB and DDG_EMDB reconstructions used the same data set so we do not expect there would be any difference in image noise. One challenge with this study was that the inter and intra reader reliability was poor. However, this poor reliability was likely because the difference in respiratory motion blur was very subtle and hard to discern. This probably made it difficult to reproduce the scoring of the images between the radiologists when scoring all patient

cases and within each radiologist when 10 cases were repeated. Based on these results of the physician evaluation, we expect that the DDG_EMDB can replace the ANZ_EMDB images having little discernable difference.

One potential limitation with this study is that although all patients that were recruited had at least one lung or liver tumor < 3 cm in diameter on prior examinations, not all tumors were present or metabolically active at the time of the examination. This was the case for 5/43 patients, and as an alternate for each of these patients a single F18-FDG focus was analyzed resulting in 1 gastric focus, 3 kidney medulla foci, and 1 splenic focus. Another limitation of the patient evaluation was that we included the results from all patients even if the Anzai respiratory waveform had issues as was the case in 11/43 patients. One of the inherent challenges of using external devices is that they are liable to failure, and so we wanted to capture how well the CBM_DDG algorithm functions in comparison to the Anzai when the Anzai failed and include this in the summary of the results. The final limitation of the patient study was that a free breathing CT was used to perform attenuation correction, and could have resulted in inaccuracies in quantification when performing attenuation correction[72].

One limitation of the phantom evaluation was that only a single sphere to background ratio, 5:1, was used in this evaluation. As the background ratio increases, it is expected that the CBM_DDG algorithm would perform better. In addition, the size of the object(s) that are moving influences the quality of the CBM_DDG signal. Future work should evaluate the CBM_DDG algorithm at lower sphere to background ratios to determine the limits of functionality for the CBM_DDG algorithm. This is an important consideration since motion correction for low contrast objects is arguably the most important task for visual detection, and it could be the case that the CBM_DDG algorithm becomes unreliable with low uptake and with small moving objects. Another limitation of the phantom study is that the CBM_DDG algorithm has been optimized to work on patient datasets, and not on phantom datasets.

Furthermore, the phantom used in this study was not anthropomorphic in design and did not represent typical biodistributions that would be seen in the patient, both of which should be considered in future investigations.

A prior study has shown that the performance of DDG algorithms degrades as the number of detected events decreases[68] and future work should investigate how this impacts the CBM_DDG algorithm. This is an investigation that could be performed by randomly removing fractions of the events from the PET LIST mode files that were already acquired for this investigation. In addition, it is not known how utilization of high table speed acquisitions used for dynamic PET imaging will impact the CBM_DDG algorithm, and this remains a topic of future investigation. In this investigation, only patients scanned with F18-FDG were included in the research protocol, and future work should investigate the performance of the CBM_DDG algorithm with radiotracers that are gaining more widespread use clinically such as Ga-68 DOTATATE and F18-Fluciclovine.

As future PET scanner technology improves, so too should the CBM_DDG algorithm. The recently introduced Siemens Biograph Vision[8], has a sensitivity that is 70.3% higher than the mCT Flow used in this study, which should improve the quality of the CBM_DDG signal, although it is likely that the higher sensitivity will be traded in to reduce the total injected activity. In addition, the time of flight resolution of the Biograph Vision has improved substantially from 540 ps to 210 ps, which could improve the signal to noise ratio of the histo-projections which are central to the CBM_DDG algorithm (Figure 3-1). This should result in an improved CBM_DDG signal.

3.6 Conclusion

This study showed that the CBM_DDG waveform produces similar results in all evaluations performed when compared to the Anzai waveforms. Consequentially, the CBM_DDG algorithm shows promise to overcome the need for external hardware to measure respiratory waveforms.

Chapter 4: Evaluation of the impact of step and shoot and continuous bed motion PET acquisition modes on respiratory motion correction

4.1 Abstract

Continuous bed motion (CBM) was recently introduced as an alternative to step-and-shoot (SS) mode for PET/CT data acquisition. In CBM, the patient is continuously advanced into the scanner at a preset speed, whereas in SS, the patient is imaged in overlapping bed positions. Previous investigations have shown that patients preferred CBM over SS for PET data acquisition. In this study, we investigated the effect of CBM versus SS on patient breathing and respiratory motion correction. One hundred patients referred for PET/CT were scanned (50 each in CBM and SS mode) using a Siemens mCT scanner. Patient respiratory waveforms were recorded using an Anzai system and analyzed using four methods: 1-2 measured the coefficient of variation (COV) of the respiratory cycle duration (RCD) and amplitude (RCA). Method 3 measured the respiratory frequency signal prominence (RSP) and method 4 measured the width of the HDChest optimal gate (OG) window when using a 35% duty cycle. Waveform analysis was performed over the abdominothoracic region which exhibited the greatest respiratory motion and the results were compared between CBM and SS. Respiratory motion correction was assessed by comparing the ratios of SUV_{max}, SUV_{peak}, and CNR of focal FDG uptake as well as Radiologists' visual assessment of corresponding image quality of motion corrected and uncorrected images for both acquisition modes also. The respiratory waveforms analysis showed that the RCD and RCA COV were 3.7% and 33.3% lower for CBM compared to SS respectively, while the RSP and OG were 30.5% and 2.0% higher respectively. Image analysis

on the other hand showed that SUV_{max}, SUV_{peak}, and CNR were 8.5%, 4.5%, and 3.4% higher for SS compared to CBM respectively, while the Radiologists' visual comparison showed similar image quality. However, for all these results there were no statistically significant differences between SS and CBM, suggesting that motion correction is not impacted by acquisition mode.

4.2 Introduction

One of the unique advances in whole-body positron emission tomography / computed tomography (PET/CT) is the acquisition of PET data with continuous bed motion (CBM) [73]. Siemens Healthineers (Erlangen, Germany) recently introduced this data acquisition technology on their PET/CT systems with the commercial name of FlowMotion [31]. Currently, the most common mode of PET data acquisition is step and shoot (SS), which advances the patient into the scanner in incremental steps, with each step being followed by acquisition of PET data while the bed is stationary.

Acquisition of PET data in CBM mode has many advantages over SS mode. For SS acquisition, it is necessary to overlap each bed position to maintain uniform levels of image noise axially. In CBM acquisition, on the other hand, the patient passes continuously through the entire PET detector, so all objects are sampled uniformly by the detector. Studies have shown that while there are minimal differences between CBM and SS when measuring the maximum and mean standardized uptake value (SUV) in tumors, the standard deviation of the SUV in both phantom and patient data were higher for SS than for CBM acquisitions [69,74]. In addition, with CBM, the end-plane images are acquired in the center of the PET detector, resulting in lower image noise in the most inferior and superior images than that in SS mode which has the lowest sensitivity at these corresponding locations. These improvements in end-plane image quality have been observed when using CBM in both patient and phantom studies

[31,69,74]. However, an assessment of image quality by radiologists blinded to the acquisition mode demonstrated no consensus in preference for CBM over SS with one study showing a significant preference for CBM images [74] while the second study showed no significant preference [69].

Another advantage of CBM is that speed zones can be prescribed in variable lengths to the nearest 0.5 cm, allowing for greater precision, flexibility, and organ-centric scan prescription than with SS acquisition. In SS mode, a whole extra bed position must be prescribed when the imaged area is slightly larger than the axial extent of the detector. In addition to the resultant increase in acquisition time, any anatomy that does not have to be imaged but is included in the SS PET prescription will be unnecessarily exposed to CT radiation. In one study, researchers compared the CBM scan prescription used in patient examinations with the SS prescription that would have been used for these patients. On average, the scan length was 3.5% shorter and the CT radiation dose was 0.5 mSv lower in CBM mode than in SS mode [75]. Another important consideration for PET scans is the patient experience, and this was investigated in a randomized crossover study in which patients were scanned in both CBM and SS mode, and the study showed that patients strongly preferred CBM because it has less abrupt motion, is quieter, and is more relaxing [69].

None of these previous studies, however, evaluated the impact of CBM and SS acquisition modes on patient breathing and the effect these two modes have on respiratory motion correction. Respiratory motion blur in PET/CT can cause a multitude of challenges, including decreased tumor detectability, underestimation of radiotracer concentrations, and misalignments with anatomical images in areas affected by respiratory motion [14,16]. Although numerous methodologies have been developed to correct for respiratory motion blur [21,22,54,76], several studies have demonstrated that the regularity of patient breathing patterns

can greatly impact the efficacy of PET images both without and with respiratory motion correction [25,77,78].

In the present study, we prospectively assessed the impact of CBM and SS acquisition modes on the regularity of patient breathing and quantitative and visual assessment of respiratory motion corrected images in PET/CT. To the best of our knowledge, this is the first time such an investigation has been performed. Should CBM or SS produce patient breathing with more regularity and consequently higher quality of motion corrected images, this would provide valuable information on which acquisition mode is superior for respiratory motion corrected studies in PET/CT.

4.3 Methods

4.3.1 Patients

100 patients with varying disease stages referred for PET/CT imaging were recruited for this study. 50 patients were assigned to CBM mode, while 50 others were assigned to SS mode. To ensure even distribution between the BMI ranges in both groups, patients were recruited to fill five body mass index (BMI) ranges ($BMI < 20$, $20 \leq BMI < 25$, $25 \leq BMI < 30$, $30 \leq BMI < 35$, and $BMI \geq 35$) at 10 patients per range.

The CBM and SS modes were assigned randomly, and patients were blinded to the acquisition mode. Fifty-seven male and 43 female patients were scanned (mean age, 56.2 ± 13.7 years; mean BMI, 28.7 ± 8.7). Contrast CT studies can be very unpleasant for patients, so to reduce potential variables which could influence patient breathing, only patients undergoing non contrast CT scans were recruited. Patients fasted before injection of 352.2 ± 39.8 MBq ^{18}F -fluorodeoxyglucose. The mean \pm standard deviation time from injection to the start of PET

acquisition was 68.5 ± 8.9 min. This study was approved by the Institutional Review Board (IRB 2015-0986), and all patients gave written informed consent to participate prior to imaging.

4.3.2 PET/CT Acquisition and Image Reconstruction

All patients were scanned using a four-ring Biograph mCT Flow system (Siemens Healthineers), which was previously characterized [7]. A free-breathing helical CT scan was acquired for attenuation correction and anatomical localization using CARE Dose4D (quality reference 90 mAs), CARE kV (quality reference: 120 kV), a 16 x 1.2 mm detector configuration, and a pitch of 1.4. For the PET acquisition, clinical CBM table speeds and equivalent SS bed times were prescribed based on BMI. For BMIs less than 40, scans from the top of head to the pelvis were acquired at 1 mm/s (2.3 min/bed), and scans of the lower extremities were acquired at 1.5 mm/s (1.5 min/bed). For BMIs greater than or equal to 40, these values were 0.8 mm/s (2.8 min/bed), and 1.5 mm/s (1.5 min/bed) respectively. For both modes of acquisition (CBM and SS), patient respiratory waveforms were recorded throughout the whole-body scanning using an AZ-733V respiratory gating system (Anzai Medical, Tokyo, Japan) with the Anzai load cell fixing belt placed between the xyphoid process and umbilicus. All respiratory waveforms were acquired using the Siemens Healthineers PET/CT software interface, which allowed for determination of when the SS table transition times occurred. PET image reconstruction was performed with and without motion correction using: 2 iterations, 21 subsets, time-of-flight information, point-spread function correction, 200 x 200 matrix, 4.07 mm x 4.07 mm x 2.03 mm voxel size, and 5-mm full width at half-maximum isotropic Gaussian post-reconstruction filter. Reconstruction without motion correction for both acquisition modes (CBM and SS) will here onwards be referred to as static whole body (SWB), while reconstructions with motion correction for both acquisition modes (CBM and SS) were

performed using a recently introduced respiratory motion correction algorithm(OncoFreeze) that utilizes elastic motion deblurring(EMDB)[54].

4.3.3 Respiratory Waveform Analysis

To evaluate the impact of the CBM and SS acquisition modes on the regularity of patient breathing, we analyzed the quality of the corresponding patient respiratory waveforms using multiple approaches. All analyses were performed at the location of the fourth bed position, as this location is most likely to cover the lower lung to upper abdominal area where respiratory motion blur is most severe. For waveform analysis corresponding to CBM acquisitions, we selected a segment of the waveform that came from an equivalent time period as bed four for the SS patients, based on the BMI dependent acquisition time of the SS protocol ($t = 6.9:9.2$ min for $BMI < 40$, $t = 8.4:11.2$ min for $BMI \geq 40$).

The regularity of the patient respiratory waveforms acquired during CBM and SS data acquisition was determined using four analysis techniques. The first, and second analysis techniques measured the coefficient of variation (COV) of the respiratory cycle durations (RCD) and the respiratory cycle amplitude (RCA) (figure 4-1) for the CBM and SS patient cohorts and the results were compared between the two acquisition modes. Patients with very repetitive breathing will have the lowest coefficients of variation for these values. The third technique calculated the respiratory frequency range signal prominence (RSP) [62]. The RSP calculates the ratio of the energy spectral density of the signals within a respiratory frequency range corresponding to human breathing to the energy spectral density of the signals outside this range, usually attributed to nonrepetitive respiratory breathing and signal noise (figure 4-1). Based on observations of our patient population, we defined the human respiratory frequency

range as 0.1-1.0 Hz (1-10 s). A high RSP is indicative of a waveform that is more repetitive than one with a lower RSP. RSP data for both CBM and SS patient cohorts were then compared. Finally, in the fourth technique, the optimal gate (OG) width was calculated according to the HD Chest algorithm with 35% of the breathing signal falling within this amplitude width [22]. All OG widths were normalized to the same amplitude range. The OG width for patients with nonrepetitive breathing should be wider and cause more respiratory motion blur than that for patients with repetitive breathing who consistently return to the same end-of-expiration location in the breathing cycle (figure 4-1). OG width data were then compared between the two acquisition modes (CBM and SS). For all analysis methods the measurements were summarized by their medians [interquartile range] and the percent changes in the medians between the two data acquisition modes (CBM and SS) were calculated with respect to the SS medians.

To assess the impact of abrupt SS transitions between bed positions immediately following the transitions, the above four waveform analyses were repeated for the first 30 s of bed position 4 and the results were compared with those for the last 30 s of that bed position. The comparisons were performed on waveforms that were acquired within the CBM and SS groups independently. All measurements comparing the first and last 30 s were summarized by their medians [interquartile range] and the percent changes in the medians were calculated with respect to the first 30 s medians.

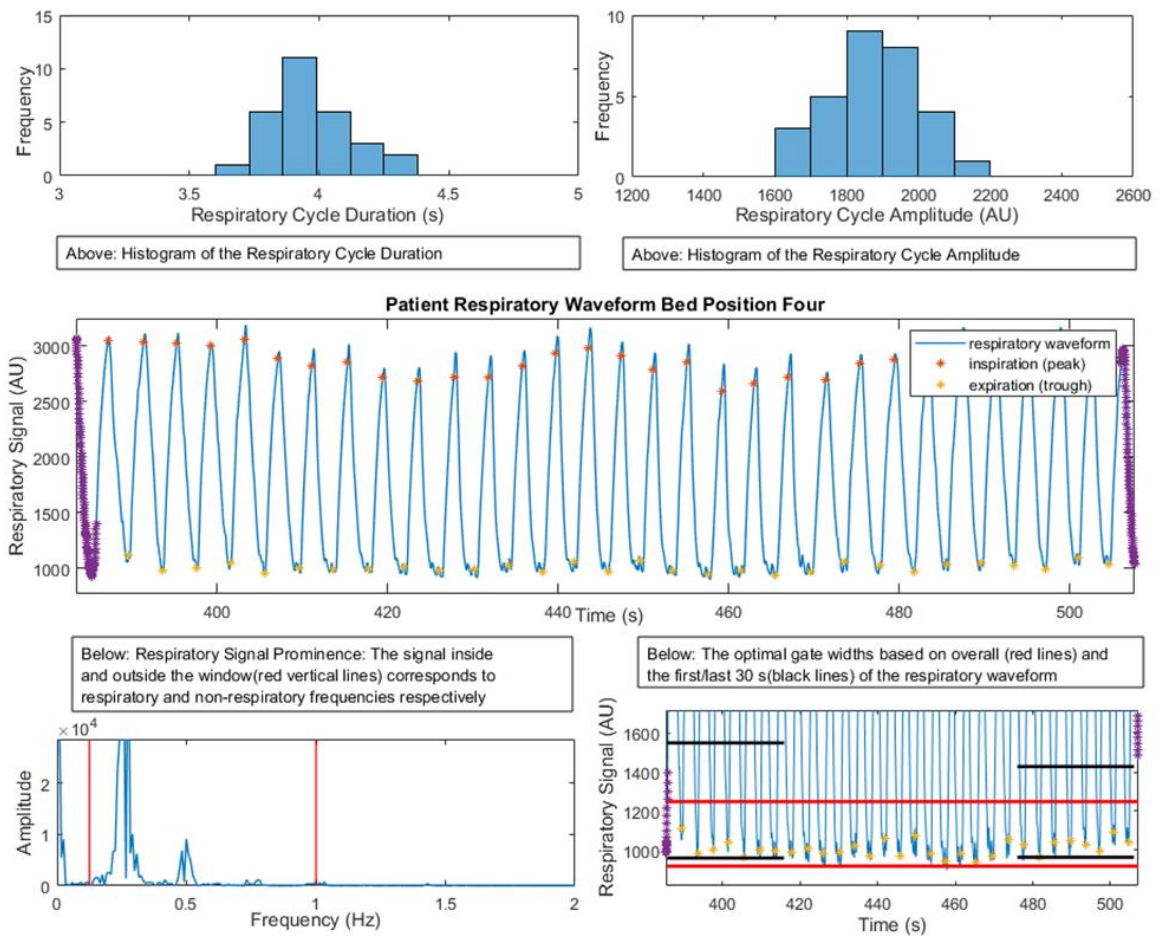


Figure 4-1 An example patient respiratory waveform at bed position four along with the four different analysis techniques

4.3.4 Respiratory Motion Quantification and Image Quality Assessment

To assess the impact of CBM and SS on image quantification and quality of motion corrected images, we measured SUVmax, SUVpeak, and CNR on various foci of FDG uptake (tumor, kidney medullae, spleen, and gastrointestinal). Since this is a non-crossover study where we cannot directly compare quantitative measurements from CBM to those of SS, we calculated the ratio of each of these metrics in motion corrected images (EMDB) to non-corrected images (SWB) and compared the results between acquisition modes (SS vs. CBM). The CNR was calculated according to equation 4-1:

$$CNR = \frac{SUV_{max,focus} - SUV_{max,liver}}{SUV_{SD,liver}} \quad (4-1)$$

where the SUV standard deviation (SUV SD) was measured in healthy liver tissue using a 3 cm diameter spherical region of interest. Only a single focus was analyzed for each patient.

All SS image measurements were made on the reconstruction from the fourth bed. To compare similar locations in the chest and abdomen for CBM datasets, only the images from the same axial range as the fourth bed position in SS acquisition were analyzed. All measurements were summarized by their medians [interquartile range] and the percent changes in the medians were calculated with respect to the SS medians.

4.3.5 Physician Assessment of Image Quality

To assess the impact of CBM and SS acquisition modes on the visual evaluation of image quality, two radiologists experienced in PET/CT interpretation were asked to compare the patients' EMDB motion corrected images to uncorrected SWB images from bed position four (Figure 4-2). In order to compare the two reconstructions, each radiologist was presented with

side by side coronal views of the SWB and EMDB reconstructions in a randomized order and only one patient was viewed at a time. The radiologists assessed if there was any difference in motion blur between the two image series. If there was no difference, both image series were assigned a score of zero. If one image series had more blur, then it was scored on a continuous scale (slightly more motion blur (1), moderately more motion blur (2), significantly more motion blur (3)). Finally, a motion blur score difference was calculated by subtracting the EMDB score from the SWB score for each patient according to equation 4-2:

$$\textbf{motion blur score difference} = \textbf{SWBscore} - \textbf{EMDBscore} \text{ (4-2)}$$

A positive difference indicates that the SWB images have more motion blur. The acquisition mode (SS or CBM) which results in the highest motion blur score difference indicates that respiratory motion correction was most effective with that mode. The motion blur score differences were summarized by their medians [interquartile range] for the CBM and SS groups respectively. To assess the intrareader reliability of each reader, 20 randomly selected patient studies were repeated.

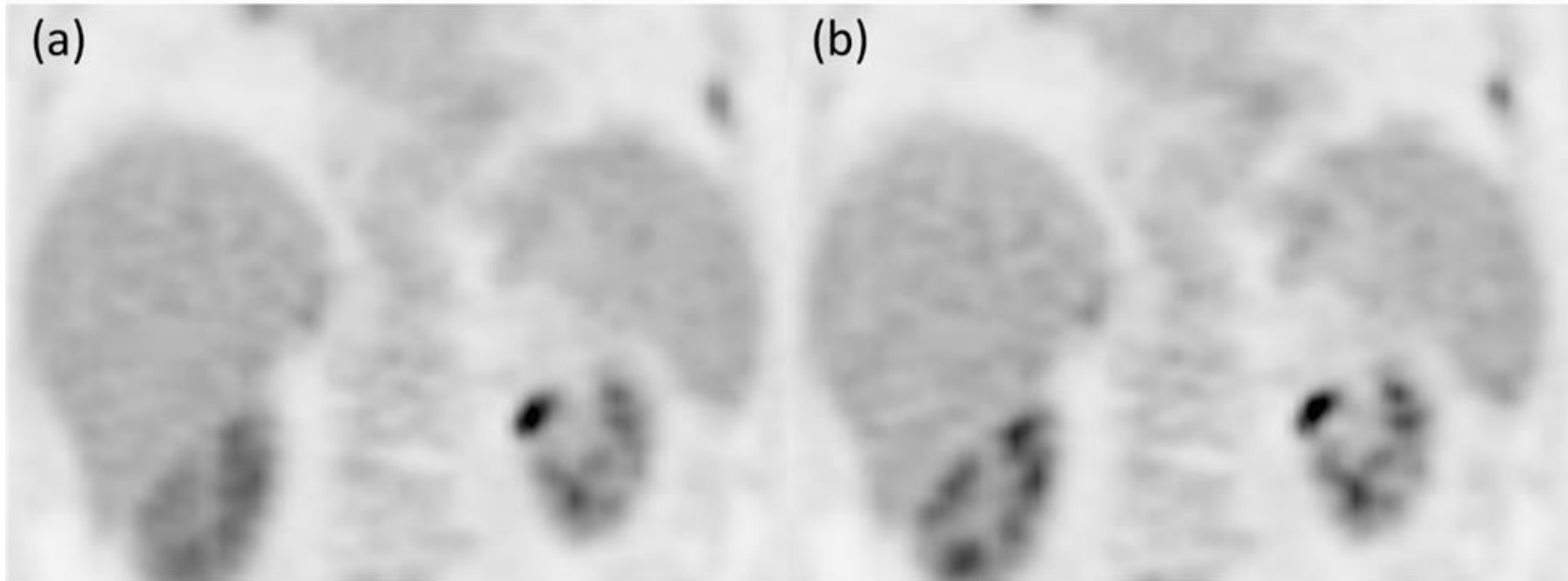


Figure 4-2 Patient images of the (a) non-motion corrected SWB and (b) the motion corrected EMDB reconstructions for physician interpretation. The images are from a CBM acquisition.

4.3.6 Statistical Analysis

All statistical analyses were performed using the Prism software program (version 7.03; GraphPad Software, San Diego, CA) and the R computing language (version 3.5.0). All waveform characteristics, respiratory motion correction measurements, and respiratory motion blur assessment scores were compared using the Mann-Whitney *U* and Wilcoxon signed rank tests for nonpaired and paired data, respectively. To control the false discovery rate due to multiple testing, the Benjamini-Hochberg procedure was used. P values less than 0.05 were considered significant. A two-way random effects, absolute agreement, multiple raters intraclass correlation coefficient was used to assess interreader reliability regarding the respiratory motion blur scores, whereas a two-way mixed effects, absolute agreement, multiple raters intraclass correlation coefficient was used to assess intrareader reliability regarding these scores [71].

4.4 Results

4.4.1 Respiratory Waveform Analysis

Results of the analysis of patient respiratory waveforms throughout the entire duration of bed position four are shown in Table 4-1. The results show that CBM has a lower COV for RCD and RCA and larger values for RSP suggesting that CBM results in more regular patient breathing; however, none of these results were statistically significant. The results also show that while RCD COV and OG had small percent changes (< 5%) in median values between the two acquisition modes, those for RCA COV and RSP had larger percent changes (> 30%).

Table 4-1 Comparison of the four different analysis methods between CBM and SS for the entire waveform duration for bed position four.

Measurement	Scan Mode	median [interquartile]	% change in median	P-value
RCD COV	SS	0.28 [0.18]	3.7%	0.86
	CBM	0.27 [0.21]		
RCA COV	SS	0.32 [0.32]	33.3%	0.55
	CBM	0.24 [0.21]		
RSP	SS	5.57 [9.04]	-30.5%	0.86
	CBM	8.02 [7.3]		
OG	SS	429.5 [293]	-2.0%	0.55
	CBM	438.4 [273.2]		

Analysis of patient respiratory waveforms of the first 30s of bed position four in comparison to the last 30 s of bed position four are shown in Table 4-2. The table shows that most results of the first 30 s were lower in comparison to the last 30 s for both the CBM and SS acquisition modes respectively, suggesting that the bed transitions in SS acquisition mode did not impact patient breathing. The results also showed that the corresponding COV values for CBM were mostly lower than SS while the RSP values were higher suggesting more regular breathing in CBM compared to SS. However, the OG results showed an opposite effect in that the CBM OG width was higher suggesting less regular breathing. Overall none of these results showed statistically significant differences between the first 30 s and the last 30 s of bed position four for both CBM and SS modes of PET acquisition respectively.

Table 4-2 Waveform analysis of the first and last 30 s of bed position four.

Measurement	Time	median	% change in	P-value
	Analyzed	[interquartile]	median	
SS RCD COV	BEG_30s	0.11 [0.19]	-47.6%	0.17
	END_30s	0.21 [0.24]		
CBM RCD COV	BEG_30s	0.14 [0.22]	-12.5%	0.98
	END_30s	0.16 [0.24]		
SS RCA COV	BEG_30s	0.2 [0.3]	-23.1%	0.98
	END_30s	0.26 [0.4]		
CBM RCA COV	BEG_30s	0.15 [0.21]	-25.0%	0.69
	END_30s	0.2 [0.2]		
SS RSP	BEG_30s	5.6 [7.6]	-13.8%	0.15
	END_30s	6.5 [9.3]		
CBM RSP	BEG_30s	6.7 [7.7]	-10.7%	0.71
	END_30s	7.5 [7.9]		
SS OG	BEG_30s	362.4 [287.4]	1.5%	0.98
	END_30s	357 [254.6]		
CBM OG	BEG_30s	405.8 [299.8]	-1.9%	0.98
	END_30s	413.6 [327.9]		

4.4.2 Respiratory Motion Quantification and Image Quality

As seen in table 4-3, the ratios of EMDB to SWB measurements for SUVmax, SUVpeak, and CNR for both acquisition modes (CBM and SS) indicated that the EMDB reconstruction improved foci quantification (ratios > 1), and detectability (ratios > 1). However, while the SS ratio was consistently higher than CBM, suggesting that motion correction was more effective in SS vs CBM for all of these measurements, none of these differences were statistically significant.

Table 4-3 Results for the motion quantification measurements. The scores are summarized as the median [interquartile].

Measurement	Scan Mode	median ratio [interquartile]	% change in median ratio	P-value
SUVmax	SS	1.28 [0.2]	8.5%	0.11
	CBM	1.18 [0.21]		
SUVpeak	SS	1.15 [0.12]	4.5%	0.11
	CBM	1.1 [0.1]		
CNR	SS	1.23 [0.41]	3.4%	0.63
	CBM	1.19 [0.36]		

4.4.4 Physician Assessment of Image Quality

The physician median [interquartile] overall score differences were 1[1] and 1[1] for CBM and SS mode, respectively ($p = 0.64$). Figure 4-3 shows the distribution of physician responses of motion blur for SS and CBM. The inter-reader intraclass correlation coefficient was 0.10 indicating poor reliability (95% confidence interval, -0.34 : 0.39). The intra-rater intraclass correlation coefficients were -0.34 and 0.24 indicating poor reliability for both readers.

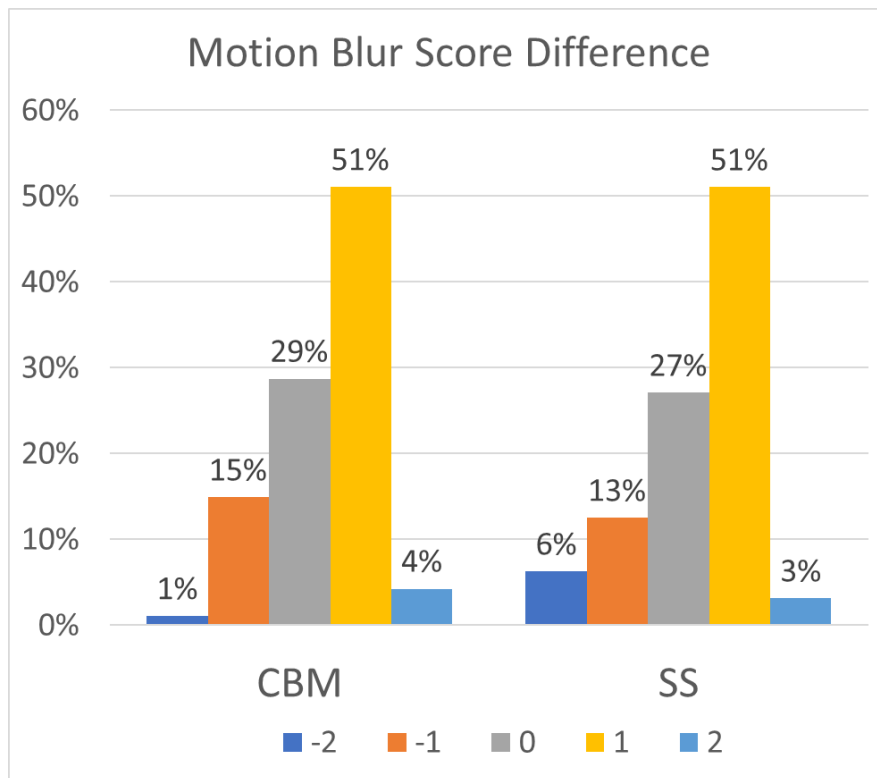


Figure 4-3 Bar Plot of the frequencies of the motion blur score differences for the CBM and SS motion blur visual analysis.

4.5 Discussion

In this work, we investigated whether CBM and SS acquisition modes impact patient breathing and consequently respiratory motion correction during PET/CT. To our knowledge, this is the first comparison study of the impact of these two acquisition modes on patients' respiratory waveforms and on respiratory motion correction. Our results showed that there is no statistically significant difference in patient breathing when PET data is acquired in CBM vs SS. Furthermore, our results showed that there was no statistically significant difference in quantitative and qualitative evaluation of motion corrected PET images when the data is acquired in CBM vs SS.

We analyzed the patient breathing waveforms using four different methods to capture all potential factors that could affect the repeatability of a patient respiratory waveform when PET data is acquired in CBM and SS. Our first overall patient respiratory waveform assessment was based on measuring the COV of the RCD. If a PET acquisition mode perturbs a patient's breathing, then the repetitiveness of the cycle duration would change, and this would be shown through an increased COV. This analysis, however, does not differentiate between normal (0.1 -1.0 Hz) and abnormal respiratory frequency ranges. For this reason, we used the RSP [62] which calculates the ratio of signals associated with normal breathing frequencies to those signals associated with abnormal frequencies. High ratios indicate repetitive breathing cycles, while smaller ratios indicate less repetitive breathing. Both of these approaches (RCD and RSP), however, do not capture any information about the breathing cycle amplitudes. For example, a patient breathing waveform might have a consistent RCD but widely varying amplitudes. In this regard we used RCA as an additional approach to assess the repeatability of the patient's respiratory cycle. Here also if a PET acquisition mode perturbs the patient's breathing, then the repetitiveness of the cycle amplitudes will change and this would be shown

through an increased COV. Finally, the choice of the OG width as another measure of the breathing cycle repetitiveness was based on its utilization in the HD Chest and OncoFreeze(EMDB) motion correction techniques. For patients with less repetitive respiratory waveforms, the OG width will be wider in comparison to more repetitive waveforms. A larger OG width is indicative of poor image quality, as it includes more respiratory motion blur in the motion corrected images. Figure 4-4 shows examples of respiratory waveforms and respective analyses of a patient with repetitive breathing and a patient with non-repetitive breathing. This figure demonstrates that when there are differences between respiratory waveforms, that the methodologies of waveform analysis used in this work captured these differences.

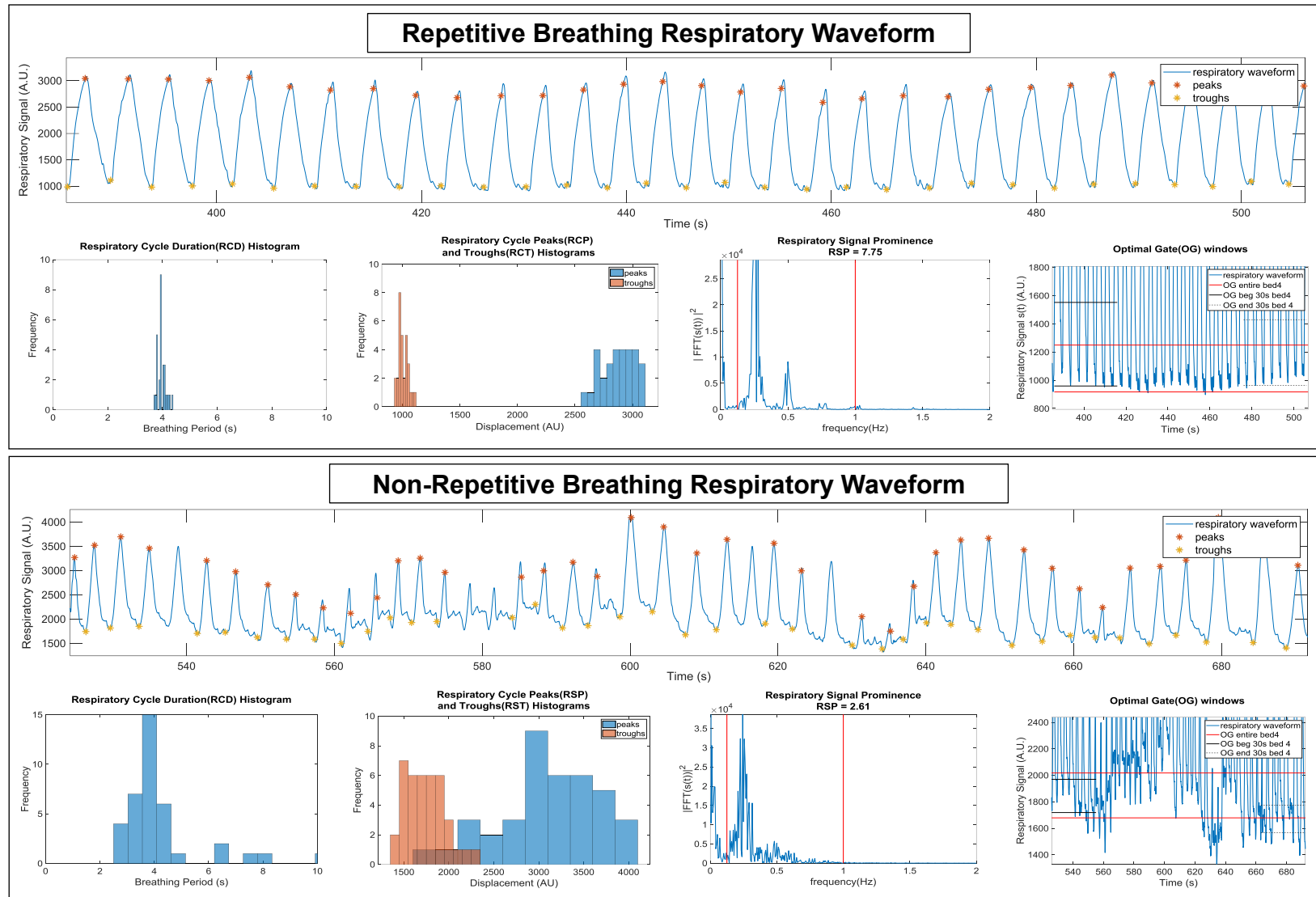


Figure 4-4 Examples of repetitive (top) and non-repetitive(bottom) respiratory waveforms and respective analyses

Although the respiratory waveform analyses over the entire duration of bed position four showed no statistical difference between CBM and SS (table 4-1), we found that the RCD COV and OG percent changes in the median between SS and CBM were very small, while the percent changes in RCA COV and the RSP were much larger. This shows that although the RCD and OG characterize certain attributes of the waveform, the RCA COV and RSP analyses captured additional information that would not have otherwise been characterized, as shown through the larger percent changes measured for these metrics. For RSP, we expected to see the SS results to be lower than those for CBM which indicates that the patient breathing was perturbed by the table transition, and our results supported this expectation although our findings were not statistically significant. On the other hand, we did not expect to see the OG width for SS to be lower than that for CBM since that would indicate that the table transition improves the repetitiveness of the patient breathing. However, here again these measurements for the whole duration of bed position four were not statistically significant. The lack of statistically significant differences in both of these cases as well as in the COV results could be explained by the possibility that any perturbations to the patient breathing that could occur immediately after the SS table transition quickly subside and are averaged out over the entire bed position time frame.

Our analysis comparing the first and last thirty seconds of bed position four was specifically conducted, so that any perturbations that might occur after the table transition will not be averaged out over the entire bed position. Our results, however, showed that there were no statistical differences in patient breathing between the first and the last 30 seconds. After the bed transition for the SS acquisition mode, we expected that all results except for the RSP would be higher in the first 30 s of bed position four due to patient breathing becoming non-repetitive as a result of the table transition, however, these values were all unexpectedly lower than the

last 30 s, except for the SS OG width. One potential explanation is that the SS table transition improves the repetitiveness of the patient breathing, a situation that needs further investigation in a future study. For CBM on the other hand we expected to see negligible differences between the first 30 s and last 30 s due to the smooth motion of the bed throughout the CBM acquisition, however, our results in table 4-2 showed that for several of the analysis methods there were unexpected differences, which for all metrics had smaller values for the first 30 s. Further analysis of this unexpected finding is warranted. Overall, most of the CBM differences were smaller in comparison to those of the SS acquisition mode, suggesting that the SS table transition has a larger impact on the patient breathing. Based on these results, we conclude that the mode of table motion has no statistically significant impact on the patient breathing. However, given that none of these results were statistically significant, we conclude that we cannot differentiate between the impact of data acquisition mode (CBM versus SS) on patient respiratory waveforms.

From the outcomes of the respiratory waveform analysis, it was not expected that the results of the respiratory motion quantification and image quality assessment would be different between the CBM and SS modes. This expectation agrees with our results which showed that although the median SS ratio was higher than the CBM ratio for SUVmax, SUVpeak, and CNR, these differences were not statistically significant. It is important to note, however, that for the ^{18}F -FDG foci that were analyzed, respiratory motion correction for both CBM and SS improved quantification and detectability as shown by the results of the ratio (>1) of EMDB to SWB for SUVmax, SUVpeak, and CNR respectively in Table 4-3.

Given the results of the respiratory waveform analysis and the respiratory motion quantification, it was also not expected to observe a statistically significant difference between the respiratory motion blur reduction of CBM and SS as determined by the radiologists. Our

results support this expectation. The median motion blur score difference was 1 and 1 respectively for CBM and SS, showing that the EMDB algorithm has a slightly perceivable reduction in motion blur in comparison to SWB, however there was no statistical difference between the two acquisition modes. Both the inter and intra reader ICC scores were poor for the physician assessment. One potential reason for this result is the slight perceivable difference in respiratory motion blur between images acquired in CBM and SS.

One limitation of this study is that most of the patients (89 of 100) in this study were scanned on an average of four times, and the majority had their last PET/CT scan at MD Anderson. These patients were aware of what to expect during a PET/CT examination, so they had much less anxiety due to fear of the unknown of being in a PET/CT scanner which could affect the regularity of their breathing independent of the acquisition mode than patients undergoing PET/CT for the first time.

Another potential limitation of this study is that it was designed as a non-crossover study. Such a study design requires a large number of patients to achieve statistical significance. Our study might not have been statistically powered with the number of patients scanned (50 patients per group) to detect differences between the two acquisition modes (CBM vs SS) for the respiratory waveform analysis, respiratory motion correction image quantification and visual assessment of motion blur score. Crossover studies require fewer patients to detect changes between two methods. However, to perform a crossover study design would require scanning the patients in both CBM and SS, thereby doubling the acquisition time, which would have been very challenging to achieve in our very busy clinic. In addition, a challenge with performing this work in a crossover study, is that the patient would have to lie on the bed for twice the amount of time, which would likely influence their breathing and consequentially the motion corrected images.

An additional limitation of the study is that we did not recruit patients specifically with lung or liver tumors in areas impacted by respiratory motion. For this reason, several patients had no lesions impacted by respiratory motion, and this is why we analyzed foci in other organs which unavoidably have varying degrees of motion perhaps less than tumors in the lung or liver. In addition, it is easier to visually assess if there is motion blur in smaller and isolated nodules, rather than assessing small structures of an organ such as the heart or the kidney, and this might have limited the radiologists' perception of respiratory motion blur if it was present in the images.

4.6 Conclusion

This study is the first to investigate and consequentially find that the choice of CBM or SS acquisition mode has no statistically significant impact on patient breathing, lesion quantification and detectability, or perceived respiratory motion blur during PET/CT examinations, suggesting that motion correction is not impacted by acquisition mode.

4.7 Acknowledgements

This work was supported in part by a research grant from SIEMENS Healthineers. We would like to thank Drs. James Hamill and Judson Jones from Siemens for their technical support in describing the recorded patient respiratory waveforms. In addition, we thank the Department of Scientific Publications for their contribution in the editing of our manuscript for publication. Finally, Christine Peterson is partially supported by NIH/NCI CCSG grant P30CA016672 (Biostatistics shared resource).

Chapter 5: Discussion

In this dissertation we sought to overcome three major challenges that hinder the routine utilization of respiratory motion correction which are: 1) poor image quality(high noise) of motion corrected images, 2) the requirement to utilize external hardware for measuring respiratory waveforms, 3) and irregular patient breathing. To address each of these challenges we validated a solution to each of these problems in three specific aims respectively: 1)use of all the data with elastic motion correction to improve image quality, 2)deviceless measurement of respiratory waveforms with data driven gating, 3) and determination of whether PET acquisition in CBM mode reduces breathing irregularities in comparison to SS acquisition mode.

5.1 Specific Aim 1

In Specific Aim 1 we sought to “*Compare the performance of a pre-commercial version of a vendor designed EMC algorithm in comparison to conventional motion correction techniques.*” The most important findings of this aim were that the EMDB algorithm had the best performance when comparing the effects of noise, resultant motion blur and contrast to noise ratio. These results are primarily due to the use of all the acquired data during reconstruction as compared to other algorithms. In contrast, conventional motion correction techniques use fractions of the acquired PET data and in this investigation we used HDChest with 35% of the data, and PBG using 12.5% of the data for each phase. As expected, when using smaller fractions of the data, the noise in the images increased in severity. We evaluated the impact on quantification in a phantom study and found that while all motion correction methodologies improved quantification, as the amplitude of the sphere motion increased, EMDB underestimated the activity concentration, HDChest was closest, and PBGmax which

uses the least amount of data had the largest overestimation of the activity concentration. In addition, EMDB had the highest CNR of the motion correction techniques.

In the patient evaluations, similar trends were seen. All motion correction methods had similar increases in SUV, except for PBGmax which had the highest increases in SUV. EMDB also had the lowest increases in image noise in the healthy lung and liver tissue. EMDB was the only method to improve the CNR. In an assessment of overall image quality, physicians preferred the currently employed clinical reconstruction, SWB, which used all the data and had no motion correction, followed in descending preference by EMDB, HDChest, and PBGmax. Even though the EMDB images had reduced respiratory motion blur in the images and had the smallest increases in image noise, the physician assessment scored SWB with the highest image quality, suggesting that noise was the most important consideration for their evaluation. SUVmax and SUVpeak are artifactually increased by image noise and so the increases we measured in this aim for all of the motion correction methodologies are influenced by image noise, but the artifactual increases for EMDB are the lowest due to utilization of all of the data in the reconstruction. Due to these combined findings, this data supported our working hypothesis which states: “due to utilization of all the acquired PET data during image reconstruction, the EMDB algorithm will have superior performance characteristics when compared to conventional motion correction methodologies”.

One limitation of the study was that a free-breathing helical CT was used for attenuation correction of the patient reconstructions, which can lead to misalignments of the PET and CT data resulting in inaccuracies in SUV quantification[72]. In addition, the EMDB algorithm applies a respiratory waveform baseline correction which can improve quantification in cases of a baseline drift in patient breathing, but this was not applied to the other motion correction methodologies. This could have given the EMDB algorithm an unfair advantage. The PET data was not acquired at the clinical table speeds, rather, a slower table speed over the chest or

abdominal region with the tumor(s) of interest was used. For this reason, the results of this study are not fully generalizable to clinical acquisition table speeds.

5.2 Specific Aim 2

In Specific Aim 2 we sought to “*Evaluate the performance of a pre-commercial version of a vendor designed CBM_DDГ technique in comparison to a conventional external device.*”

The motivation of this specific aim was to show that this CBM_DDГ technique is sufficient to replace external hardware and consequentially overcome the challenges associated with utilization of external devices which impede the routine utilization of respiratory motion correction. In the phantom evaluation, our study showed that as the amplitude of the spheres increases, the correlation between the CBM_DDГ and the ANZ waveforms increased. Respiratory motion correction becomes more urgent as the amplitude of the respiratory motion increases, and this shows that the algorithm’s performance is improved when there is a need to correct for respiratory motion. In the patient study, we found that when removing cases in which the ANZ respiratory waveform was poor, the average correlation coefficient between ANZ and CBM_DDГ was 0.80. Similar to what was observed in the phantom, for the patient with the highest correlation coefficient there were large amounts of respiratory motion, and conversely for the patient with the lowest correlation coefficient, there were small amounts of motion. To test the similarity of quantification of the CBM_DDГ images to the ANZ images, non-inferiority tests showed that the CBM_DDГ images remained with a non-inferiority margin of -5% of ANZ for both SUVmax and SUVpeak in tumors impacted by respiratory motion. The physician evaluation of the presence of respiratory motion blur showed that visually the CBM_DDГ images are non-inferior to the ANZ images. Given these findings this data

supported our working hypothesis which states: “CBM_DDG motion corrected images will be non-inferior to hardware-based motion corrected images”.

The CBM_DDG algorithm was designed and optimized for patient data. Therefore, one of the limitations of the phantom evaluation is that the phantom did not represent the more complicated biodistribution of activity in the body with moving and non-moving activity distributions. The CBM_DDG algorithm relies on determining the anterior-posterior motion of the chest and abdominal wall. This phantom did not provide this motion and so, the CBM_DDG algorithm’s performance might have been underestimated in the phantom. In the patient evaluation, some of the patients did not have lung or liver tumors and for these patients we assessed F18-FDG foci which were impacted by respiratory motion. It is possible for the visual evaluation of the images that evaluating foci in sites other than the lung or liver could have biased the results, but only 5/43 patients were evaluated in this manner.

5.3 Specific Aim 3

In Specific Aim 3 we sought to: *“Evaluate the impact of step and shoot (SS) and CBM PET acquisition modes on respiratory motion correction.”* In the previous aims, EMDB and CBM_DDG have demonstrated great promise to overcome the challenges of image noise and the requirement for external hardware. However, the efficacy of these and other motion correction methodologies is still hindered by patients who have irregular respiratory waveforms. For this reason, in Specific Aim 3, we sought to determine whether CBM could reduce the incidence of irregular respiratory waveforms in comparison to SS. In CBM the patient is continuously advanced through the scanner during the PET acquisition, while in SS the patient is incrementally advanced into the PET scanner in overlapping positions. Due to these differences in acquisition, we expected that the patient would be more relaxed in CBM and therefore have more regular breathing in comparison to SS.

We assessed the regularity of the respiratory waveforms by characterizing the respiratory cycle duration, respiratory cycle amplitude, respiratory signal prominence, and optimal gate width. The waveform analysis showed no statistically significant differences between SS and CBM. Given the above findings, we did not expect for there to be a difference when comparing the reduction of respiratory motion blur by measurement of quantification, detectability, and Physicians' assessment of respiratory motion blur reduction. Although both methodologies of motion correction improved quantification and detectability, there were no statistically significant differences between SS and CBM respectively. Finally, the Physicians' assessment showed there was no statistically significant difference in the motion blur reduction between SS and CBM. Given the lack of any statistically significant findings, this data did not support our working hypothesis which states: "CBM acquisition will reduce breathing irregularities in comparison to SS acquisition and therefore, the motion corrected CBM images will have superior motion reduction in comparison to the SS images."

Regarding limitations, this study had 50 SS and 50 CBM patients, and so it might have been underpowered to detect any statistically significant differences. To increase power, more patients could have been recruited or the study could have been performed as a crossover study in which each patient was scanned in each mode. For a crossover study it is uncertain if this prolonged acquisition time would have an impact had on the patient respiratory waveform. In this study, the patients had been scanned on average around four times, and so they were familiar with what to expect in a PET/CT scan and the difference in acquisition modes might not have impacted them as much in comparison to someone being scanned for the first time. A final limitation is that these patients were not recruited to have lung or liver tumors, so in many patients the evaluation of the impact on respiratory motion was performed using foci of ^{18}F -FDG in any organ impacted by respiratory motion, possibly making it not as easy to assess in comparison to isolated lung and liver nodules.

5.4 Future Applications

For Specific Aim 1, to overcome the mentioned challenges of misalignment with a free breathing CT, future work could explore methodologies of aligning the EMDB PET data to the free breathing CT. One method to align the PET data with the free breathing CT selects the PET data from the same respiratory waveform amplitude range that the CT scan was acquired at over that respective PET bed position[79]. This achieves improved alignment, but the PET acquisition time must be lengthened to overcome using only a fraction of the data. In a collaborative effort, we are currently evaluating a methodology that selects PET data which is aligned based on amplitude with the CT at each axial CT slice position rather than for the entire PET bed position. This alignment is performed based on an analysis of both the CT and PET waveforms [52]. This aligned PET data, which is a fraction of the total data, is then used as the reference image for the EMDB algorithm which should improve image quality. In this dissertation, we found that the radiologists preferred the SWB images and we presume that this is due to these images having a lower amount of noise in comparison to the EMDB images. However, further investigation is warranted to determine why they preferred the SWB images over the EMDB images. For the PET acquisition, the table speed was half of the default clinical speed over the abdomen or thoracic region of interest, and so the image quality and resultant quantitative measurements are not reflective of what would result with our clinical protocols. To simulate the same clinical table speeds and while using the same patient population, this could be performed by removing the necessary fraction of events from the range acquired at the slower table speed. Likewise, it is important to know how the EMDB algorithm performs in low count studies such as low activity injections, Y-90 post SIRT verifications, or multi timepoint studies. The increase in noise that the EMDB images have is a result of the determination of the blurring kernel between a noisy HDChest and the SWB image. For very

low count studies, the accuracy of the registration and increases in EMD image noise could severely worsen. Likewise, this study could be achieved, by removing the requisite fractions of the already acquired PET LIST mode data to simulate different levels of noise.

For Specific Aim 2, one of the most important future investigations to perform is a phantom study to determine the lower limits of sphere to background ratios that the CBM_DD algorithm can reliably produce a respiratory waveform. Determining these limits is important because correction of respiratory motion blur, especially for small objects with low contrast, is needed the most as these objects are the hardest to visually detect and assess. This is especially important in the lung in the scenario when the tumors are the only source of moving radioactivity due the myocardium having low radiotracer uptake as well as the liver and spleen being out of the field of view. A simulation of this scenario could be performed with patient data, by inserting moving lesions of progressively decreasing contrast into the LIST mode data set. A superior-inferior motion could be provided to the lesions based on the patient's Anzai respiratory waveform. Additionally, future work needs to investigate the impact that count rate has on the CBM_DD algorithm. Decreasing the total number of detected events increases the noise in the time of flight histogram volumes which are used by the CBM_DD algorithm to determine the respiratory waveform. This could be performed with our patient data set by removing progressively larger fractions of the LIST mode PET data. These concerns are important for studies with very low counts such as Y-90 with a very low yield of positrons, or multi-timepoint acquisitions. Another future investigation to perform is to determine how well the CBM_DD algorithm performs with newer radiotracers which have different biodistributions and are being used routinely such as ^{68}Ga -DOTATATE and ^{18}F -Fluciclovine.

In Specific Aim 3 no statistically significant differences were found between the two acquisition modes, perhaps due to the study being underpowered. To rule out that these findings were caused by a lack of statistical power, a larger study is warranted. If this future

investigation shows that CBM does not reduce the incidence of irregular respiratory waveforms, then alternative options will need to be explored. One class of options that could reduce irregular breathing is to invasively minimize respiratory motion through deep inspiration breath holds, abdominal compression, or pulsatile flow ventilation,[33,53,80]. One challenge for deep inspiration breath hold is that sick patients can have a hard time complying with the repeated breath holds required to obtain enough breath-hold PET data. However, as the sensitivity and timing performance of PET scanners improves, the total breath hold time needed will reduce and make these interventions more practical. This could be achievable in a single breath hold(15-30 s) with the whole-body United Imaging uEXPLORER PET system[81], but this scanner is prohibitively expensive being equal in axial length to 6.5 times the next longest clinically available PET scanner (uMI 780 PET/CT scanner (United Imaging Healthcare (UIH), Shanghai, China)). Breathing motion can be reduced mechanically through abdominal compression or pulsatile flow ventilation, but the major drawback is that they are both uncomfortable, invasive, and require extra setup time. An additional benefit is that these methods would achieve improved alignment between the CT and the PET data. Radiologists prefer CT images of the lungs when fully expanded, and so pulsatile flow ventilation and deep inspiration breath hold could provide this benefit. However, 60% of patients were shown to have regular breathing[25], and to avoid subjecting this majority of patients who would not benefit would require a-priori identification of patients with irregular breathing [82], or identification of patients with irregular breathing during the examination and repeat a portion of the scan. If these invasive solutions are to be used clinically, it will be requisite to minimize the burden posed to patients and to the clinic. A more feasible option is one that requires no intervention from the clinic or the patient, and this would be to develop respiratory motion correction reconstructions that work for patients with irregular breathing. Recently, a NIH funded grant (R01CA224140-02), “Personalized Task-Based Respiratory Motion Correction for

Low-Dose PET/CT”, has set out to develop methods to triage the most time effective motion correction approach and reconstruction type utilized for each patient depending on the degree of breathing irregularities that are present. Successful completion of this research goal and translation to a clinical product, is the ideal solution to the problem of breathing irregularities, rather than using invasive methodologies.

For Specific Aim1 and Aim 2, the next step would be to perform a clinical evaluation on the impact that the EMDB algorithm has on patient diagnosis, staging, and management. The number of research studies which have evaluated the clinical impact on patient care when using respiratory motion corrected images is relatively small and potential reasons for this is that the motion corrected studies involve acquiring the PET data for a longer time to maintain acceptable levels of image noise, the added complexity of needing external devices for waveform measurement and the burden of prospectively identifying and consenting patients for these studies. With the combination of EMDB and CBM_DDГ, respiratory motion correction research studies could be performed retrospectively by applying these motion correction methodologies to LIST mode data acquired with the clinical default acquisition parameters.

5.5 Conclusion

In this work we demonstrated that poor image quality which is characteristic of conventional respiratory motion correction techniques is greatly reduced with the EMDB algorithm while improving image quantification due to reductions of respiratory motion blur. We also found that the Anzai external device which requires extra set-up time and is prone to failure, can be replaced by the CBM_DDG algorithm to measure the patient's respiratory waveform. However, irregular patient breathing and the resultant degradations in image quantification and quality were not mitigated by utilization of CBM in comparison to SS for PET data acquisition. Therefore, our central hypothesis which states, "the application of EMC, DDG, and CBM for respiratory motion correction in PET imaging will result in improved image quantification and quality, decreased workflow complexity, and reduced patient breathing irregularity during PET/CT imaging", was not proven in entirety.

Appendix

6.1 EMOCO Supplemental materials

The following is taken from:

http://jnm.snmjournals.org/content/suppl/2019/02/01/jnumed.118.213884.DC1/213884_Supplemental_Data.pdf

The phantom was designed to move 5 spheres in three planes to simulate the elastic motions of the thorax and abdomen. To achieve this 3D motion, the CIRS dynamic thorax phantom (Norfolk, Virginia) motor moved the shaft of the phantom in the superior inferior direction as shown in figure-6-1.

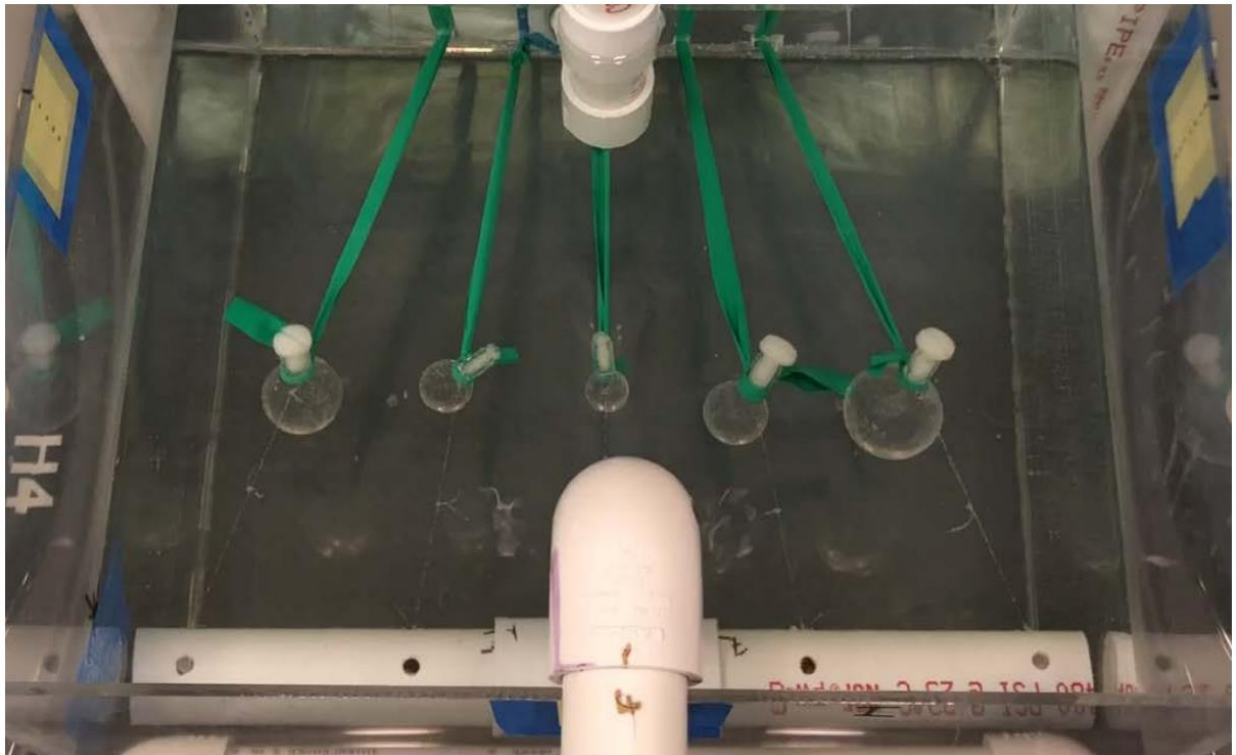


Figure 6-1 Top view of the phantom tank.

To simulate the anterior posterior motion of lung tumors, the stationary, superior attachment point of the spheres was placed at a depth of 11 cm, and the inferior mobile connection point of the spheres was placed at 6 cm, so that the depth of the spheres changed as the phantom moved.

Furthermore, the attachment points of the spheres were spaced with less distance on the superior, stationary attachment point, in comparison to the inferior attachment point, such that the spheres paths diverged with inhalation, and converged with exhalation. The connection to the spheres from the superior location was made with elastic bands, while the connection to the mobile inferior shaft was non-elastic.

The spheres had inner diameters of 10, 13, 17, 22, and 28 mm. The spheres were placed in an acrylic tank containing 16 liters of water. The spheres to background ratio was set to 5:1. A motor drove the spheres using a repeated patient respiratory cycle that had a duration of 6 s. Four acquisitions were performed in which the spheres were driven with 0, 1, 2, and 3 cm amplitudes. The phantom motion was programmed such that the spheres always returned to the same location for all acquisitions. During PET acquisition, the respiratory waveform was acquired with the AZ-733V respiratory gating system (Anzai Medical Co., Ltd.; Tokyo, Japan), by wrapping the belt around the surrogate motor platform as shown by the red arrow in the figure 6-2.



Figure 6-2 Setup of motion phantom. Surrogate motion platform and set up of Anzai belt on the platform (red arrow).

Bibliography

- [1] Röntgen WC. ON A NEW KIND OF RAYS. *Science*. 1896;3(59):227-231.
doi:10.1126/science.3.59.227
- [2] Cherry SR, Sorenson JA, Phelps ME. *Physics in Nuclear Medicine*. 4th ed. Philadelphia: Elsevier/Saunders; 2012.
- [3] Rahmim A, Zaidi H. PET versus SPECT: strengths, limitations and challenges. *Nucl Med Commun*. 2008;29(3):193-207. doi:10.1097/MNM.0b013e3282f3a515
- [4] Ryu H, Meikle SR, Willowson KP, Eslick EM, Bailey DL. Performance evaluation of quantitative SPECT/CT using NEMA NU 2 PET methodology. *Phys Med Biol*. 2019;64(14):145017. doi:10.1088/1361-6560/ab2a22
- [5] Moses WW. Fundamental limits of spatial resolution in PET. *Nucl Instruments Methods Phys Res Sect A Accel Spectrometers, Detect Assoc Equip*. 2011;648:S236-S240.
doi:10.1016/J.NIMA.2010.11.092
- [6] Pan T, Einstein SA, Kappadath SC, Grogg KS, Lois Gomez C, Alessio AM, Hunter WC, El Fakhri G, Kinahan PE, Mawlawi OR. Performance evaluation of the 5-Ring GE Discovery MI PET/CT system using the national electrical manufacturers association NU 2-2012 Standard. *Med Phys*. May 2019;mp.13576. doi:10.1002/mp.13576
- [7] Rausch I, Cal-González J, Dapra D, Gallowitsch HJ, Lind P, Beyer T, Minear G. Performance evaluation of the Biograph mCT Flow PET/CT system according to the NEMA NU2-2012 standard. *EJNMMI Phys*. 2015;2(1):26. doi:10.1186/s40658-015-0132-1
- [8] van Sluis J, de Jong J, Schaar J, Noordzij W, van Snick P, Dierckx R, Borra R, Willemsen A, Boellaard R. Performance Characteristics of the Digital Biograph Vision PET/CT System. *JNM*. 2019;60(7):1031-1036. doi:10.2967/jnumed.118.215418

- [9] Kinahan PE, Fletcher JW. Positron Emission Tomography-Computed Tomography Standardized Uptake Values in Clinical Practice and Assessing Response to Therapy. *Semin Ultrasound, CT MRI*. 2010;31(6):496-505. doi:10.1053/J.SULT.2010.10.001
- [10] Lassen ML, Kwiecinski J, Dey D, Cadet S, Germano G, Berman DS, Adamson PD, Moss AJ, Dweck MR, Newby DE, Slomka PJ. Triple-gated motion and blood pool clearance corrections improve reproducibility of coronary ^{18}F -NaF PET. *Eur J Nucl Med Mol Imaging*. August 2019;1-11. doi:10.1007/s00259-019-04437-x
- [11] Daou D. Respiratory motion handling is mandatory to accomplish the high-resolution PET destiny. *Eur J Nucl Med Mol Imaging*. 2008;35(11):1961-1970. doi:10.1007/s00259-008-0931-x
- [12] Farwell MD, Pryma DA, Mankoff DA. PET/CT imaging in cancer: Current applications and future directions. *Cancer*. 2014;120(22):3433-3445. doi:10.1002/cncr.28860
- [13] Korreman SS. Motion in radiotherapy: Photon therapy. *Phys Med Biol*. 2012;57(23). doi:10.1088/0031-9155/57/23/R161
- [14] Nehmeh SA, Erdi YE, Ling CC, Rosenzweig KE, Squire OD, Braban LE, Ford E, Sidhu K, Mageras GS, Larson SM, Humm JL. Effect of respiratory gating on reducing lung motion artifacts in PET imaging of lung cancer. *Med Phys*. 2002;29(37):72504-76221. doi:10.1118/1.1448824
- [15] Guerra L, De Ponti E, Elisei F, Bettinardi V, Landoni C, Picchio M, Gilardi MC, Versari A, Fioroni F, Dziuk M, Koza M, Ahond-Vionnet R, Collin B, Messa C, Carla Gilardi M, Versari A, Fioroni F, Dziuk M, Koza M, Ahond-Vionnet R, Collin B, Messa C, Guerra L, Elisei F, Messa C, De Ponti E, Bettinardi V, Landoni C, Picchio M, Gilardi MC, Versari A, Fioroni F, Dziuk M, Koza M, Ahond-Vionnet R, Collin B. Respiratory gated PET/CT in a European multicentre retrospective study: added diagnostic value in detection and characterization of lung lesions. *Eur J Nucl Med Mol Imaging*. 2012;39(9):1381-1390.

doi:10.1007/s00259-012-2148-2

- [16] Crivellaro C, De Ponti E, Elisei F, Morzenti S, Picchio M, Bettinardi V, Versari A, Fioroni F, Dziuk M, Tkaczewski K, Ahond-Vionnet R, Nodari G, Todde S, Landoni C, Guerra L. Added diagnostic value of respiratory-gated 4D 18F-FDG PET/CT in the detection of liver lesions: a multicenter study. *Eur J Nucl Med Mol Imaging*. 2018;45(1):102-109. doi:10.1007/s00259-017-3795-0
- [17] Frood R, McDermott G, Scarsbrook A. Respiratory-gated PET/CT for pulmonary lesion characterisation—promises and problems. *Br J Radiol*. February 2018:20170640. doi:10.1259/bjr.20170640
- [18] IMV. PET Imaging Market Summary Report 2019 - IMV Medical Information Division. <https://imvinform.com/product/pet-imaging-market-summary-report-2019/>. Published 2019. Accessed May 1, 2019.
- [19] Robin P, Bourhis D, Bernard B, Abgral R, Querellou S, Le Duc-Pennec A, Le Roux P-Y, Salaün P-Y. Feasibility of Systematic Respiratory-Gated Acquisition in Unselected Patients Referred for 18F-Fluorodeoxyglucose Positron Emission Tomography/Computed Tomography. *Front Med*. 2018;5:36. doi:10.3389/fmed.2018.00036
- [20] Bettinardi V, Rapisarda E, Gilardi MC. Number of partitions (gates) needed to obtain motion-free images in a respiratory gated 4D-PET/CT study as a function of the lesion size and motion displacement. *Med Phys*. 2009;36(12):5547-5558. doi:10.1118/1.3254431
- [21] Hope TA, Verdin EF, Bergsland EK, Ohliger MA, Corvera CU, Nakakura EK. Correcting for respiratory motion in liver PET/MRI: preliminary evaluation of the utility of bellows and navigated hepatobiliary phase imaging. *EJNMMI Phys*. 2015;2(1):21. doi:10.1186/s40658-015-0125-0

- [22] Van Elmpst W, Hamill J, Jones J, De Ruyscher D, Lambin P, Öllers M. Optimal gating compared to 3D and 4D PET reconstruction for characterization of lung tumours. *Eur J Nucl Med Mol Imaging*. 2011;38(5):843-855. doi:10.1007/s00259-010-1716-6
- [23] Kinahan P, Wollenweber S, Alessio A, Kohlmyer S, MacDonald L, Lewellen T, Ganin A. Impact of respiration variability on respiratory gated whole-body PET/CT imaging. In: *Journal of Nuclear Medicine*. Vol 48. Society of Nuclear Medicine; 2007:196P-196P. http://jnm.snmjournals.org/content/48/supplement_2/196P.1.short. Accessed May 9, 2019.
- [24] Teo B-K, Saboury B, Munbodh R, Scheuermann J, Torigian DA, Zaidi H, Alavi A. The effect of breathing irregularities on quantitative accuracy of respiratory gated PET/CT. *Med Phys*. 2012;39(12):7390-7397. doi:10.1118/1.4766876
- [25] Chi L, Larry II AP, Adam MA, Paul EK, Liu C, Pierce II LA, Alessio AM, Kinahan PE. The impact of respiratory motion on tumor quantification and delineation in static PET/CT imaging. *Phys Med Biol*. 2009;54(24):7345-7362. doi:10.1088/0031-9155/54/24/007
- [26] Masaoka Y, Homma I. The effect of anticipatory anxiety on breathing and metabolism in humans. *Respir Physiol*. 2001;128(2):171-177. doi:10.1016/S0034-5687(01)00278-X
- [27] Grilo A, Vieira L, Carolino E, Oliveira C, Pacheco C, Castro M, Alonso J. Anxiety in Cancer Patients during 18 F-FDG PET/CT Low Dose: A Comparison of Anxiety Levels before and after Imaging Studies. *Nurs Res Pract*. 2017;2017:1-9. doi:10.1155/2017/3057495
- [28] Fürst S, Grimm R, Hong I, Souvatzoglou M, Casey ME, Schwaiger M, Nekolla SG, Ziegler SI. Motion correction strategies for integrated PET/MR. *JNM*. 2015;56(2):261-269. doi:10.2967/jnumed.114.146787
- [29] Hong I, Jones J, Casey M. Ultrafast Elastic Motion Correction via Motion Deblurring. In:

2014 IEEE Nuclear Science Symposium and Medical Imaging Conference (NSS/MIC).

IEEE; 2014:1-2. doi:10.1109/NSSMIC.2014.7430841

- [30] Kesner AL, Schleyer PJ, Büther F, Walter MA, Schäfers KP, Koo PJ. On transcending the impasse of respiratory motion correction applications in routine clinical imaging - a consideration of a fully automated data driven motion control framework. *EJNMMI Phys.* 2014;1(1):8. doi:10.1186/2197-7364-1-8
- [31] Panin VY, Smith a M, Hu J, Kehren F, Casey ME. Continuous bed motion on clinical scanner: design, data correction, and reconstruction. *Phys Med Biol.* 2014;59(20):6153-6174. doi:10.1088/0031-9155/59/20/6153
- [32] Schleyer P, Hong I, Jones J, Hamill J, Panin V, Fuerst S. Data-Driven Respiratory Gating Whole Body PET Using Continuous Bed Motion. In: Institute of Electrical and Electronics Engineers (IEEE); 2019:1-5. doi:10.1109/nssmic.2018.8824401
- [33] Nehmeh SA, Erdi YE, Meirelles GSP, Squire O, Larson SM, Humm JL, Schöder H. Deep-inspiration breath-hold PET/CT of the thorax. *JNM.* 2007;48(1):22-26. <http://www.ncbi.nlm.nih.gov/pubmed/17204695>. Accessed June 21, 2017.
- [34] Dawood M, Büther F, Lang N, Schober O, Schäfers KP. Respiratory gating in positron emission tomography: A quantitative comparison of different gating schemes. *Med Phys.* 2007;34(7):3067-3076. doi:10.1118/1.2748104
- [35] Qiao F, Clark JW, Pan T, Mawlawi O. Joint model of motion and anatomy for PET image reconstruction. *Med Phys.* 2007;34(12):4626-4639. doi:10.1118/1.2804721
- [36] Chang G, Chang T, Pan T, Clark JW, Mawlawi OR. Joint correction of respiratory motion artifact and partial volume effect in lung/thoracic PET/CT imaging. *Med Phys.* 2010;37(12):6221-6232. doi:10.1118/1.3512780
- [37] Nehmeh SA. Respiratory Motion Correction Strategies in Thoracic PET-CT Imaging. *Positron Emiss Tomogr.* 2013;8(1):29-36. doi:10.1016/j.cpet.2012.10.004

- [38] Kesner AL, Meier JG, Burckhardt DD, Schwartz J, Lynch DA. Data-driven optimal binning for respiratory motion management in PET. *Med Phys*. 2018;45(1):277-286. doi:10.1002/mp.12651
- [39] Frey K, Hamill J, Jones J, Koeppe R. Respiratory motion gated PET with end-expiratory, amplitude based gating. *JNM*. 2009;50(supplement 2):348-348.
http://jnm.snmjournals.org/content/50/supplement_2/348.abstract?sid=33fffc61-93ad-4cb1-9514-cd559712f33d. Accessed April 3, 2018.
- [40] Van Der Gucht A, Serrano B, Hugonnet F, Paulmier B, Garnier N, Faraggi M. Impact of a new respiratory amplitude-based gating technique in evaluation of upper abdominal PET lesions. *Eur J Radiol*. 2014;83(3):509-515. doi:10.1016/j.ejrad.2013.11.010
- [41] Grootjans W, De Geus-Oei L-F, Troost EGC, Visser EP, Oyen WJG, Bussink J. PET in the management of locally advanced and metastatic NSCLC. *Nat Publ Gr*. 2015;12:395-407. doi:10.1038/nrclinonc.2015.75
- [42] Hamill J, Ghosh P. HD•Chest Respiratory Gating for PET. In: *PN0002262 Rev. A (White Paper)*. Siemens Medical Solutions; 2011.
- [43] Dawood M, Buther F, Xiaoyi Jiang, Schafers KP. Respiratory Motion Correction in 3-D PET Data With Advanced Optical Flow Algorithms. *IEEE Trans Med Imaging*. 2008;27(8):1164-1175. doi:10.1109/TMI.2008.918321
- [44] Hong L, Jones J, Hamill J, Michel C, Casey M. Elastic motion correction for continuous bed motion Whole-body PET/CT. In: *2016 IEEE Nuclear Science Symposium, Medical Imaging Conference and Room-Temperature Semiconductor Detector Workshop, NSS/MIC/RTSD 2016*. Vol 2017-Janua. IEEE; 2017:1-2.
doi:10.1109/NSSMIC.2016.8069587
- [45] Poesse S, Hong I, Mannweiler D, Buether F, Jones J, Schafers M, Schaefer K. Respiratory motion compensation in PET/CT: Evaluation of a fast elastic motion

- compensation technique based on motion deblurring. *JNM*. 2017;58(supplement 1):1349-1349. http://jnm.snmjournals.org/content/58/supplement_1/1349.abstract?sid=5f9a8dac-501c-4adc-98ec-e733a5fed842. Accessed April 2, 2018.
- [46] Dawood M, Gigengack F, Jiang X, Schäfers KP. A mass conservation-based optical flow method for cardiac motion correction in 3D-PET. *Med Phys*. 2013;40(1):012505. doi:10.1118/1.4770276
- [47] Li XA, Stepaniak C, Gore E. Technical and dosimetric aspects of respiratory gating using a pressure-sensor motion monitoring system. *Med Phys*. 2005;33(1):145-154. doi:10.1118/1.2147743
- [48] Krippendorff K. Reliability in Content Analysis. *Hum Commun Res*. 2004;30(3):411-433. doi:10.1111/j.1468-2958.2004.tb00738.x
- [49] Liu C, Alessio A, Pierce L, Thielemans K, Wollenweber S, Ganin A, Kinahan P. Quiescent period respiratory gating for PET/CT. *Med Phys*. 2010;37(9):5037-5043. doi:10.1118/1.3480508
- [50] Pan T, Mawlawi O, Nehmeh SA, Erdi YE, Luo D, Liu HH, Castillo R, Mohan R, Liao Z, Macapinlac HA. Attenuation correction of PET images with respiration-averaged CT images in PET/CT. *JNM*. 2005;46(9):1481-1487. <http://www.ncbi.nlm.nih.gov/pubmed/16157531>. Accessed April 2, 2018.
- [51] Erdi YE, Nehmeh SA, Pan T, Pevsner A, Rosenzweig KE, Mageras G, Yorke ED, Schoder H, Hsiao W, Squire OD, Vernon P, Ashman JB, Mostafavi H, Larson SM, Humm JL. The CT motion quantitation of lung lesions and its impact on PET-measured SUVs. *JNM*. 2004;45(8):1287-1292. <http://www.ncbi.nlm.nih.gov/pubmed/15299050>. Accessed April 2, 2018.
- [52] Hamill J, Mawlawi O, Meier J. Respiratory Phase Matching in PET/CT Using Fast Spiral CT. In: *Journal of Nuclear Medicine*. Vol 58. Society of Nuclear Medicine; 2017:577-

577. http://jnm.snmjournals.org/content/58/supplement_1/577.abstract?sid=aa003d68-35f7-4ad8-ba87-4c83d75e91b4. Accessed April 3, 2018.
- [53] Prior JO, Péguret N, Pomoni A, Pappon M, Zeverino M, Belmondo B, Lovis A, Ozsahin M, Vienne M, Bourhis J. Reduction of Respiratory Motion During PET/CT by Pulsatile-Flow Ventilation: A First Clinical Evaluation. *JNM*. 2016;57(3):416-419. doi:10.2967/jnumed.115.163386
- [54] Meier JG, Wu CC, Betancourt Cuellar SL, Truong MT, Erasmus JR, Einstein S, Mawlawi O. Evaluation of a novel elastic respiratory motion correction algorithm on quantification and image quality in abdomino-thoracic PET/CT. *JNM*. 2018;60(2):279-284. doi:10.2967/jnumed.118.213884
- [55] Lu Y, Fontaine K, Mulnix T, Onofrey JA, Ren S, Panin V, Jones J, Casey ME, Barnett R, Kench P, Fulton R, Carson RE, Liu C. Respiratory Motion Compensation for PET/CT with Motion Information Derived from Matched Attenuation-Corrected Gated PET Data. *JNM*. 2018;59(9):1480-1486. doi:10.2967/jnumed.117.203000
- [56] Dutta J, Huang C, Li Q, El Fakhri G. Pulmonary imaging using respiratory motion compensated simultaneous PET/MR. *Med Phys*. 2015;42(7):4227-4240. doi:10.1118/1.4921616
- [57] Hoisak JDP, Sixel KE, Tirona R, Cheung PCF, Pignol J-P. Correlation of lung tumor motion with external surrogate indicators of respiration. *Int J Radiat Oncol Biol Phys*. 2004;60(4):1298-1306. doi:10.1016/j.ijrobp.2004.07.681
- [58] Gierga DP, Brewer J, Sharp GC, Betke M, Willett CG, Chen GTY. The correlation between internal and external markers for abdominal tumors: Implications for respiratory gating. *Int J Radiat Oncol*. 2005;61(5):1551-1558. doi:10.1016/J.IJROBP.2004.12.013
- [59] Fayad H, Pan T, François Clement J, Visvikis D. Technical Note: Correlation of respiratory motion between external patient surface and internal anatomical landmarks.

Med Phys. 2011;38(6Part1):3157-3164. doi:10.1118/1.3589131

- [60] Klein GJ, Reutter BW, Botvinick EH, Budinger TF, Huesman RH. Fine-scale motion detection using intrinsic list mode PET information. In: *Proceedings IEEE Workshop on Mathematical Methods in Biomedical Image Analysis (MMBIA 2001)*. IEEE Comput. Soc; 2001:71-78. doi:10.1109/MMBIA.2001.991701
- [61] Büther F, Ernst I, Dawood M, Kraxner P, Schäfers M, Schober O, Schäfers KP. Detection of respiratory tumour motion using intrinsic list mode-driven gating in positron emission tomography. *Eur J Nucl Med Mol Imaging*. 2010;37(12):2315-2327. doi:10.1007/s00259-010-1533-y
- [62] Feng T, Wang J, Sun Y, Zhu W, Dong Y, Li H. Self-Gating: An Adaptive Center-of-mass Approach for Respiratory Gating in PET. *IEEE Trans Med Imaging*. 2017:1-1. doi:10.1109/TMI.2017.2783739
- [63] He J, O’Keefe GJ, Gong SJ, Jones G, Saunder T, Scott AM, Geso M. A Novel Method for Respiratory Motion Gated With Geometric Sensitivity of the Scanner in 3D PET. *IEEE Trans Nucl Sci*. 2008;55(5):2557-2565. doi:10.1109/TNS.2008.2001187
- [64] Yang J, Khalighi M, Hope TA, Ordovas K, Seo Y. Technical Note: Fast respiratory motion estimation using sorted singles without unlist processing: A feasibility study. *Med Phys*. January 2017. doi:10.1002/mp.12115
- [65] Kesner AL, Bundschuh RA, Detorie NC, Dahlbom M, Ziegler SI, Czernin J, Silverman DH. Respiratory Gated PET Derived in a Fully Automated Manner From Raw PET Data. *IEEE Trans Nucl Sci*. 2009;56(3):677-686. doi:10.1109/TNS.2009.2016341
- [66] Schleyer PJ, O’Doherty MJ, Barrington SF, Marsden PK. Retrospective data-driven respiratory gating for PET/CT. *Phys Med Biol*. 2009;54(7):1935-1950. doi:10.1088/0031-9155/54/7/005
- [67] Thielemans K, Rathore S, Engbrant F, Razifar P. Device-less gating for PET/CT using

- PCA. In: *2011 IEEE Nuclear Science Symposium Conference Record*. IEEE; 2011:3904-3910. doi:10.1109/NSSMIC.2011.6153742
- [68] Thielemans K, Schleyer P, Marsden PK, Manjeshwar RM, Wollenweber SD, Ganin A. Comparison of different methods for data-driven respiratory gating of PET data. In: *IEEE Nuclear Science Symposium Conference Record*. IEEE; 2013:1-4. doi:10.1109/NSSMIC.2013.6829055
- [69] Schatka I, Weiberg D, Reichelt S, Owsianski-Hille N, Derlin T, Berding G, Bengel FM. A randomized, double-blind, crossover comparison of novel continuous bed motion versus traditional bed position whole-body PET/CT imaging. *Eur J Nucl Med Mol Imaging*. 2016;43(4):711-717. doi:10.1007/s00259-015-3226-z
- [70] Ahn S, Park SH, Lee KH. How to Demonstrate Similarity by Using Noninferiority and Equivalence Statistical Testing in Radiology Research. *Radiology*. 2013;267(2):328-338. doi:10.1148/radiol.12120725
- [71] Koo TK, Li MY. A Guideline of Selecting and Reporting Intraclass Correlation Coefficients for Reliability Research. *J Chiropr Med*. 2016;15(2):155-163. doi:10.1016/j.jcm.2016.02.012
- [72] Meier JG, Einstein SA, Diab RH, Erasmus LJ, Xu G, Mawlawi OR. Impact of free-breathing CT on quantitative measurements of static and quiescent period-gated PET Images. *Phys Med Biol*. 2019;64(10):105013. doi:10.1088/1361-6560/ab1cdd
- [73] Dahlbom M, Reed J, Young J. Implementation of true continuous bed motion in 2-D and 3-D whole-body PET scanning. *IEEE Trans Nucl Sci*. 2001;48(4):1465-1469. doi:10.1109/23.958381
- [74] Osborne DR, Acuff S, Cruise S, Syed M, Neveu M, Stuckey A, Bradley Y. Quantitative and qualitative comparison of continuous bed motion and traditional step and shoot PET/CT. *Am J Nucl Med Mol Imaging*. 2015;5(1):56-64.

<http://www.ncbi.nlm.nih.gov/pubmed/25625027>. Accessed August 3, 2018.

- [75] Everding M, Emery D, Mawlawi O, Millican-Campbell, Richelle Palendat T, Pan T, Peirsol L, Simon B, Swanston N, Rohren E. Impact of continuous bed motion (CBM) PET/CT scanners on clinical operation. *JNM*. 2014;55(supplement 1):2511-2511.
http://jnm.snmjournals.org/content/55/supplement_1/2511.abstract?sid=0917b0ac-faf0-4d89-8b51-ae3c8e03cb90. Accessed August 29, 2018.
- [76] Bouyeure-petit A-C, Chastan M, Edet-Sanson A, Becker S, Thureau S, Houivet E, Vera P, Hapdey S. Clinical respiratory motion correction software (reconstruct, register and averaged—RRA), for 18 F-FDG-PET-CT: phantom validation, practical implications and patient evaluation. *Br J Radiol*. 2017;90(1070):20160549. doi:10.1259/bjr.20160549
- [77] Bowen SR, Pierce LA, Alessio AM, Liu C, Wollenweber SD, Stearns CW, Kinahan PE. Assessment of patient selection criteria for quantitative imaging with respiratory-gated positron emission tomography. *J Med imaging (Bellingham, Wash)*. 2014;1(2):026001. doi:10.1117/1.JMI.1.2.026001
- [78] Wang S, Bowen SR, Chaovalitwongse WA, Sandison GA, Grabowski TJ, Kinahan PE. Respiratory trace feature analysis for the prediction of respiratory-gated PET quantification. *Phys Med Biol*. 2014;59(4):1027-1045. doi:10.1088/0031-9155/59/4/1027
- [79] Chang G, Chang T, Pan T, Clark JW, Mawlawi OR. Implementation of an Automated Respiratory Amplitude Gating Technique for PET/CT: Clinical Evaluation. *JNM*. 2010;51(1):16-24. doi:10.2967/jnumed.109.068759
- [80] Huang T-C, Wang Y-C, Chiou Y-R, Kao C-H. Respiratory Motion Reduction in PET/CT Using Abdominal Compression for Lung Cancer Patients. Gelovani JG, ed. *PLoS One*. 2014;9(5):e98033. doi:10.1371/journal.pone.0098033
- [81] Cherry SR, Jones T, Karp JS, Qi J, Moses WW, Badawi RD. Total-Body PET: Maximizing Sensitivity to Create New Opportunities for Clinical Research and Patient

Care. *JNM*. 2018;59:3-12. doi:10.2967/jnumed.116.184028

- [82] Liu S, Wang S, Chaovalitwongse WA, Bowen SR. Cost-effectiveness of patient-specific motion management strategy in lung cancer radiation therapy planning. *Eng Econ*. April 2019:1-19. doi:10.1080/0013791X.2019.1597239

Vita

Joseph Gabriel Meier, was born in Dallas, Texas, the son of Patricia Rose Meier and Kenneth John Meier. After completing his high school education at Cistercian Preparatory School, Dallas, Texas in 2003, he entered the University of Dallas in Irving, Texas. He received a Bachelor of Science in Physics and a Bachelor of Arts in English in May, 2008. For the next 5 years, he worked as a Physics Technologist in the Imaging Physics Department at MD Anderson Cancer Center. In August of 2014 he entered The University of Texas MD Anderson Cancer Center UTHealth Graduate School of Biomedical Sciences to pursue a doctoral degree in Medical Physics. Most noteworthy, he married his wife, Kristine Elisa Norvik Meier on December 13, 2014.

Permanent address:

4022 Cheena Drive
Houston, Texas 77025